EUROPEAN COMMISSION

Community Research

SEVENTH FRAMEWORK PROGRAMME

CARBOWASTE

Treatment and Disposal of Irradiated Graphite and Other Carbonaceous Waste

Grant Agreement Number: FP7-211333

Deliverable D-4.2.1

Decontamination Factors Obtained by Thermal Treatment in an Inert Atmosphere

Author(s):
Katrin Baginski, Tatiana Podruzhina, Monika Florjan, Corrado Rizzato, Dirk Vulpius;
Forschungszentrum Juelich GmbH

Document Number: CARBOWASTE-D-1303-4.2.1
Date of issue of this report: 25/03/2013

Start date of project: **01/04/2008** Duration: **60 Months**

Project co-funded by the European Commission under the Seventh Framework Programme (2007 to 2011) of the European Atomic Energy Community (EURATOM) for nuclear research and training activities		
Dissemination Level		
PU	Public	
RE	Restricted to the partners of the CARBOWASTE project	
CO	Confidential, only for specific distribution list defined on this document	**X**

Distribution list

Person and organisation name and/or group	Comments
WP4 members	
Executive Board	
Co-ordinator	

CARBOWASTE		
Work package: 4 **Task:** 4.2	**CARBOWASTE document no:** CARBOWASTE-1303-D-4.2.1 (e.g. May 2008 as date of issue: 0805)	**Document type:** D=Deliverable
Issued by: Forschungszentrum Juelich GmbH (DE) **Internal no.:** CW1303-Deliverable-4-2-1-I		**Document status:** Final

Document title

Decontamination Factors Obtained by Thermal Treatment in an Inert Atmosphere

Executive summary

Graphite Decontamination by 'Physical Treatment' is addressed within Task 4.2. Contaminated graphite samples (powder, granulate or solid specimens) have been heated in an inert atmosphere. The radionuclide release rates have been measured in the off-gas as function of the temperature. In particular, the influence of adsorbed gases on the graphite porous surface before thermal treatment have been investigated, as these gases may have a significant influence on the separation of ^{14}C from the ^{12}C-containing matrix. FZJ is performing most of the experimental work together with ITU, which operates a Knudsen Cell to reach temperatures up to 2000 °C with micro-samples.
The main results from this task are as follows:
Thermal treatments in inert atmosphere (TTIA) showed to be effective for the removal of Tritium with high selectivity and relatively high Decontamination Factors (DFs), thanks to its diffusion-like migration mechanism: temperatures higher than 1100°C resulted in a significant decontamination from Tritium, with values depending on i-graphite´s history. For what concerns C-14, several experiments proved that its removal is linkable to the presence of oxidants, already adsorbed/embedded or provided by an external source. Accordingly, TTIA are not suitable for an effective removal of C-14 since, after the adsorbed/embedded oxidising species have reacted, no further decontamination takes place due to lacking of reactants: low DFs for C-14 reflected this fact. Inert gas treatments, however, could be a valid option in the case a re-loading of reactants on the graphite surfaces occurred, preferentially in separate steps in order to avoid significant mass losses. In addition it has to be underlined that lower Decontamination Factors (DFs) are generally achieved for C-14, compared to H-3, due to its nature and localization in the graphite matrix: part of the C-14 is embedded in the structure and, since its behaviour is chemically identical to the C-12, it is not possible to separate it in an efficient way without implying isotopic separation techniques in conjunction with the application of destructive techniques; however, another fraction of C-14 is labile/loosely bound and, consequently, removable through a proper thermal treatment, even without significantly affecting the graphite structural integrity depending on the chosen treatment gases/parameters.
It is possible to use TTIA as analytical tool to get an indication on the treatability of the graphite in question: different nuclear graphite, coming from different reactors, can be classified in such a way and, moreover, the selectivity of C-14 can be evaluated.
In addition, it has to be taken into account that very high temperature TTIA start changing graphite´s structure, particularly in the case on which graphite was irradiated at low temperatures, allowing in such a way the migration of vacancies and interstitials: more than favouring a partial removal of volatile radionuclides, a high temperature TTIA could improve the containment of several radioisotopes inside the graphite matrix due to the enhancement of the structure order and the immobilization of radionuclides in a more stable way. This finding is particularly important for the waste management of irradiated graphite.

Revisions						
Rev.	Date	Short description	Author	Internal Review	Task Leader	WP Leader
00	dd/mm/yyyy	Issue	Name, Organisation	Name, Organisation *Signature*	Name, Organisation *Signature*	Name, Organisation *Signature*
00	21/01/2010	First issue	Baginski FZJ	von Lensa FZJ	Vulpius FZJ	Vulpius FZJ
01	26/03/2010	2nd Issue	Rizzato, Vulpius FZJ	von Lensa FZJ	Vulpius, FZJ	von Lensa FZJ

Table of Content

1. OBJECTIVES OF THE TASK 7

2. SIMULATIONS AND MECHANISMS 7

2.1 Molecular dynamics study of C-14 transport in nuclear graphite 7

2.2 Transport mechanism of C-14 8

2.3 Effect of Grain Boundaries 10

3. INVESTIGATED SAMPLES 11

3.1 Merlin Graphite 11
3.1.1 Merlin samples: Origin and preparation 11

3.2 AVR (Arbeitsgemeinschaft VersuchsReaktor) 13
3.2.1 AVR Reflector Graphite 13
3.2.2 AVR Virgin Samples: Origin and Preparation 17

3.3 Saint-Laurent A2 21
3.3.1 General considerations about UNGG reactors 21
3.3.2 Saint-Laurent A2: reactor history 21
3.3.3 Graphite stack description 22
3.3.4 SLA2 Graphite 23
3.3.5 Core sampling 24

3.4 Oldbury 2 25
3.4.1 The reactor 25
3.4.2 Oldbury 2 samples: Origin and preparation 25
3.4.3 Sample Preparation for small scale thermal treatment facility 26

4. DESCRIPTION OF EXPERIMENTAL FACILITIES 28

4.1 Small Scale Facility at FZJ 28
4.1.1 Equipment 28
4.1.2 Reagents and investigated materials 28
4.1.3 Performance of experiments 29
4.1.4 On-going experiments and changes of the facility 33

4.2 Induction Furnace Facility at FZJ 39
4.2.1 Equipment 39
4.2.2 Modifications of the facility 47
4.2.3 Performance of experiments 53

5. Experimental Results 58

5.1 Small Scale Facility at FZJ 58
5.1.1 Tritium release 58
5.1.2 Radiocarbon release 61

5.1.2 Calculation method of ^{3}H and ^{14}C release 63

5.2 Induction Furnace at FZJ 65

6. DECONTAMINATION FACTORS 71
6.1. Decontamination Factors for Merlin Graphite 72
6.2. Decontamination Factors for SLA2 Graphite 75
6.3. Decontamination Factors for Oldbury 2 Graphite 78
6.4. Decontamination Factors for AVR Graphite 81
6.5 Removal of other radionuclides 83
6.6 Overview of Decontamination Factors for Different Graphite 83

7. INTERPRETATION OF RESULTS 86

7.1 Release Mechanisms and Kinetics 86
7.1.1 Release of Tritium 86
7.1.2 Release of Radiocarbon 96

7.2 Release Isotherms – Merlin and Oldbury2 106

7.3 Special case: Detection and removal of surface contaminations 109

7.4 Waste Management Strategies 111

CONCLUSIONS 113

8. REFERENCES 117

9. APPENDIX 121

9.1 Summary Thermal Treatment with Decontamination Factors 121

9.2 Summary Thermal Treatment with Enrichment Factors 123

List of Figures 124

List of Tables 128

1. Objectives of the Task

Tritium and other radioisotopes, including ^{36}Cl and ^{129}I, can be removed from graphite by thermal treatment under inert conditions, as shown in former and current KUEFA experiments on HTR fuel elements. It has to be checked whether significant parts of the ^{14}C inventory can be selectively mobilized, since a significant part of ^{14}C may be adsorbed on the surface of the crystallites in the pore structure and not integrated into the crystal lattice. This has been demonstrated in principle by early experiments performed at FZJ and by separate work in the UK on GLEEP reactor graphite. This task will perform detailed investigations of this decontamination process in order to discriminate physical from chemical effects, which might take place in parallel to each other. The general temperature dependence of radioisotope release will be examined up to temperatures of 2000 °C. The graphite samples will be characterised before and after treatment in order to determine the decontamination rate. The results will be interpreted with regards to optimized processes for graphite purification.

2. Simulations and Mechanisms

In the present chapter some simulations performed at INBK (Institut für Nuklearen BrennstoffKreislauf, RWTH Aachen) by Dr. R. Nabbi and H. Probst are presented. The main purpose of such simulations, performed with Monte Carlo method, was to contribute to a deeper understanding of C-14 creation mechanism and transport in nuclear graphite, in order to predict the binding state and location of such radionuclide and, consequently, to establish a selective removal process, where it is applicable.

2.1 Molecular dynamics study of C-14 transport in nuclear graphite

The work in the field of modeling and simulation has been focused on the description of the formation of the radionuclide C-14 and its transport in the nuclear graphite as a result of recoil process. In view of a potential decontamination of the irradiated graphite, the knowledge of the binding state of the ^{14}C-atoms and their local distributions in the graphite structure as well as the release mechanism is of particular importance.
As nuclear material, graphite is characterized by a well-defined crystalline structure as given in Fig. 2.1.1 (hexagonally shaped). The individual ^{14}C-Atoms are located in layers with a distance of 3.5 Å which are shifted against each other. In the case of irradiation elastic and inelastic interaction with fast neutrons take place in parallel to the formation of ^{14}C by activation leading to the creation of Frenkel-pairs (interstitials and vacancies). Due to the high cross section for this process the concentration of the defect pairs are higher than ^{14}C concentration by orders of magnitude. However as a consequence of low energy for potential recombination and temperature dependent self-diffusion the concentration vacancy-interstitial takes place resulting in a reduction of their concentration (0.15 eV).
C-14 is formed as a result of the activation of captured trace elements like oxygen and nitrogen existing in nuclear graphite and particularly by activation of carbon-isotopes. The formation by activation of C-13 is less than over the N-14 activation which is embedded in graphite

during the manufacturing process or reactor operation. The reason for higher activation rate is the higher cross section as depicted in Figure 2.1.2.

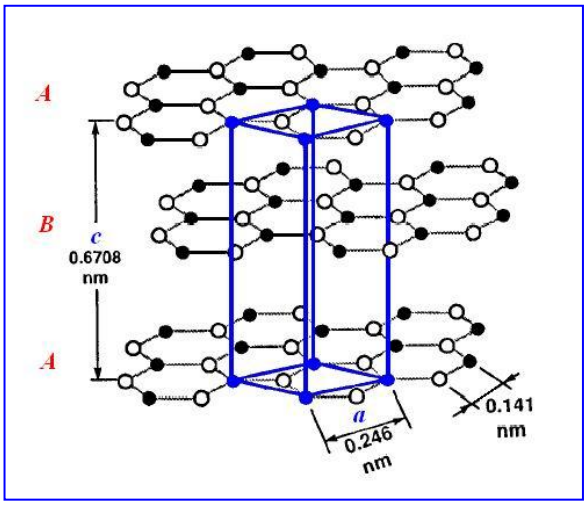

Figure 2.1.1: Criytalline structure of graphite

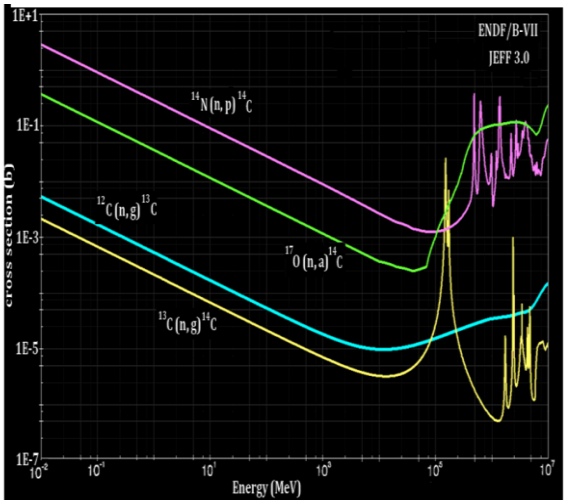

Figure 2.1.2: Cross sections for production of C14.

2.2 Transport mechanism of C-14

The mechanism of the transport/distribution and release of C-14 inside the irradiated graphite structure is a complex issue and is studied by the application of molecular dynamic (MD) method which allows the simulation of the interaction mechanisms at atomistic level in the lattice structure of graphite. The result of such a simulation is given in Figures 2.2.1-2 that show the configuration and state of the graphite lattice at beginning and end of recoil atom transport (C-14). Accordingly the C-14 atom is located in an interstitial position accompanied with a deformation of the lattice structure due to the cascade process. For this aim the program LAMMPS was used to investigate the behavior and the configuration of the defects (^{14}C). The MD works with the solution of Newton's equation of motion for atoms and molecules, coupled together by certain atomic interaction potentials. The transport process and the binding of C-14 were initially investigated in pure graphite with a crystalline structure under various initial and boundary conditions; in addition, a possible effect of the grain boundaries, pores and impurities was studied. The formation process of ^{14}C is associated with the recoil of ^{14}C atoms with a kinetic energy in the range of some keV (2.56 keV for the ^{13}C activation and 42 keV by ^{14}N) leading to the removal from the lattice site. This transfer of ^{14}C is accompanied by various interaction and ionization processes which result in a disorder of the lattice structure as well as in the formation of further displacements (interstitial atoms and vacancies).

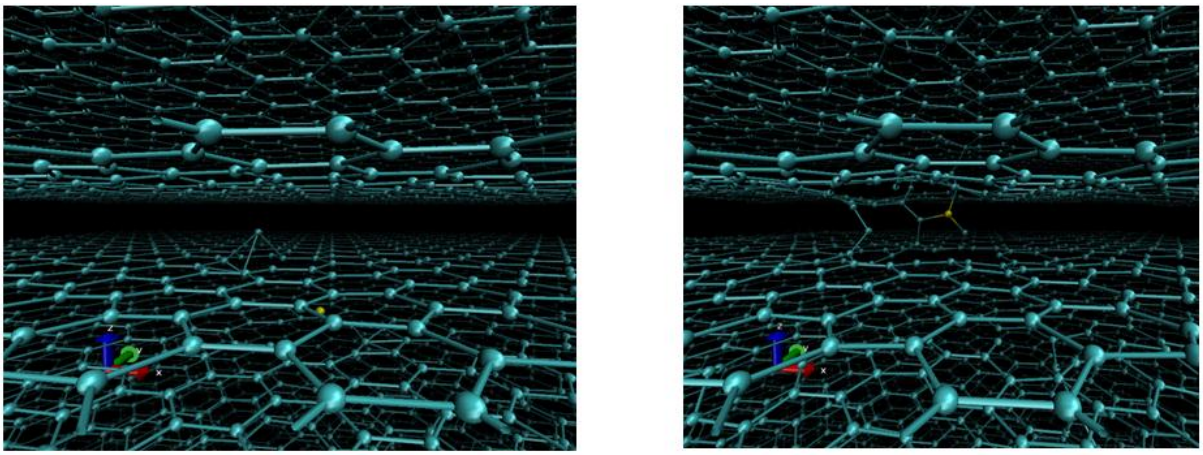

Figure 2.2.1-2: Initial and Final state of single cascade in perfect lattice structure (yellow: C14)

The MD simulation showed that at an initial energy of 10 keV, for example, the recoil atom is displaced after the generation by a mean distance of 60-130 angstrom in the crystal structure, being influenced by the interacting potentials (see Figure 2.2.3). However the result depends on the type of the potentials governing the interaction between the individual atoms in the short range and recoil direction relative to the orientation of the crystal lattice.

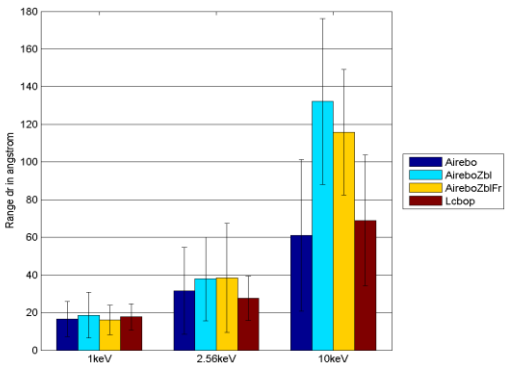

Figure 2.2.3: Range of C-14 in dependence of recoil energy and for different potentials

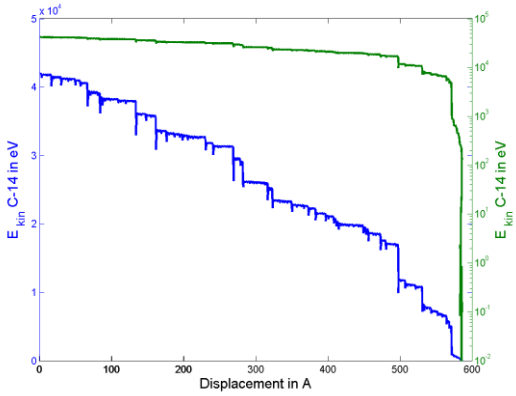

Figure 2.2.4: Displacement and energy loss of C-14 in crystalline graphite for 40 keV(right)

Resulting from the symmetrical character of the individual atoms at the c-layers, the mean range and the transport of the primary C-14 is not significantly influenced by the temperature variation. This result, however, needs to be verified by detailed modeling of the boundary conditions.

In addition, specific and stepwise energy loss of the ^{14}C atoms taking place during the transport process was studied as given in Fig. 2.2.4 for an example of 42 keV (^{14}C produced by ^{14}N). Accordingly, a smooth energy loss takes place with a specific value of approx. 100 eV per Å. After getting lower energy (5 keV) the energy loss shows a sudden drop probably caused by electronic interaction and ionization.

2.3 Effect of Grain Boundaries

Due to the complex manufacturing process the reactor graphite consists of polycrystalline configuration and no specific alignment, which lead partly to the formation of grain boundaries. To answer the question of the grain boundaries on the ^{14}C transport a polycrystalline model consisting of individual monocrystalline grains was generated for MD simulation. For the model different orientation and angle respectively between the individual crystalline grains were assumed as given in Fig. 2.3.1-a,b. In this configuration, the recoil ^{14}C-Atom was started under various angles with recoil energy of 40 keV (^{14}C by activation of ^{14}N). Due to the fact that no particular potentials are acting at the interface (representing the pores) the ^{14}C atoms cross the grain boundaries and pores without any deflection and path change. The results of the simulation have been summarized and depicted in Fig. 2.3.2-a,b for different orientation of individual crystalline grains. Accordingly the starting ^{14}C atom undergoes a transport without being influenced by the adjacent boundary layers but by the orientation of the subsequent grain layers. The figure shows that a significant accumulation of C-14 in the vicinity of grain boundaries or surfaces (pores) caused only by the stopping processes (potentials) is not expected (Fig. 2.3.2-a,b).

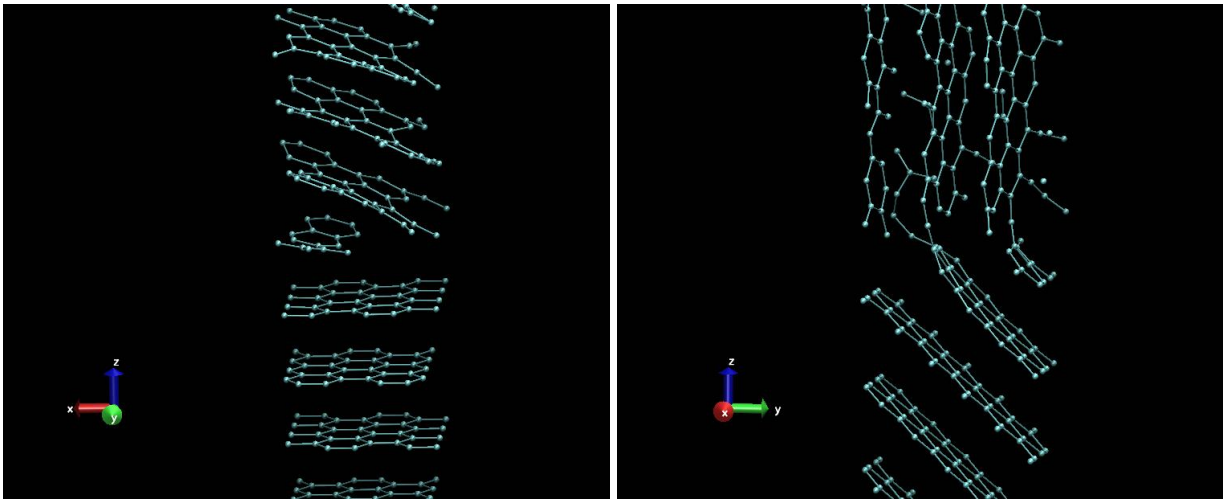

Figure 2.3.1-a,b: Configuration of crystaline grains for Md simulation of the boundary effect

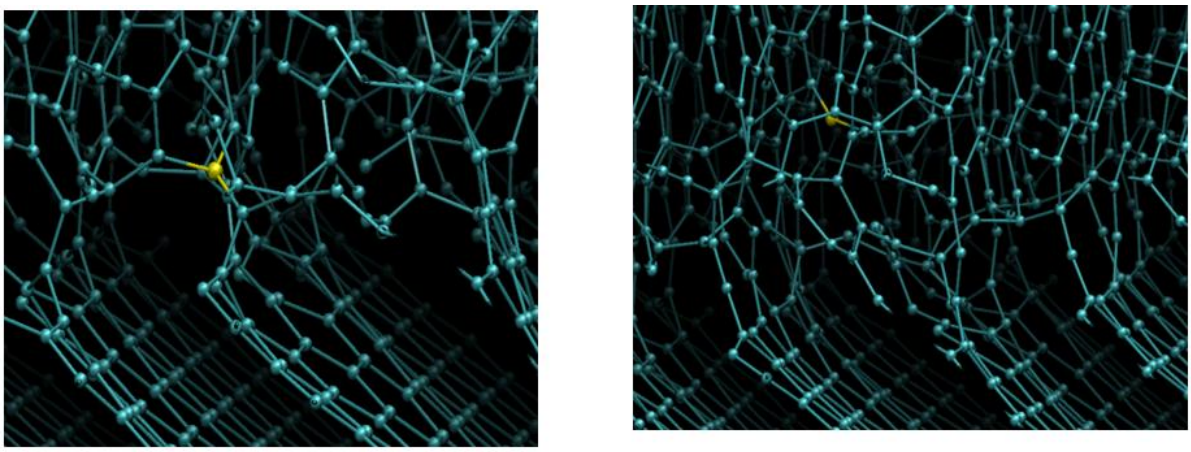

Figure 2.3.2-a,b: Final states of C14 near grain boundaries

3. Investigated Samples

3.1 Merlin Graphite

The MERLIN reactor (Medium Energy Research Light-Water-Moderated Industrial Nuclear Reactor, called also FRJ-1) at the research centre of Juelich was a light-water-moderated and -cooled swimming pool reactor. It was built between 1958 and 1962 and was subsequently used for various irradiation experiments, especially in the field of material science. Such reactor implied nuclear-grade graphite in a thermal column (see Figure 3.1-a,b) and operated from 1964 till 1985. After 10 years its dismantling began and was completed in 2009: the reactor has been completely decommissioned and reached the so-called “green field” status. The thermal power was initially 5 MW, raised later on up to 10 MW with a thermal neutron flux up to $1.1 \cdot 10^{14}$ n/cm^2·s. The 10 tons of graphite are presently placed in an intermediate storage. Several samples of the thermal column have been used for the investigations on graphite treatments within the scope of this report.[8]

3.1.1 Merlin samples: Origin and preparation

The samples used in the following tests were removed from the thermal columns during the reactor block's demolition. The thermal columns were used to slow down the fast neutrons, released during the nuclear reaction, to thermal neutrons for test purposes. The following figures 3.1.1-a and 3.1.1-b show the reactor block's structure.

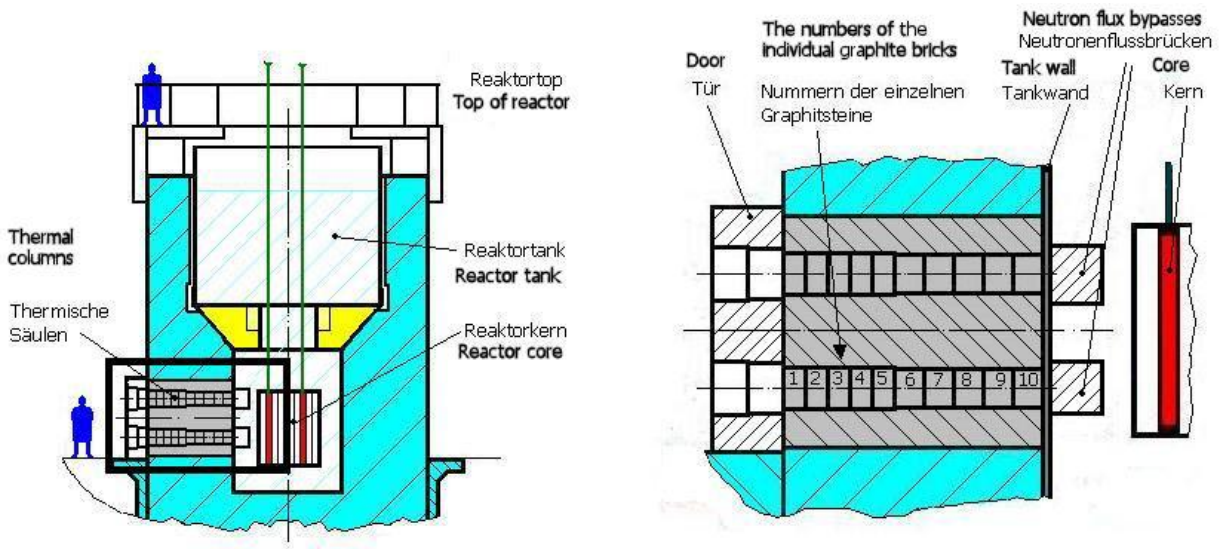

Figure 3.1.1: (a) Cross section of the reactor block (left) and (b) position of the individual graphite bricks inside the reactor block (right)

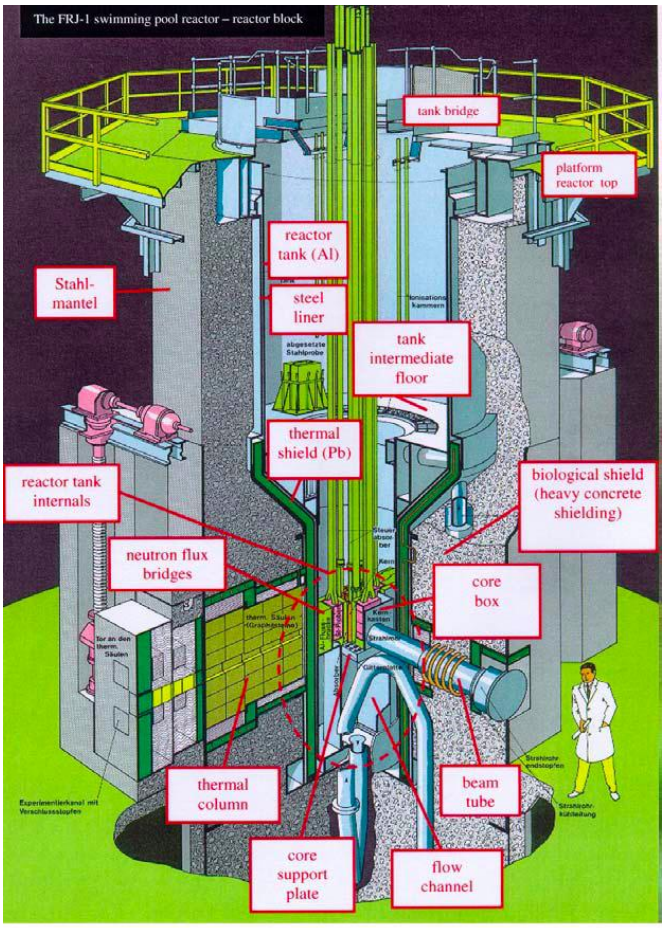

Figure 3.1.2: MERLIN Material Test Reactor (FRJ-1)

Ten individual graphite bricks were removed from the bottom right channel of thermal column II in the reactor block (see Figure 3.2 for structure). A sample was removed from each one of these graphite bricks: each specimen was analyzed by LSC in order to qualify and quantify the present radionuclides.[1] The samples were obtained by core drilling, leading to cylindrical-shaped specimens in the range of 0.6-1.5 g.

The results of the above-mentioned analyses showed the samples containing the following radionuclides: ^{3}H, ^{14}C, ^{60}Co, ^{133}Ba, ^{152}Eu, ^{154}Eu and ^{155}Eu. A quantification of the specific activity for the most important radioisotopes of interest revealed about 4700 Bq/g for ^{3}H, about 450 - 500 Bq/g for ^{14}C, and about 1000 Bq/g for ^{60}Co.

[1] Since LSC analyses need the preparation of a liquid clear solution, the measurement a priori is not possible. The complete analyses have been performed ex post by burning the sample in oxygen and by adding the released radionuclides´ activities to the one removed during the thermal treatment.

3.2 AVR (Arbeitsgemeinschaft VersuchsReaktor)

The AVR (Arbeitsgemeinschaft VersuchsReaktor) was the first experimental high temperature reactor of pebble bed type worldwide on industrial scale. Main aim of this experimental reactor was the test of the pebble bed core concept and the test of many different types of pebble shaped fuel elements. It started working in 1967 and its definitive shut-down dates back to 1988. The electrical power output was 15 MWe (46 MW_{th}). It was helium cooled and high-purity graphite was used both as moderator and reflector. In particular, the present paper deals with some investigations on the reflector graphite. The bottom, side and top reflectors as well as the so-called "reflector noses" consisted of polycrystalline graphite (needle-coke graphite, ARS/AMT grade made by SIGRI-Elektrographit [10]), chosen due to its chemical and physical properties and behaviour under fast neutron irradiation. The graphite reflector wall of 50 cm thickness [9] surrounded the reactor core containing the spherical fuel elements (see Fig. 3.2.1). The graphite brick reflector vessel is enclosed in a 50 cm envelope made of “baked carbon” bricks (“early stage graphite”, with larger amounts of impurities), which provides shielding and thermal insulation. Double wall steel liner surrounds all the ceramic structure. The bottom and top reflector consist also of graphite, surrounded by “baked carbon” bricks. A peculiarity of the here presented graphite is the method of manufacture: extrusion was implied, leading to highly anisotropic properties of the final product.

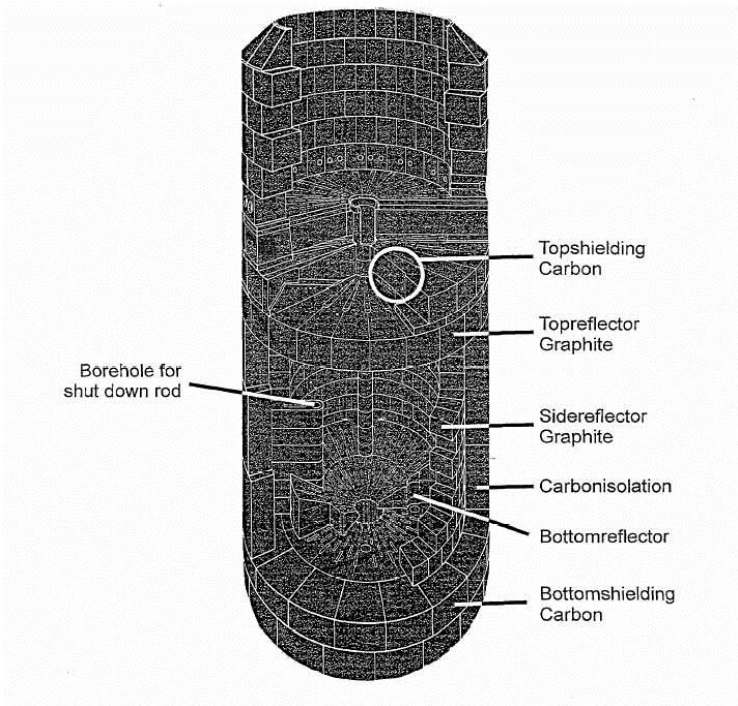

Figure 3.2.1: Internal structure of AVR’s core and heat exchanger chamber

3.2.1 AVR Reflector Graphite

The reactor graphite's total inventory of contaminants was determined by B. Bisplinghoff [11] with ICP-MS measurements. There is no other information available about the type and characteristics of the reactor graphite.

Nature of radionuclide contamination:

Radioactivity in graphite and carbon/slag results from the neutron capture reaction on carbon itself and on impurities like cobalt, iron, lithium, nitrogen, etc. In case of AVR impurity concentration in reflector graphite and insulation layers of carbon bricks are different (Table 3.2.1). The other contributions to the total inventory of radionuclides in the graphite must be considered. Besides the activation of carbon and of stable impurities in the graphite these are the fission of natural uranium present in the graphite as an impurity and the possibility of primarily surface contamination from the other regions of the reactor. Unfortunately, no virgin material was available from MERLIN graphite. It can be assumed that similar amounts of impurities will be present.

Element	Concentration, ppm		Activation product
	Isolation carbon	Reflector graphite	
Li	30	2	^{3}H
B	10	2	^{3}H
C	9.90E+05	1.00E+06	^{14}C
N	4500	30	^{14}C
Cl	15	0.2	^{36}Cl
K	1600	30	^{40}K
Ca	1500	100	^{41}Ca
Fe	7000	1000	^{55}Fe
Co	10	0.2	^{60}Co
Ni	40	10	^{63}Ni
Nb	2.5	0.05	^{94}Nb
Mo	10	2	^{93}Mo, ^{99}Tc
Cs	1	0.01	^{134}Cs
Ba	100	20	^{133}Ba
Sm	2	0.02	^{151}Sm, ^{155}Eu
Eu	0.1	0.02	^{152}Eu, ^{154}Eu

Table 3.2.1: Concentrations of impurities in AVR graphite

<u>Tritium</u>

The radionuclide ^{3}H, tritium has a half-life time of 12.3 years. The contribution of radioactivity in nuclear graphite arising from tritium is significant [12−14]. It will be produced by the following reactions:

- Fission reaction, such as $^{235}U(n,f)^{3}H$ reactions,

- $^{6}Li(n,\alpha)^{3}H$ reactions, lithium presents as an impurity in the graphite matrix of the fuel element and in the reflector,

- $^{3}He(n,p)^{3}H$ reactions of the ^{3}He isotope present in the helium coolant,

- $^{10}B(n,2\alpha)^{3}H$ reactions in the absorber rods (negligible for designs without core rods).

Main contribution to accumulation of tritium in graphite is given by neutron reactions with ^{6}Li and ^{3}He nuclei. Tritium generated from lithium impurities present in graphite is mostly produced in graphite bulk. The release of tritium is controlled by its diffusion out of the grain boundaries and into the pore system.

The chemical properties of tritium are essentially the same as those of ordinary hydrogen. One of the most important reactions is isotopic exchange where tritium can substitute hydrogen atom in water molecule or in organic molecule. The exchange process

$$HT + H_2O \Leftrightarrow HTO + H_2 \qquad \text{Eq. (1)}$$

is rather slow at room temperature (equilibrium constant K = 6 at 25°C) because the hydrogen is tightly bound.

Radiocarbon

Radionuclide ^{14}C has a half-life time of 5730 years. It is mainly produced in the reactor graphite through following neutron reactions:

Reaction	Capture cross section in barns ($10^{-24}cm^2$)	Abundance of isotope in %
^{13}C (n, γ) ^{14}C	$0.9 \cdot 10^{-3}$	1.1 ^{13}C/carbon
^{14}N (n, p) ^{14}C	1.81	99.63 ^{14}N/nitrogen
^{17}O (n, a) ^{14}C	0.235	0.04 ^{17}O/oxygen

Table 3.2.2: Activation reactions producing ^{14}C

In the reactor core materials nitrogen is present only as an impurity, whereas carbon and oxygen are in some cases major constituent elements of the coolant, moderator or fuel. In spite of this fact, the ^{14}N activation reaction is usually the most important contributor to ^{14}C production because of its larger cross section and high isotopic abundance of ^{14}N in natural nitrogen. Nitrogen in graphite is in bound state, substituting for carbon atoms in nodes of crystal lattice, or in gaseous form filling pores in graphite. The kinetic energy of formed ^{14}C atom is about 470 kJ/mol. This value is equivalent to the bond energy between C-C bound and C=C bond. It was suggested [15] that the formed ^{14}C atom stays in the same position as ^{14}N locates. Thus the level and location of nitrogen impurity in all reactor core materials is an important parameter. The nitrogen levels vary widely from 10 to 100 ppm in different reactor graphite sorts [16] and sometimes they are not known very precisely. It was shown that nitrogen content is the largest on the surface [15]. From surface to about 30 nm in depth, nitrogen concentration decreases.

Caesium

The three radioactive caesium isotopes ^{134}Cs, ^{135}Cs and ^{137}Cs are produced by nuclear fission and neutron capture reaction:

$$^{235}U \rightarrow {}^{137}Cs, {}^{135}Cs$$

$$^{235}U \rightarrow {}^{133}Cs(n,\gamma){}^{134}Cs$$

^{134}Cs can be also produced from the stable isotope impurity during reaction:

$$^{133}Cs(n,\gamma){}^{134}Cs$$

The half-life of Cs isotopes is two years for ^{134}Cs, $2 \cdot 10^6$ for ^{135}Cs and 30.1 for ^{137}Cs. The sources of radioactive Cs contamination are: uranium impurities in reactor graphite, uranium present in the circuit from fuel elements externally contaminated during manufacture, volatilisation of Cs from defective fuel due to its high vapour pressure. This Cs can be absorbed in graphite and form the interstitial compounds [17].

Europium

^{152}Eu, ^{154}Eu, ^{155}Eu are produced by fission reaction and their half-life amounts to 12.4 years, 8.5 years and 4.5 years. The isotopes can be also formed by activation of impurities ^{151}Eu, ^{153}Eu and ^{154}Sm.

Cobalt

Cobalt-60 originates from neutron activation of stable Co-59, which is present as an impurity in nuclear reactor graphite, and has a half-life 5.3 years.

Table 3.2.3 shows the calculated total radioactivity in AVR graphite in the end of 1988 [18].

Radionuclide	Total radioactivity, Bq	
	Reflector graphite	Isolation carbon
^{3}H	8.8E+14	6.9E+15
^{14}C	4.6E+12	2.9E+14
^{36}Cl	1.5E+09	5.9E+10
^{41}Ca	5.8E+10	4.5E+11
^{55}Fe	1.1E+15	4.0E+15
^{60}Co	4.2E+13	1.1E+15
^{63}Ni	4.1E+12	8.5E+12
^{93}Mo	2.5E+08	4.1E+08
^{99}Tc	2.8E+07	3.5E+07
^{134}Cs	8.9E+11	3.1E+13
^{133}Ba	3.5E+11	7.1E+11
^{151}Sm,	4.5E+08	1.8E+10
^{152}Eu	1.4E+07	2.9E+07
^{154}Eu	1.5E+11	3.0E+11
^{155}Eu	6.3E+10	2.5E+12
^{166m}Ho	2.2E+09	4.3E+10

Table 3.2.3: Total radioactivity in AVR graphite

3.2.2 AVR Virgin Samples: Origin and Preparation

In this work virgin materials, in particular AVR reflector graphite, have been selected to perform some investigations on the effects of thermal treatments and to prove the existence of many embedded chemical species. The reasons behind this choice have been various. In particular, even at the beginning of its life nuclear-grade graphite is unique under many aspects, because of the particular receipt used for its production, the raw materials and the manufacture process. After a temporary storage, the materials are used in the designated reactor: such time period could affect significantly the radionuclide production during the reactor operation. Normally, after the final product is ready, the manufacturer seals it in proper packages in order to avoid the contact with pollutants: as previously mentioned, the prolonged contact with air could lead to adsorption of many gases and humidity on the graphite surfaces and porous structure. A possible problem could arise during the building of the reactor, when the graphite positioning takes place under atmospheric conditions (air with moisture). It is probable that most of the materials used in the past were positioned without any precaution in that way.
Moreover, the study of virgin materials could help to understand the sources of different precursors (see Fig. 3.2.2), in order to avoid in future application such pre-contaminations and resulting, at the end of the reactor life, in a lower activity of the involved materials. Indeed, many factors are influencing the radionuclide production and migration: even by using the same material in different reactors or in different reactor zones, different amounts of contamination are expected. Neutron fluence, temperature and temperature excursions, gases present in the environment of operation are some of the determinant factors which will affect the inventory, contamination and the leaching behaviour under different conditions. From these considerations it follows that a full understanding of the entire contamination route results to be difficult by investigations only on the final radioactive product.

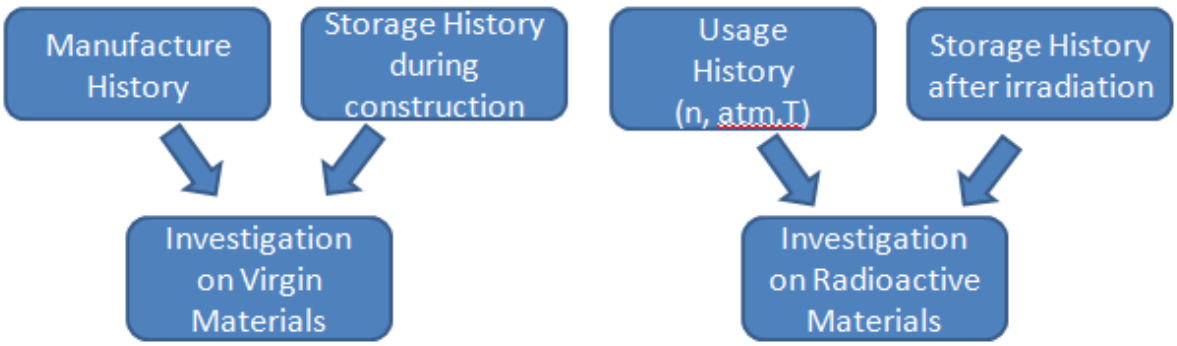

Figure 3.2.2: Scheme of different histories of a nuclear-grade graphite

Another advantage of using virgin materials stands on the lack of activity, so their handling and treatment will not be dangerous and will not request the safeguards measures necessary in controlled areas. Certainly the development of a purification treatment cannot be focused only on virgin materials, but its development could go through that and, probably, it could be even

accelerated. From this point of view, on the basis of the small samples (~ 1-3g) acquired in the past, the activity of a larger sample (200 g) of irradiated AVR graphite was estimated in the order of some GBq. In addition, there are no massive samples available, due to the fact that only a borehole has been drilled through the irradiated reflector regions. The access to larger samples of i-graphite is a general problem, as most graphite components reside in the cores, awaiting their future retrieval.

It is true that irradiated and virgin graphite show much different behaviour under some aspects, but it is believed that the driving physical-chemical mechanisms are the same: this is the main hypothesis of this work.
Other experiments performed in FZJ revealed some uncertainties and not fully understood results. In particular the high initial high release of radionuclides, during thermal treatment and under argon atmosphere, was not well explainable: it was hypothesized that many oxidants could be already embedded in the graphite matrix, resulting in the creation of oxide products that are affecting the release of some radionuclides (e.g. tritium and radiocarbon).

In Fig. 3.2.2 a schematic view of the different histories of nuclear-grade graphite is shown. By investigating virgin materials, the first two, i.e. manufacture history and storage during construction, can be better understood, together with their influence on the successive employment in the designated reactor.

Virgin samples were found in a container next to the AVR building. For the investigations on virgin materials, AVR graphite (ARS-AMT grade[2]) has been considered, whereas the unknown-grade graphite has been used to check the proper running of the induction oven.
The cutting technique used to produce the samples consisted of using CNC machines to produce a dry cut, in the way to contaminate as less as possible the samples surfaces (e.g. with water). On the other side it is impossible to have a perfect cut without changing the superficial structure: the cutting itself consisted on a sort of superficial pre-treatment, developing high local temperature and generating consistent amounts of carbon powder; the only way to avoid this artefact would be to cut the big block (see Fig. 3.2.3) keeping untouched one external surface: for what concerns the samples here presented this was not done, but it could be a future task to prove to which extent the sample preparation is affecting the results. Some SEM analyses confirmed this fact (see deliv. 3.3.2). Despite the not-ideal cutting technique, the bulk material is believed to be pristine; from this point of view, massive samples would be affected the less by the preparation than small ones: for this reason, and many others[3], different samples of different size were prepared (Figs. 3.2.4, 3.2.5).

[2] ARS/AMT grade graphite from Sigri Elektrographit, used in the AVR as reflector and structural material
[3] The TGA is able to operate with cylindrical samples up to few grams, as well as the small facility installed in FZJ. The Carbolite Oven and the Induction Oven, installed at FZJ, are able to work with larger massive samples, up to some hundreds of grams.

Figure 3.2.3: Coarse virgin material before being cut in smaller samples.
Left: Unknown grade graphite, Right: AVR reflector virgin graphite

Figure 3.2.4: Massive virgin samples of AVR reflector graphite, H50Ø50 mm

Figure 3.2.5: Small sample used both in the TGA, in the small electric oven and in the Carbolite Oven, H20Ø8 mm

3.3 Saint-Laurent A2

3.3.1 General considerations about UNGG reactors

EDF (Electricite De France) operated in France six gas-cooled reactors, all shutdown now for at least fifteen years. These reactors are of so-called in French, "UNGG" reactor type (Uranium Naturel Graphite Gaz). They were graphite moderated, cooled by carbon dioxide and fuelled with natural metallic uranium.
The design of UNGG reactors is, in its general principle, very close to that of the British Magnox reactors, which was developed independently at the same period in United Kingdom. In the absence of uranium enrichment, graphite was used as a moderating material with a very high level of purity due to the necessity of the highest transparency to neutrons. Graphite has been also chosen as a mechanical support of the fuel cartridges (graphite sleeves) and as a biological shield in some reactors. A scheme of the main possible uses of graphite in UNGG reactors is shown in figure 3.3.1. The irradiated graphite from the pile or from the biological shield still lies in the reactors. The graphite sleeves that are not already shipped to the final repository are stored in silos.

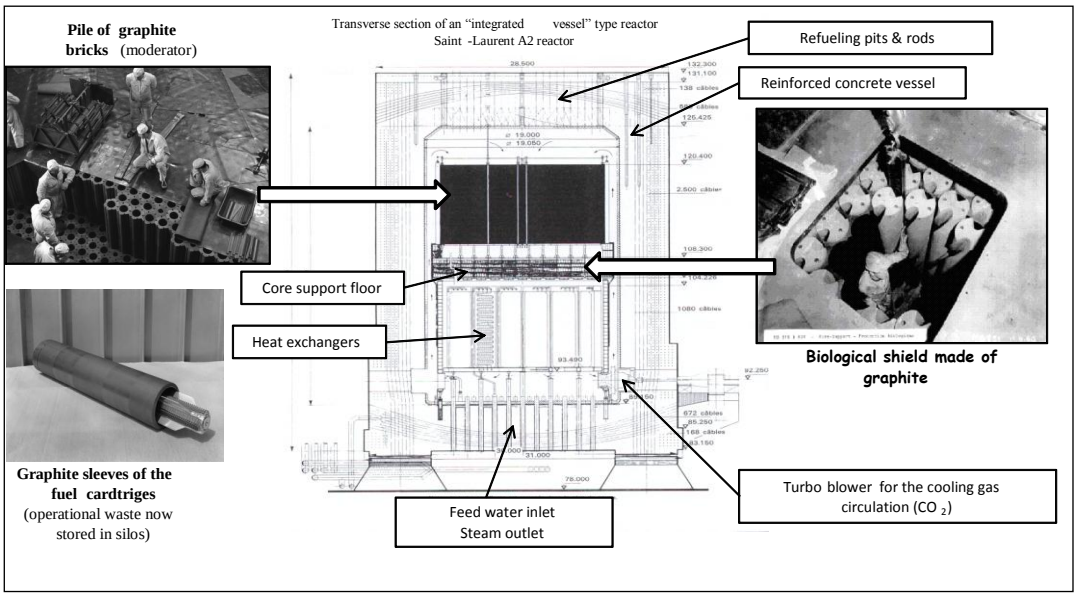

Figure 3.3.1: Uses of graphite in EDF UNGG reactors; different designs were developed, in this scheme an "integrated vessel" type reactor is presented (approximate external dimensions: 50 m height / 28.5 m diameter)

3.3.2 Saint-Laurent A2: reactor history

The Saint-Laurent A2 (SLA2) reactor was commissioned in August 1971. The pressure vessel of this reactor is built of prestressed concrete which also acts as biological shielding. The coolant is CO_2 which circulates from top to bottom at a pressure of 29 bar in the space between the graphite and the Mg-Zr alloy fuel cladding. The operating temperature ranges between 240°C (top) and 470°C (bottom). The thermal power is 1,700 MW. The gross electrical power is 530 MWe and the net electrical power in nominal operation is 515 MWe. The thermal neutron flux (from 10^{-5} eV to 0.5 eV) in the central zone of the core and in the maximum flux plane is 3.12 10^{13} $n.cm^{-2}.s^{-1}$.

It should also be noted that this reactor was shut down between March 1980 and September 1982 following an incident which led to the melting of two fuel elements at the bottom of the F5 M19 C14 channel (loss of cooling of the channel as a result of its obstruction by a metal plate, leading to overheating of the fuel elements).
The SLA2 reactor was finally shutdown on May 25, 1992. It was operated during 11 years full equivalent operating power. It has been defuelled and has been placed in a safe enclosure mode (ventilated by air with a moisture content limited to 50 %) until the final dismantling is performed.
EDF received the authorization to fully dismantle the SLA2 reactor by decree 2012-510 of May 18, 2010. All non-nuclear parts of SLA2 nuclear unit have been dismantled (dismantling IAEA level II achieved - figure 3.3.2). Up to now, final dismantling (level III) is planned by 2030-2040.

Figure 3.3.2: Saint-Laurent A1 (left) and Saint-Laurent A2 (right) UNGG reactors (current state 2012)

3.3.3 Graphite stack description

The graphite stack of the SLA2 reactor has the form of a cylinder with a vertical axis 15.73 metres in diameter (13.43 metres of moderator surrounded by a 1.15 m thick reflector) and 10.2 metres high. The total mass of graphite is 2,440 tons including 1,580 tons of moderator and 860 tons of reflector (figure 3.3.3).
The stack's network of graphite bricks is a hexagonal mesh with a pitch of 225.16 mm. The elementary graphite blocks are prismatic bars with a hexagonal base whose distance between two opposite faces is equivalent to the network mesh. The side-by-side juxtaposition of 4,429 bars forms a bed, the SLA2 stack consisting of 8 superimposed beds (bed No. 1 is that at the bottom of the stack). Thus, the bars are superimposed and the stack may also be regarded as the juxtaposition of 4,429 columns. The graphite stack comprises:

- The lateral reflector consisting only of 828 solid columns surrounding the core;
- The moderator (or core) consisting of 3,601 columns: 345 solid columns, 181 bored to 84 mm for the control rods and 3,075 columns bored to 140 mm (basically for the fuel elements).

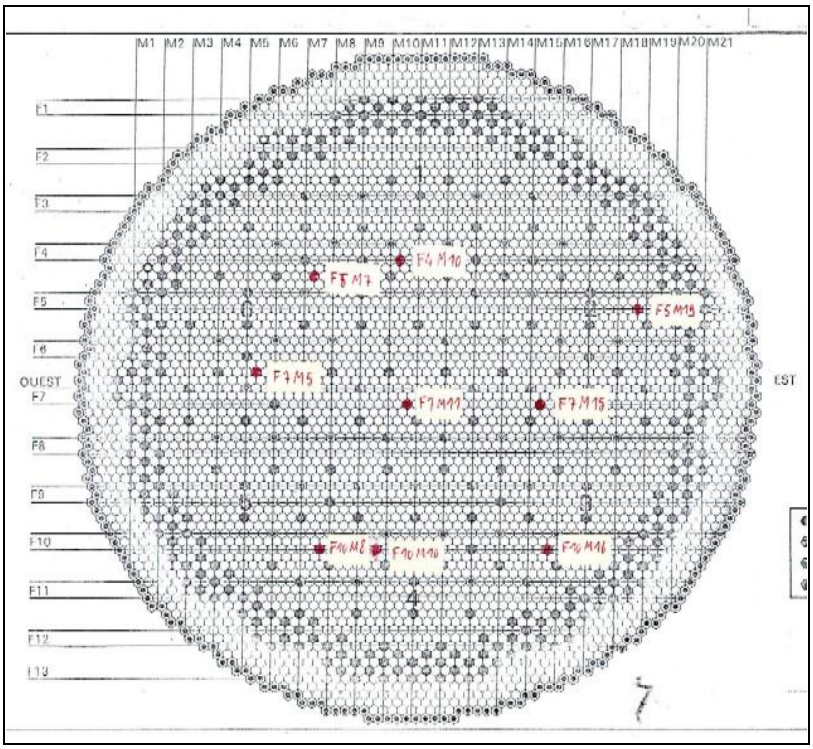

Figure 3.3.3: Section through the graphite stack of the Saint-Laurent A2 reactor - Juelich graphite cores were sampled from the F4M10 (hexagonal cell) C19 (fuel channel).

3.3.4 SLA2 Graphite

The graphite of SLA2 stack was manufactured by the Pechiney/SERS company between May 1966 and November 1967. This graphite was made from Lima coke, underwent one impregnation and was purified using MgF2. During its manufacture it was tested particularly with regard to effective cross-sections, density measurements and other properties described in the table 3.3.1.

Ashes (ppm)	B (ppm)	Li (ppm)	Co (ppm)	Cl (ppm)	Thermal neutron absorption cross section (mbarn)	density
98	0.11	0.07	0.05	-	3.76	1.68

Table 3.3.1: Some impurities and characteristic values of SLA graphite

^{3}H	^{10}Be	^{14}C	^{36}Cl	^{41}Ca	^{60}Co	^{63}Ni	^{137}Cs
$8.9\ 10^{4}$	19.1	$7.7\ 10^{4}$	37.9	83.7	$4.0\ 10^{3}$	$3.5\ 10^{4}$	47.0

Table 3.3.2: Estimated radionuclide inventory of SLA2 graphite (Bq/g)

Concerning radionuclide inventory of the irradiated SLA2 graphite from the pile, it has been determined as described in Carbowaste report T-3.4.3 and corresponds to the values reported in table 3.3.2, for the main radionuclide of interest: these values are in Bq / g and related to January 2017. They take no account of the influence of leaching phenomena of the underwater

dismantling process. They are over-estimated mean values as described in Carbowaste report T-3.4.3.
The radionuclide inventory for Caesium 137, a trace element for the fission reactions, shows that the decontamination operations adopted following the fuel element melting have been effective. In fact, this incident has no detectable effects in terms of contamination of the graphite. The levels of Caesium 137 are equivalent in all the EDF reactors whether fusion of fuel elements has occurred or not. The presence of Caesium 137 in very low quantities and the heavy nuclei produced are explained by the fission of traces of uranium present in the original graphite. These traces were identified in the analyses performed on the graphite at the time of their manufacture and now evidenced by the identification calculation-measurement method used for the radionuclide inventory assessment.

3.3.5 Core sampling

The SLA2 reactor stack was subjected to core drilling in 2005 during which 180 cores were extracted. Remote controlled tools introduced into the fuel channels of the stack were used. This technique is the same to the technique implemented for monitoring the wear of the graphite during operation. The remote-control tool (figure 3.3.4) was introduced from accesses through the refuelling pits at the top of the reactor into the channels, and performed coring on either side of the graphite bricks (figure 3.3.5) in the direction perpendicular to the channels with a diameter of about 20 mm.

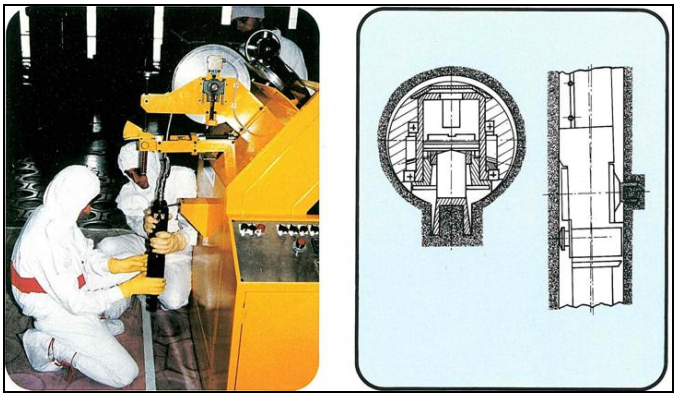

Figure 3.3.4: Remote controlled tool used for graphite stack sampling in UNGG reactors

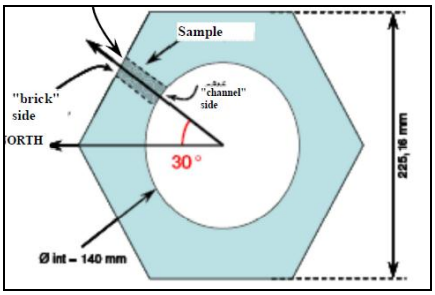

Figure 3.3.5: Schematic view of coring in a graphite brick

Five Samples were received by Forschungszentrum of Juelich coming from F4M10 cell C19 channel. They were chosen as being distributed over the height of the fuel channel in order to correspond to the operating temperature range in SLA2 reactor, as shown in table 3.3.3.

Adress	Height	Temperature °C	dose rate µSv/h	Mass sample (g)
F4M10C19	1680	443	185	17,5
F4M10C19	2460	446	193	22
F4M10C19	5120	391	462	20,5
F4M10C19	7880	294	107	20,5
F4M10C19	9260	258	9	23

Table 3.3.3: Position, temperature and dose rate of the samples delivered to FZJ.

3.4 Oldbury 2

3.4.1 The reactor

The Oldbury nuclear power station consists of two Magnox class reactors; reactor 1 was connected to the electricity grid on 07/11/67 and reactor 2 on 06/04/67. Reactor 1 was shut down on 29/02/12 and reactor 2 on 30/06/11 [3]. The Oldbury reactors were the first nuclear power station in the UK to have a pressure vessel made from pre-stressed concrete instead of steel. Reactor 2 had a gas outlet temperature of 365 °C and produced an average power output of 434MW during its lifetime, a reduction from the original design specification of 600MW. Reactor 2 produced 893 thermal power MW(t), the graphite was manufactured from pile grade A (PGA) graphite, weighing 2061 tonnes with a reactor graphite total of 2090 tonnes (including reflector and shield graphite).

3.4.2 Oldbury 2 samples: Origin and preparation

Samples provided for CARBOWASTE research where supplied by NNL. The present information is what has been made available to the author. The samples were taken from an installed set, these were located in pot 634, position 4, which was placed in Channel S77 (BNL Channel 3) of Oldbury Reactor 2 from commissioning to June 2005. The Mean Core Irradiation of these installed sets is 30658 MWd/t. Dosimetry calculations have not been specifically carrier out for these samples. However, a suitable reference sample from Oldbury Reactor 1 trepanned in 2004 has had full dosimetry calculations performed. On this basis the information reported in table 3.4.1 have been provided [3].

Irradiation Conditions	
Irradiation temp	543 K
Adjacent fuel dose	52827 MWd/t
DIDO equivalent dose	40.27×10^{20} n/cm^2
Calder equivalent temperature	543 K
DIDO equivalent temperature	597 K
DPA	5.28

Table 3.4.1: Irradiation conditions of Oldbury 2 graphite provided by NNL

3.4.3 Sample Preparation for small scale thermal treatment facility

From the above mentioned description of samples, several samples with different shapes and different histories arrived at FZJ. The equipment needs special shape for obtaining good results. For what concerns thermal treatment equipment in FZJ, cylinders with a diameter of 8 mm were drilled from the received samples in glove boxes. Sample preparation of radioactive material was a great challenge. The material from Saint-Laurent differs in hardness from the Oldbury 2 material. The Oldbury 2 material was easy to drill, the Saint-Laurent material caused problems. Drilling tools got hot and broke, so it was decided to use new suitable drilling tools in collaboration with the drilling tool manufacturer.

Hardness measurements could be suitable for future experiments to make correlations about hardness and release. At the present state, in FZJ, there is no measurement equipment available in a controlled area. Figures 3.4.1 to 3.4.5 show respectively the received samples of Saint-Laurent A2 graphite and Oldbury 2 graphite, the glove box for sample preparation used in a laboratory fume hood and the drilled Saint-Laurent A2 samples.

Figure 3.4.1: Saint-Laurent 2 sample

Figure 3.4.2: Oldbury 2 sample

Figure 3.4.3: Oldbury 2 sample

Figure 3.4.4: Glove box with tools for sample preparation

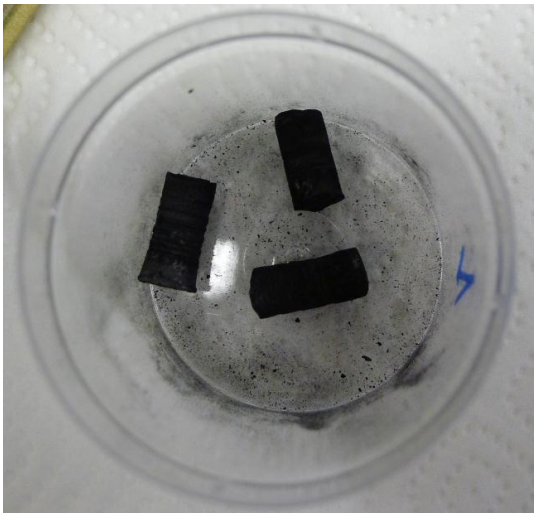

Figure 3.4.5: Drilled Saint-Laurent 2 samples

4. Description of Experimental Facilities

4.1 Small Scale Facility at FZJ

4.1.1 Equipment

The following technical equipment was used:

Main Furnace:	combustion furnace C-5500 from Ströhlein Instruments, tube furnace adjustable up to 1550°C
Furnace for catalyst reaction:	Ströhlein Instruments, tube furnace run at 550°C with copper oxide catalyst
Balance:	MP-3000, YMC Europe GmbH
CO, CO_2 analyser:	NGA 2000 MLT analyser from Fisher-Rosemount, concentration range 0-4000 ppm
Peltier-cooling unit:	Bühler Technologies GmbH, gas drying was needed for analysis with CO, CO_2 analyser
Flow controller:	mass flow controller 5850E from Brooks, range: 0-70 L/h to 0-200 L/h
Liquid scintillation counter:	TRICARB 2700 from Packard
γ-spectrometer:	High-Purity Germanium Well Detector from EG&G Ortec
Water purification:	Elga Elgastat maxima HPLC, specific resistance of purified water is 18.2 mΩ
Washing bottles:	Special glass equipment manufactured by ZAT, Research Center Jülich

4.1.2 Reagents and investigated materials

The following chemicals were used:

NaOH, CuO, HCl, HNO_3

All chemicals were from MERCK, Darmstadt, and of analytical grade. They were used without preliminary treatment.

Investigated materials:

Merlin reactor graphite:	bottom right channel of thermal column II
AVR graphite:	inner reflector

Gases:

Argon:	purity >99.999%, MESSER Griesheim
Oxygen:	purity >99.5%, LINDE

Calibration gas: mixture: CO - 1880 ppm, CO_2 - 2180 ppm, O_2 - 0.516 vol%, H_2 - 4 vol%, N_2 - rest; MESSER Griesheim

4.1.3 Performance of experiments

A scheme of the installation for graphite treatment is shown in Figure 4.1.3.2. It consisted of a gas bottle, a flow controller, a tube furnace with quartz reaction tube (T. Podruzhina) or with a ceramic reaction tube (M. Florjan), 5 washing bottles and a CO-CO_2 IR detector. M. Florjan replaced the quartz tube in the furnace with a ceramic one in order to reach higher reaction temperatures. Before the experiment started, the graphite sample was placed in a ceramic boat and weighed. Then, the ceramic boat was inserted into the preheated furnace tube and heated up to the foreseen temperature. The experimental details of the samples used by T. Podruzhina are listed in Table 4.1.1; the details of the ones used by M. Florjan are listed in Table 4.1.2. This work is continued by the PhD thesis of K. Baginski to optimise the treatment parameters.

Sample	Mass, g	T, °C	Time, hours	Flow rate, L/min
Merlin graphite bulk sample	1.3644	866	18	0.12
Merlin graphite powder	0.4023	969	9	0.12
Merlin graphite powder	0.15	1050	15	0.175
Merlin graphite bulk sample	0.9116	1063	13.5	0.12
AVR graphite	0.213	1057	15	0.08

Table 4.1.1: Radioactive graphite treatment in argon atmosphere (T. Podruzhina)

Sample	Mass, g	T, °C	Time, hours	Flow rate, L/min
Merlin graphite bulk sample	3.925	1280	7	0.24
Merlin graphite powder	0.564	900	7	0.24
Merlin graphite powder	0.787	1280	7	0.24
AVR graphite (reflector)	0.338	900	7	0.24
AVR graphite (reflector)	0.316	1280	7	0.24
AVR graph., pebble spalling	0.308	900	7	0.24
AVR graph., pebble spalling	0.367	1280	15	0.24

Table 4.1.2: Radioactive graphite treatment in nitrogen atmosphere (M. Florjan)

Nitrogen or argon gas was flushed through the system. Volatile radionuclides were caught in washing bottles. The first washing bottle was filled with 40 ml 0.1 mol/l nitric acid. Tritium as HTO was absorbed in this bottle. After first washing bottle the concentration of CO and CO_2 in gas flow was detected by CO-CO_2 analyser. Then carrier gas passed through reactor tube with CuO at temperature 550°C in order to oxidise tritium, also presenting as tritiated molecular hydrogen in the gas mixture, and carbon monoxide to H_2O and CO_2 correspondingly. Oxidised molecular hydrogen was absorbed in the second and third bottles with 0.1 mol/L nitric acid. $^{14}CO_2$ passed the first three bottles and was absorbed in the fourth and fifth washing bottles,

which are filled with 40 mL 4 mol/L NaOH. The third and fifth bottles were set to control that all tritium and ^{14}C had been absorbed in the previous washing bottles.

The determination of mass loss of the sample during the time was detected by IR spectrometer from CO and CO_2 concentration in flow. Before every run the detector was calibrated with a calibration gas with known concentration of CO and CO_2.

After the oven has been heated up to the defined temperature, samples of the solutions of the washing bottles, every sample taking time 3 mL, have been taken from washing bottles in certain time intervals.

When the experiment was finished, the solutions in the washing bottles were replaced by fresh solutions and graphite was burnt completely in oxygen atmosphere in the same equipment. Then the content of washing bottles was analysed in order to determine the total amount of tritium and ^{14}C in the graphite sample after treatment.

After complete combustion the ceramic boat was put in a beaker with 30 mL of hot concentrated HCl, heated for 2 hours and left for 24 hours. The liquid was evaporated up to dry residue and dissolved in 5 ml of 2 M HNO_3.

In order to determine the radionuclide transport during treatment procedure reactor tube was divided into several sectors (Figure 4.1.1, sectors 1-4) and washed out step by step with concentrated HCl plus 1 mL of HF.

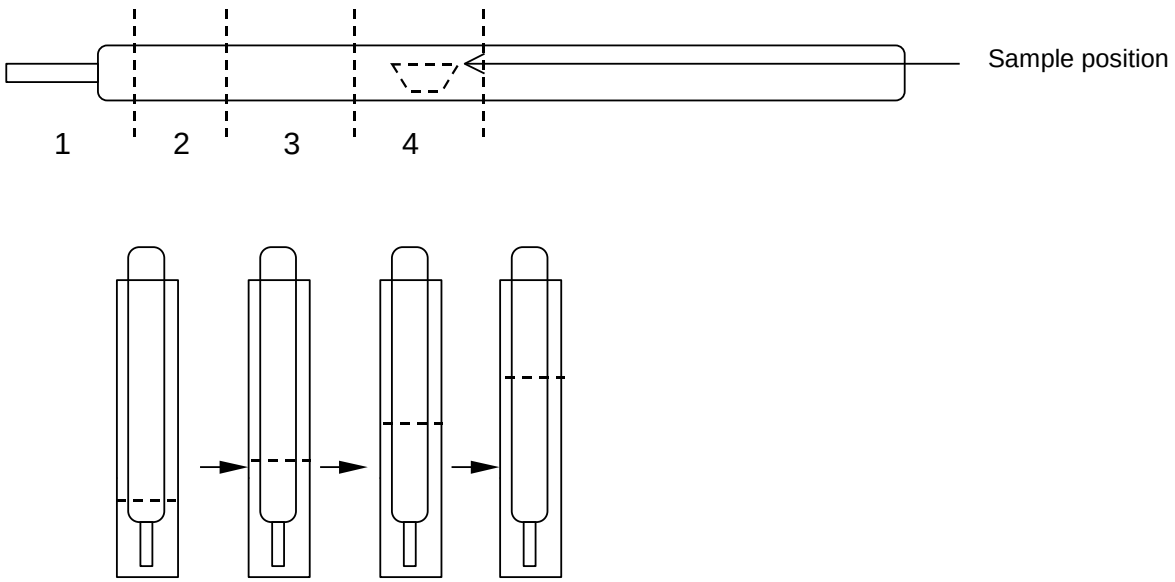

Figure 4.1.1: Washing procedure of reactor tube

Then the washing liquid was evaporated up to dry residue and recovered with 5 mL of 2 M HNO_3 (the same procedure as with boat). Also after the washing procedure the reactor tube and the ceramic boat were analysed by γ spectrometry in order to ensure that all radioactivity was removed.

Determination of ^{3}H

Tritium was retained in three first bottles with 0.1 M HNO_3 solution. In the experiments with Merlin graphite an aliquot of 2 mL was mixed with 18 mL Instant Scint-Gel Plus™ and

measured directly by LSC. In the experiments with AVR graphite an aliquot 100 µL was taken from bottles with HNO_3 mixed with 1.9 mL distilled water and 18 mL of Instant Scint-Gel Plus™.

Determination of ^{14}C

An aliquot of 1 mL of solution from fourth and fifth washing bottles was taken, mixed with 1 mL disstilled water and 18 mL of HIONIC FLUOR™ and directly measured with LSC.

Determination of total β,γ-activity

An aliquot of 100 µL from the dissolved residue was diluted with 1.9 mL H_2O and mixed with 18 mL of Instant Scint-Gel Plus™ and then directly measured by LSC.

Determination of γ-activity

An aliquot of 0.5 mL from the solution of dissolved residue was taken, diluted with 9.5 mL of H_2O in plastic 10 mL bottle and measured with γ-spectrometry.

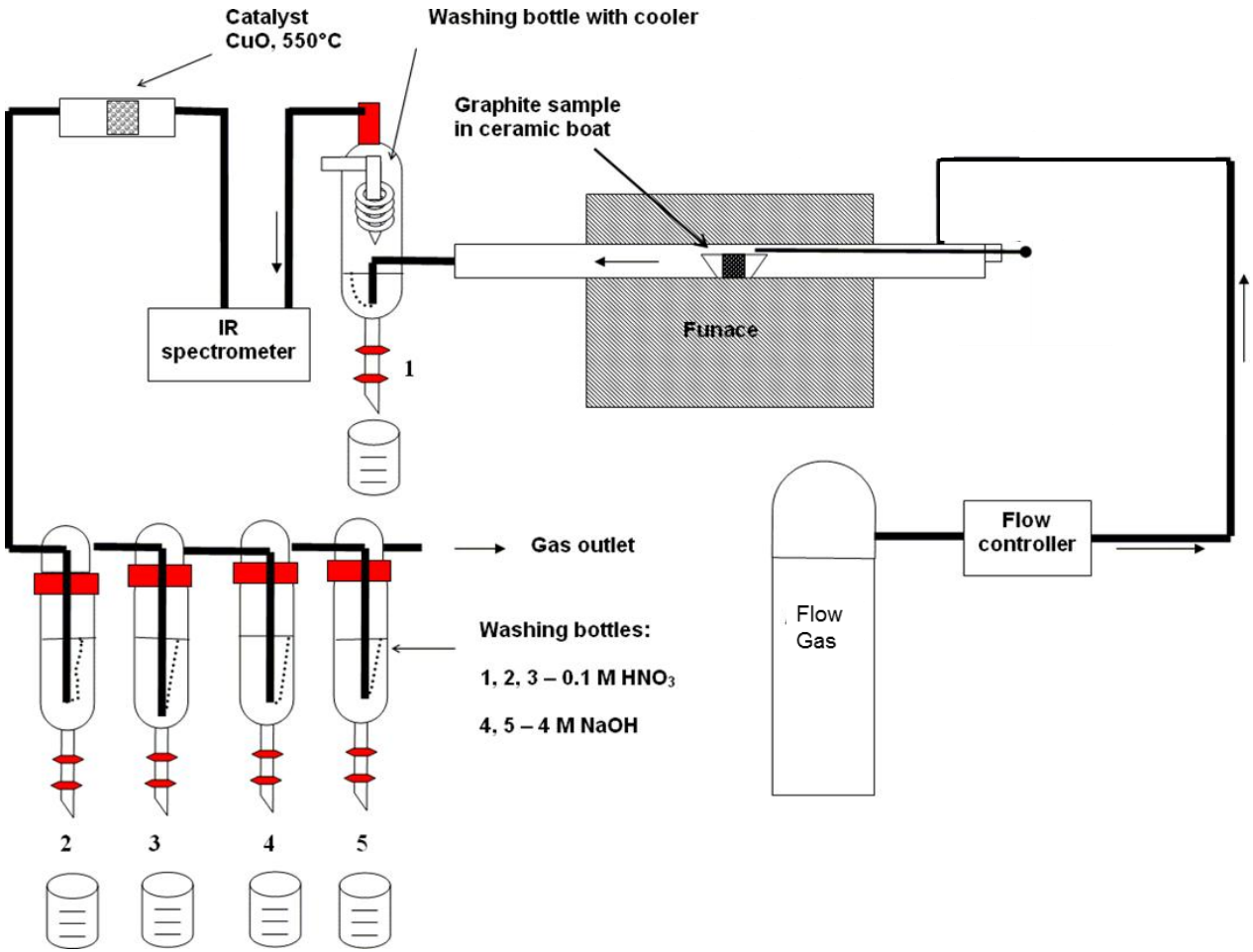

Figure 4.1.2: Installation for graphite thermal treatment with inert gas (T. Podruzhina, M. Florjan)

4.1.4 On-going experiments and changes of the facility

Comparing the results of M. Florjan and T.Podruzhina some unsolved questions occur. The given sample mass loss by M. Florjan is very low in comparison with sample mass loss of T. Podruzhina. Mass loss was only calculated from integral calculus of the CO and CO_2 curves from the off-gas written by software of the infrared measurement apparatus. After thermal treatment, samples were incinerated directly for determining the rest content of tritium and ^{14}C. With further experiments, it is necessary to check the repeatability of M. Florjan's results and how to reach even more release with variations of time and temperature and to have a closer look to the measurement conditions, especially to sample mass loss.

Another question concerns the release of tritium and ^{14}C. Will tritium be released as tritium gas (HT) or tritiated water (HTO) and ^{14}C be released as ^{14}CO or $^{14}CO_2$? In order to solve this question, the copper oxide catalyst was connected between two bottles of nitric acid as well as two bottles of sodium hydroxide solution for trapping HTO and $^{14}CO_2$ and two bottles of nitric acid as well as two bottles of sodium hydroxide solution for trapping HT and ^{14}CO. So there is now an installation for thermal treatment with a total of eight washing bottles. Figure 4.1.3 shows a drawing of the new installation for thermal treatment. Figure 4.1.4 shows a photo of the new installation for thermal treatment. But here is still the question to solve how soluble is hydrogen or HT in water and if there is an isotopic exchange between water and HT in the first two bottles of the equipment for thermal treatment and in what amount occurs this exchange.

It should be noted that the sequence of washing bottles increases the pressure in the reaction tube because the height of all liquid columns within the washing bottles needs to be compensated for pressing the carrier gas through the whole arrangement. Thus, the pressure needs to be determined to calculate the pressure dependency of the related reactions.

Regarding samples after thermal treatment it is visible that the surface of the sample lying at bottom of the sample holder seems untreated. Therefore, flow patterns were calculated (figs. 4.1.5-6) and with the help of flow patterns a new sample holder was developed (Fig. 4.1.7), in substitution of the conventional one (Fig. 4.1.8).

Because the facility was complex and the ingress of air was not complete excluded also not by flushing with nitrogen overnight and heating at a closed and flushed system the last step was the comparison of tests in the small scale facility performed with a quartz tube as oven tube and tests performed in the ceramic tube. With quartz tube, tests could only run up to 1100 °C for about 20 hours because the softening temperature of glass is around this temperature and heating more than this temperature for a long time would cause damages to the test tube. So quartz tube tests were carried out with as low air content as possible, flushing with nitrogen overnight. Tests with a ceramic tube as testing tube could be heated up to 1300 °C or even 1450 °C, the ceramic tube was fixed with two clamps of metal for opening and closing the test tube quick, so that samples could be inserted in the testing tube when the test temperature was already reached. The disadvantage was that the inserting of samples brought amounts of oxygen from the environment into the test region which could not be determined with the flow gas detection because the flow gas detection system depends on a stable pressure. So at ceramic tests at test beginning surface corrosion with remaining, but not quantitative determined oxygen was the first reaction.

At this state of art all tests are running with flexible rubber tube connections because they are easy to fix and to change. But there is still diffusion of oxygen and hydrogen through this tubes

and a change in purity would be to construct the connections of the equipment of stainless steel tubes. Discussions with companies to construct a stainless steel connection system are on-going and planned for next tests. The remaining oxygen concentration can be measured in a region of 4000 ppm and below, but a higher concentration will destroy this sensor. So purity of "inert state" has to be considered for an accurate determination of low oxygen content.

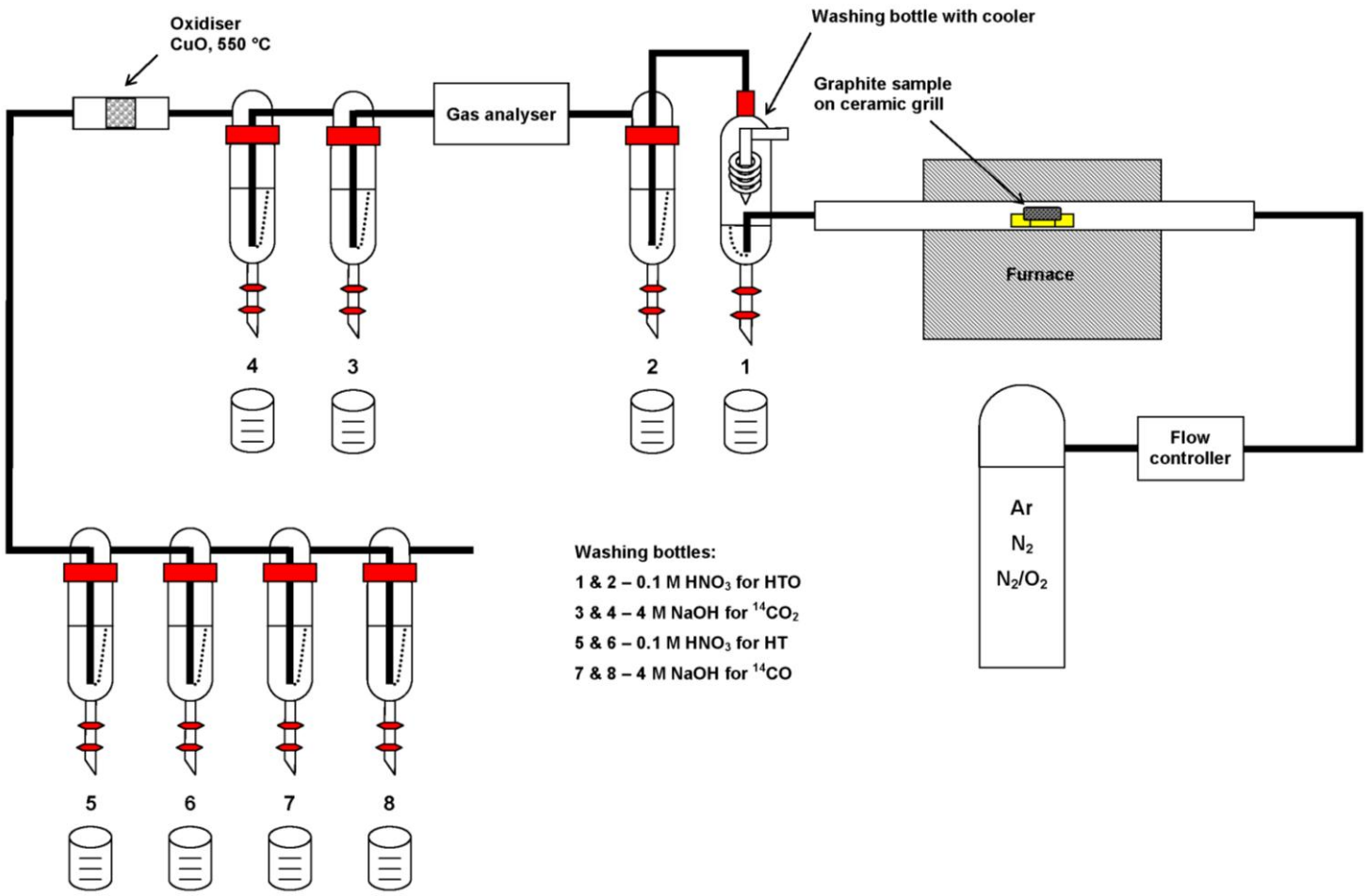

Figure 4.1.3: New installation for graphite thermal treatment with given washing solutions in each bottle (K. Baginski)

Figure 4.1.4: Photo of the new installation for graphite thermal treatment (K. Baginski)

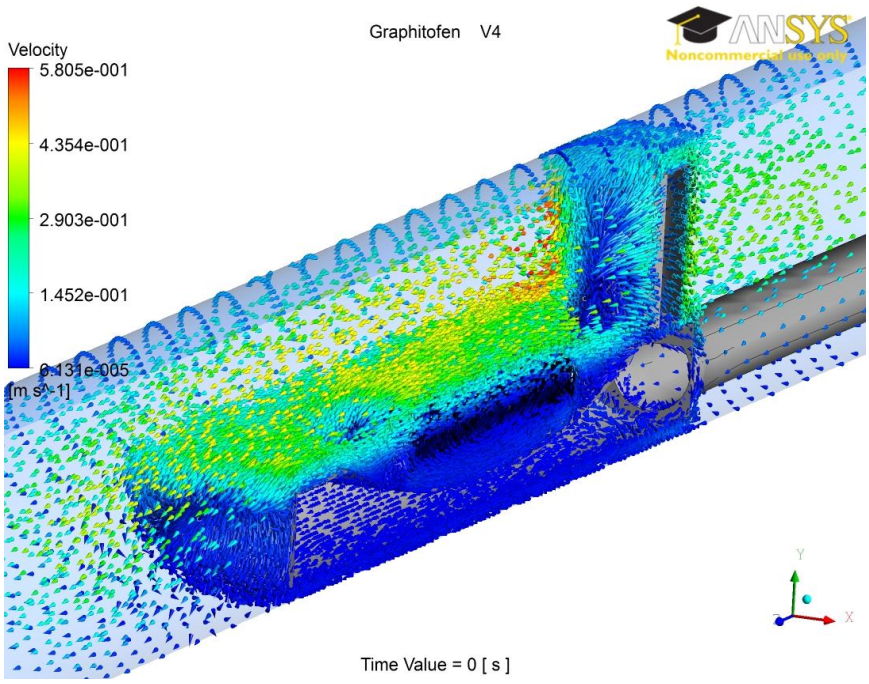

Figure 4.1.5: Flow pattern of velocity of flow gas, vector modus (nitrogen, 1.42 L/min)

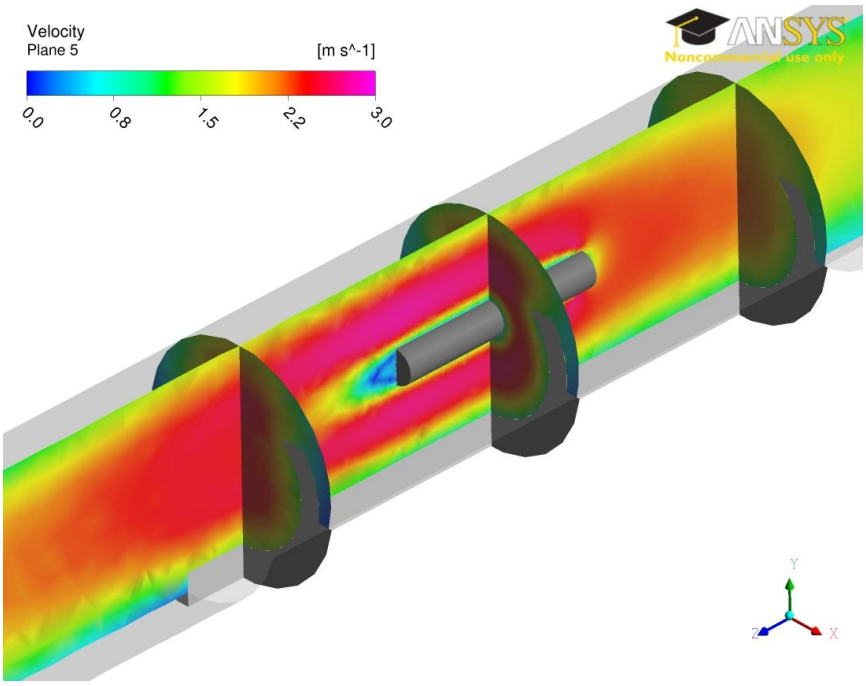

Figure 4.1.6: Flow pattern of velocity of flow gas, sample position with new sample holder (nitrogen, 1.42 L/min)

Figure 4.1.7: New sample holder with a virgin untreated graphite sample for the apparatus of graphite thermal treatment

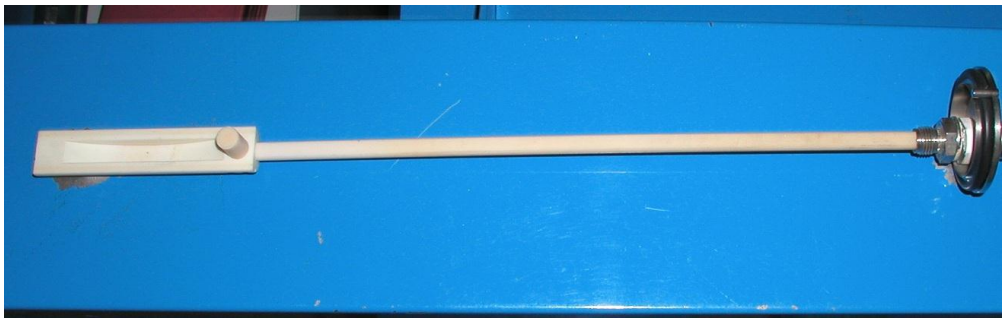

Figure 4.1.8: Conventional sample holder for graphite thermal treatment.

4.2 Induction Furnace Facility at FZJ

4.2.1 Equipment

The Induction oven facility is formed by the following main components:
- Middle frequency generator
- Power supply and Control Unit
- Cooling Unit
- Induction Oven
- Pyrometer

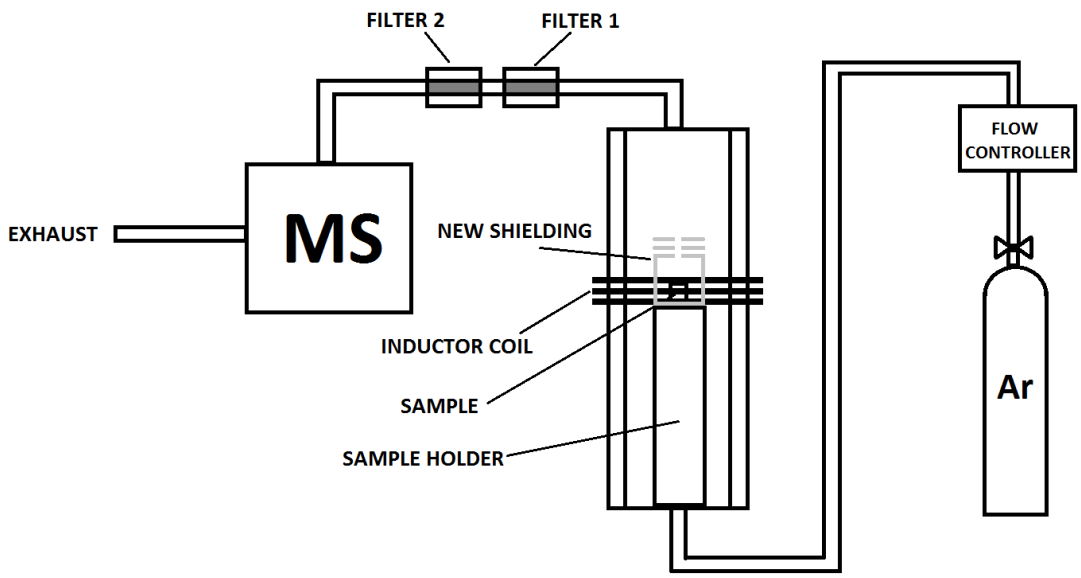

Figure 4.2.1: Overview of the experimental set up with the induction oven

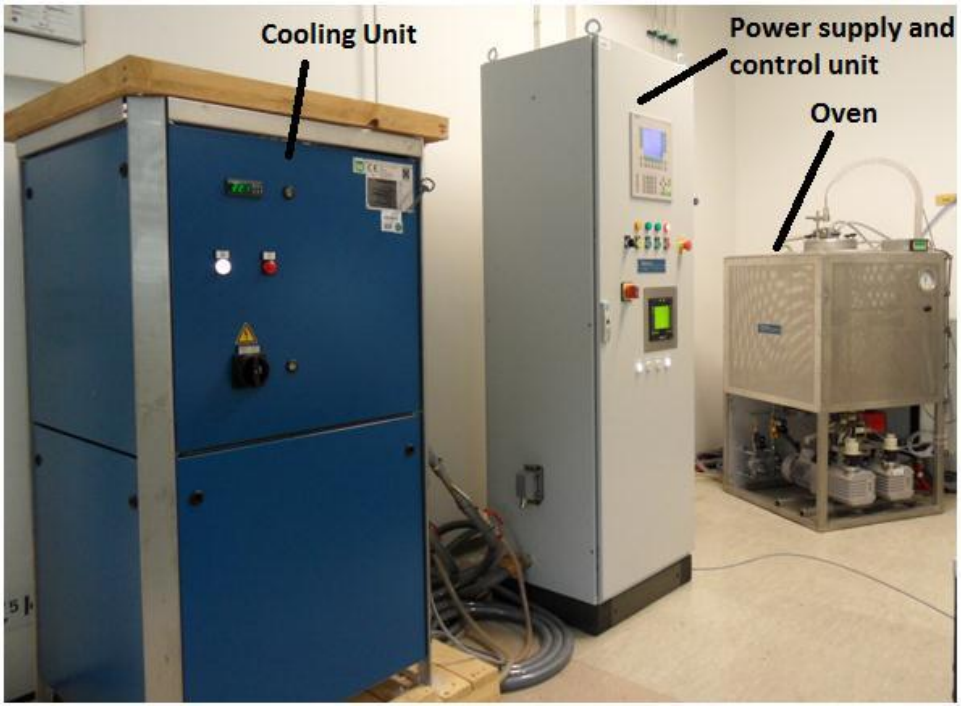

Figure 4.2.2: Overview of the Induction Oven Facility

Working principle of Inductive Heating

The working principle is based on induction heating: an electrically conducting sample is heated by electromagnetic induction because of eddy currents (or Foucault currents) generated within the material; due to the electrical resistance, Joule heating takes place. In the induction heater an electromagnet is placed, in which a middle-frequency current (AC) is imposed. The working method is aswith an electrical transformer: the sample behaves like a short-circuited secondary loop (leading to high currents), whereas the coil connected to the AC power supply represents the primary circuit. Generally speaking, the AC frequency used depends on the object size, material type, coupling (i.e. energy transfer between the work coil and the object to be heated) and the penetration depth.

Middle frequency generator

The 3-phase main supply goes first through a 3-phase rectifier inside the "Power supply and control unit", and it is transformed to DC voltage of about 580V. Then capacitors are used to filter the current. The converter transistors transform DC into middle frequency AC. The current is led over connecting capacitors to the primary side of the output transformer, placed at the oven side. The secondary transformer is connected in series with 2 capacitors (the tank capacitors amount to 17 µF total) and the induction coil.

The oscillator exciting is realized through the control electronics. The control pulses for the converter are frequency modulated and because of this the output power is regulated through changing the oscillating frequency.

Rectifier, capacitors, transformer, transistors, inductor coil are water cooled and protected with water flow switch and thermo switch.
The inductor coil, connected at the converter, can work with the tank capacitance in the frequency range from 10 to 30 kHz.

Control unit

A Siemens control system is installed on the "Power supply and control unit". Because of the complexes operations it was preferred to install a secondary control unit, directly connected to the Siemens' one, for the normal operations concerning heat treatments.In the same cabinet the power supply and all the safety tools to prevent overloads and overheating are placed.

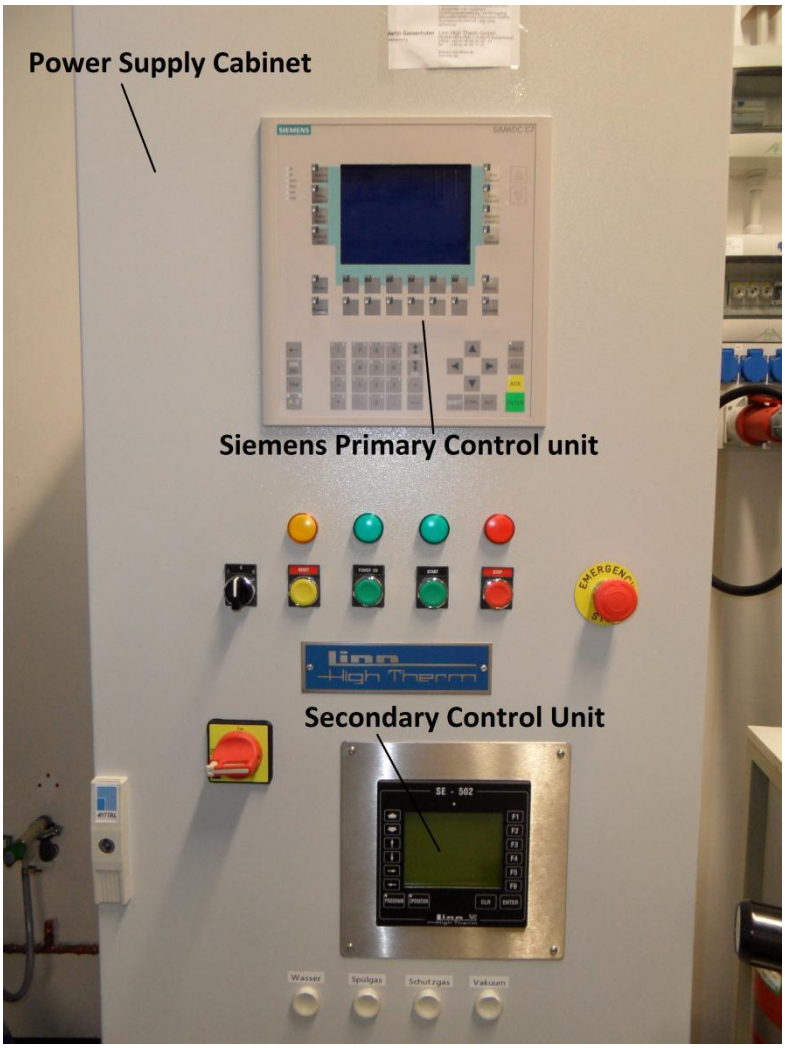

Figure 4.2.3: Front view of the control and power supply unit

Cooling unit

A cooling unit is used in order to obtain stationary conditions or in any case proper conditions to safeguard all the heat generating and heat sensitive equipment. In particular the oven, the power supply unit and the middle frequency generator have to be cooled. A water tank, an air-cooled chiller and a control unit for the water temperature form the unit. The chiller uses R407C gas with a cooling power of 10.7 kW at the limit operative temperature of 37°C. The evaporator consists of a heat exchanger gas-water immersed into the water tank. The condenser is formed by a gas-air heat exchanger provided with a fan.

The water is mixed with a special compound to prevent the corrosion of the evaporator. The water tank is connected to two separated circuits, one for the cooling of the power supply and the other for the cooling of the induction oven. A water pump guarantees a continuous water flow of 1.4 m^3/h with a pressure of 4 bar. The control unit measures the temperature of the water tank: as it rises over the set value, a switch is automatically closed to activate the chiller. When the temperature of the water reaches one grade below the set value the switch is opened again.

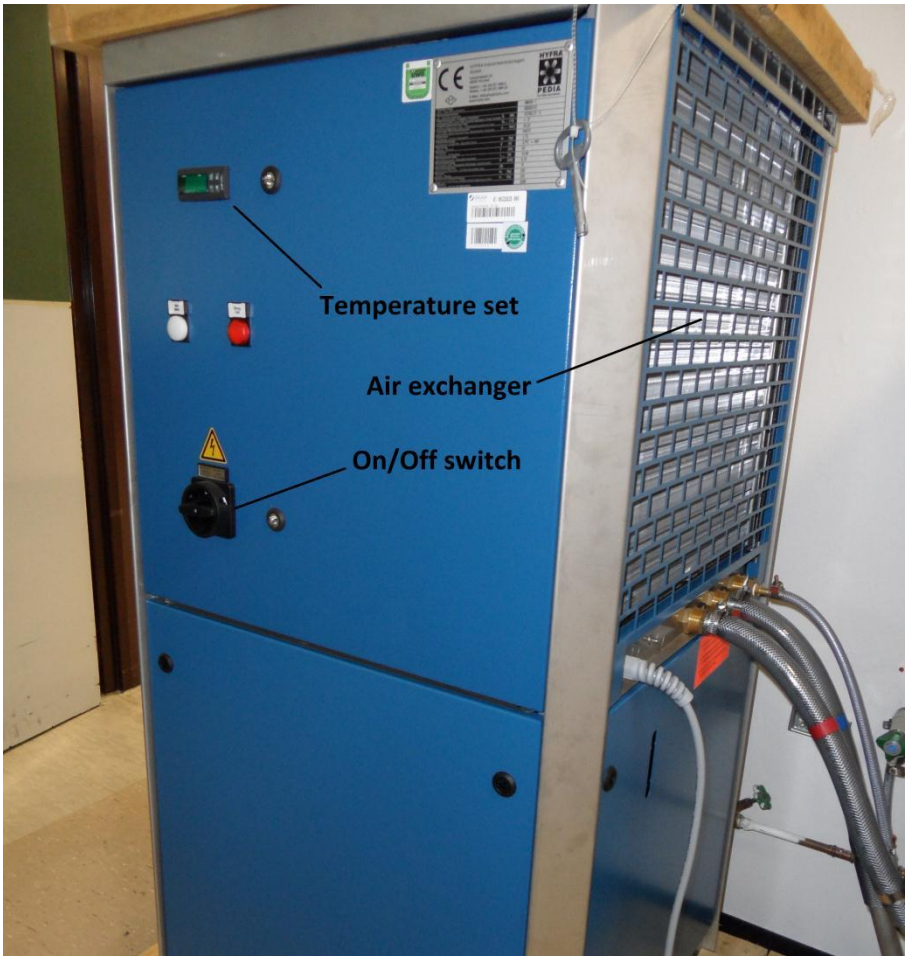

Figure 4.2.4: Overview of the cooling unit

Induction Oven

The induction oven, produced by Linn High Therm GmbH, is the heart of the facility. It has been specifically designed for treating massive samples of graphite. The central part is formed by the sample to be treated upon a holder. Two concentric quartz tubes are surrounding it, with water coolant flowing in the middle. The induction coil is placed outside these tubes and it is connected to the middle frequency generator, at the oven side. On the top, a pyrometer probe is placed, necessary to point indirectly the sample and to measure the high temperatures reached in the oven. At the bottom two vacuum pumps, working in parallel, are placed together with two flushing gas valves. In the backside there are input connectors for the process gases. The gas outlet is placed on the oven top, the inlet on the bottom. The gases are provided via 50 liters bottles and a centralized gas-distribution line.

For safety reasons a grid is surrounding the oven to prevent further damage in case of quartz glass breaking. At the oven outlet, two filters in series are installed: their purpose is to avoid the contamination of the Mass Spectrometer with carbon particles. The mean pore size is 140 μm for the first one and 5 μm for the second.

The usage of an induction oven allows the establishment of a clean and well-controllable heating process compared to most of the other means of heating.

Figure 4.2.5: Overview of the Induction Oven

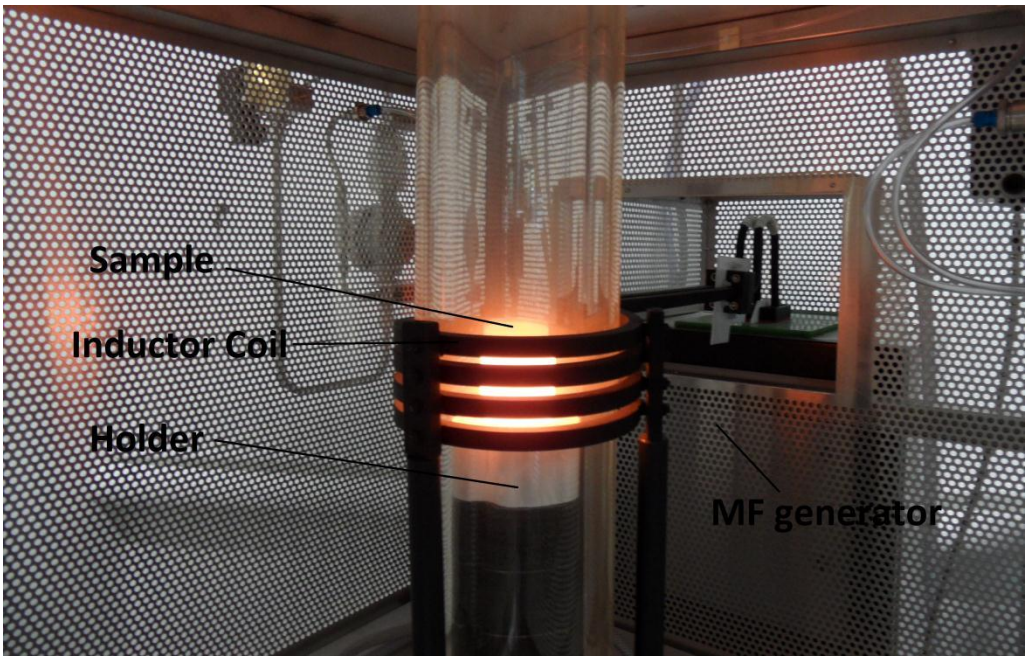

Figure 4.2.6: Inside view of the Induction Oven during at treatment

Pyrometer

A Pyrometer is a measurement device whose working principle is based on electromagnetic radiation emitted in the infrared range (wavelength approx 0.74-300 μm). The IR radiation is measured immediately outside of the oven through a receiver, connected in turn with an optic fibre to the device. The receiver is furnished with a laser pointer, in order to point precisely the surface to be measured. The manufacturer has calibrated the optimal distance by adjusting the pointer focus: the fixed distance is the one between the receiver and the top surface of the sample.

The pyrometer is used as a feedback-control device (Fig. 4.2.7) with respect to the Middle Frequency Generator, allowing in such way the power regulation and subsequently the control of the sample temperature.

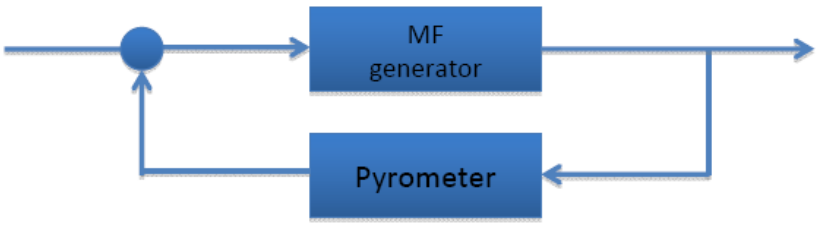

Figure 4.2.7: Schematic representation of the pyrometer feedback action

Mass Spectrometer

The system consists of a quadrupole Mass Spectrometer QMS 200 (PRISMA™), the vacuum recipient, the pumping station, a control unit (PCU201) and the Computer (PC). The Mass Spectrometer (MS) is equipped with a crossbeam ion source (double wire) to obtain a good linearity over a wide range of concentrations and a Channeltron (Secondary Electron Multiplier) detector. Furthermore, a Faraday detector is built in, less precise that SEM and used to measure high gaseous concentrations and to check the reliability of the calibrations. One detector or the other can be chosen via software interface: the IPI QuadStarTM Software controls the MS via PC.

Vacuum is generated by a rotary vane vacuum pump in combination with a turbo molecular pump. The first is able to work up to 10^{-5} bar, the second one is able to reach 10^{-9} bar. Because of the high revolution speed of the turbomolecular pump (up to 120,000 rpm) a purge gas (Argon) is necessary to prevent materials depositions. A pressure gauge PKR 261 is installed in the recipient for service purposes. By means of this gauge the rest gas and the operating pressure can be measured.

A set of calibration gases of well-known concentrations are needed to calibrate the MS; the calibration step is the most important for this equipment and it is fundamental to obtain good results. The system is naturally air-cooled. Figs. 4.2.8 and 4.2.9 show respectively the vacuum scheme of the MS and the outside view of the machine.

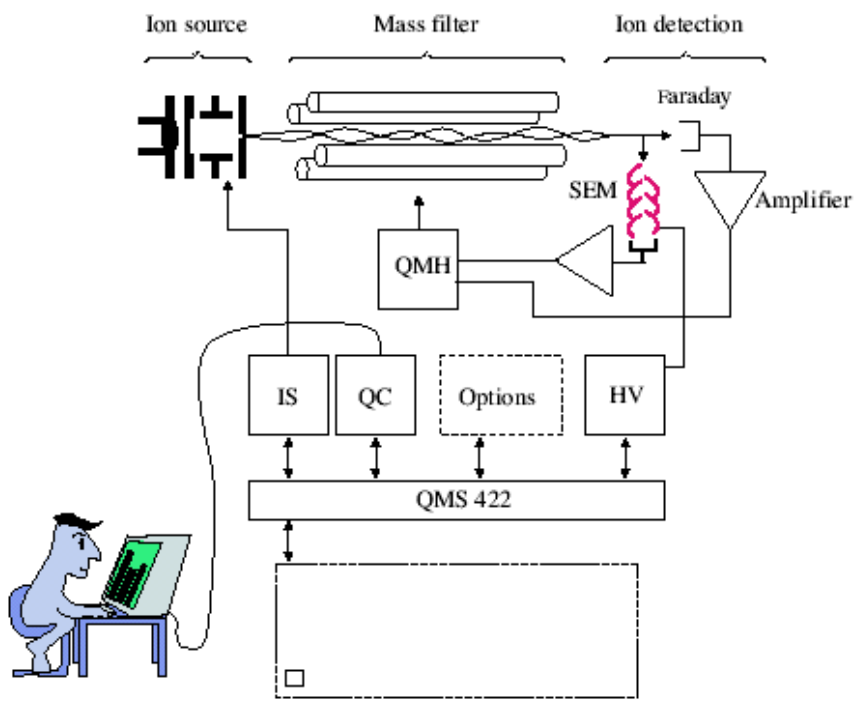

Figure 4.2.8: Scheme of the Mass Spectrometer System (Courtesy of InProcess Instruments)

Figure 4.2.9: View of the Mass Spectrometer (left) next to the Induction Oven (right)

4.2.2 Modifications of the facility

Before starting the experiments with AVR virgin graphite in the oven, many tests have been performed with other graphite grade samples to check the response of the equipment during different regimes and temperatures. The oven behaviour was found to be not optimal and the temperature revealed strong uncertainties, due to the non-linear response of the system on the one hand and due to the wrong measurements of the pyrometer on the other hand. In addition it was found that the treatment chamber was not perfectly sealed: many interventions were necessary to find the leakages. As a result of that, with the exception for the first experiment, several improvements have been achieved resulting in a cleared on-line measurement, less affected by secondary gaseous sources overlapping the real emissions. The interventions were, in particular, the following:

- Substitution of all the original sealing with high-vacuum ones made of aluminum instead of rubber;

- Helium leakage tests, through a Helium bottle and the mass spectrometer, to check the tightness of every single connection;

- Substitution and improvement of the vacuum line, in particular it was also inserted a manual valve to exclude the vacuum line when not necessary;

- Design of a new sample holder, in order to have a less porous media;

- Cycles of vacuum and flushing with Argon, before starting an experiment, revealed to remove part of the water present in all the inner surfaces of the treatment chamber. Such water was probably originated by the exposure to ambient air (with moisture). A pre- treatment would have been the best case, with the oven emptied, in order to thermally remove all the adsorbed water; unfortunately, since the oven is an induction one, a conductive specimen would have been necessary to obtain a temperature rise. It was performed a trial with a vanadium specimen but the oven revealed strong instabilities, leading to the failure of the cooling unit and to the necessity of shutting down the facility. The first experiment ("AVR 1") was performed before the above-mentioned interventions, so it was repeated ("AVR 2") in order to check the reliability of the on-line emissions (see section 5.2).

4.2.2.1 The new Sample Holder

The original sample holder was made of two parts:

- The upper part, in contact with the sample, made of porous Al_2O_3
- The lower part made by several layers of graphite wool, insulated on the top in order to avoid the establishment of an axial flow

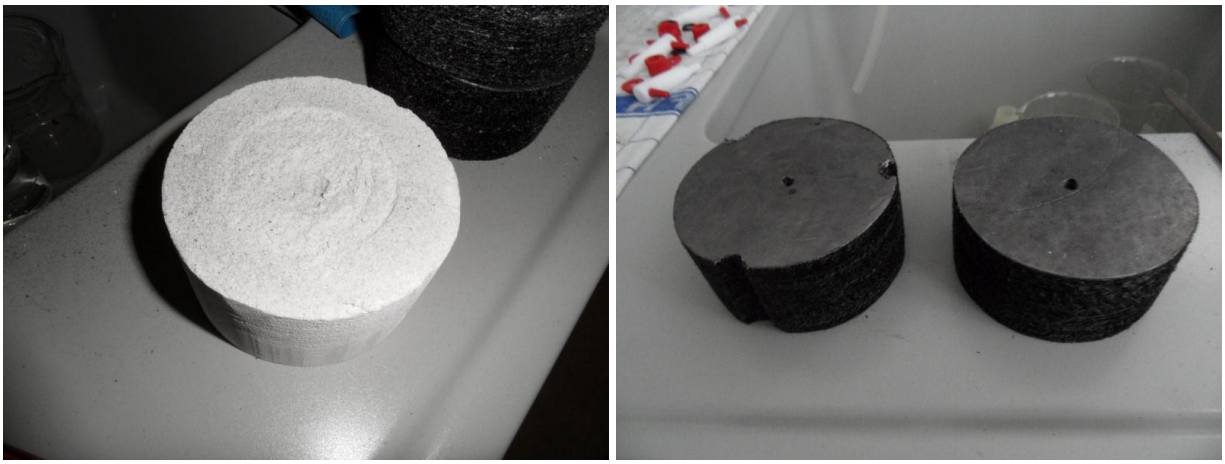

Figure 4.2.10-11: Upper part (left) and lower parts (right) of the original sample holder

The main reasons that led to abandon such holder are listed in the following:

- Inefficient fluid dynamics
- Porosity: gas and water adsorption are favoured. In this way, a secondary emissions of these gases could occur at high temperatures, overlapping so the real emissions of the sample
- Pyrolysis at high temperatures: it could lead to products or carbon particles emitted during the treatment

Because of the above-listed reasons, a thermo-fluid dynamic simplified simulation was performed with the purpose of building a new, more inert, sample holder. The key-features of the new holder, used to choose the proper material and geometry, were:

- Improved fluid dynamics
- High temperature resistance
- Inert as much as possible, both in reducing and oxidizing ambient
-Thermal shielding, in order to reduce the thermal radiation of the inner oven surfaces, made of fused quartz
- Maximum costs/benefits ratio

The chosen material was Al_2O_3 Alsint(R) 99.7%. Due to economic reasons and difficulty in manufacturing the holder, the bottom part has been designed in a special-grade steel (Iconel(R) alloy 617) able to bear up to 1000 °C; moreover, the geometry of the holder has been simplified as much as possible, considering the requested features.

In figs. 4.2.3-4 the results of the simplified thermodynamic simulation are shown, performed with the following hypothesis:

- Geometry 2D, axial symmetry
- Steady State
- Irradiative heat exchange between the sample and the inner walls of the oven (assumed $\varepsilon_{walls} = 0.7$ and $\varepsilon_{sample} = 1$)
- Conduction in the fused quartz walls

- Adiabatic top and bottom of the treatment chamber
- External walls with irradiative heat exchange with the environment $\varepsilon_{walls} = 0.7$
- Air flow 7 l/h
- Sample temperature of 1100 °C (maximum advised temperature without a thermal shield)

For what concerns the CFD simulation, the following assumptions have been considered:

- Geometry 2D, axial symmetry
- Steady State
- Low inlet gas velocity (0,1 m/s)
- Sample holder not porous

The CFD simulation results are reported in Fig. 4.2.14. The performed simulations allowed the design of an improved sample holder (Figs. 4.2.15-16) Together with a thermal shielding, able to operate at temperatures higher than 1100 °C (up to 1600 °C by design). A comparison between the old and new holder, installed in the induction oven, is shown in figs. 4.2.17.a-b).

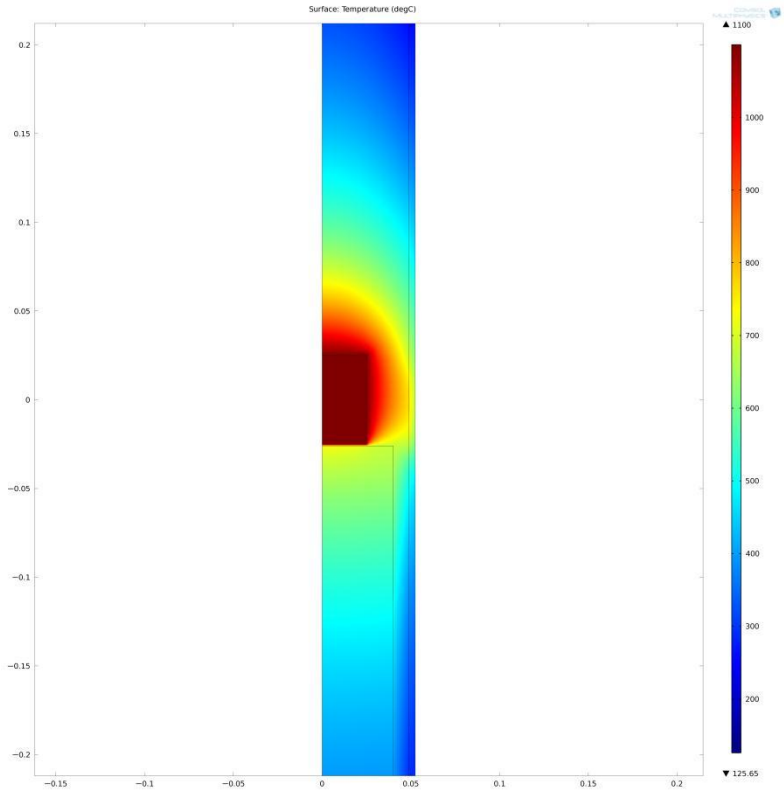

Figure 4.2.12: Thermodynamic simulation of the original sample holder

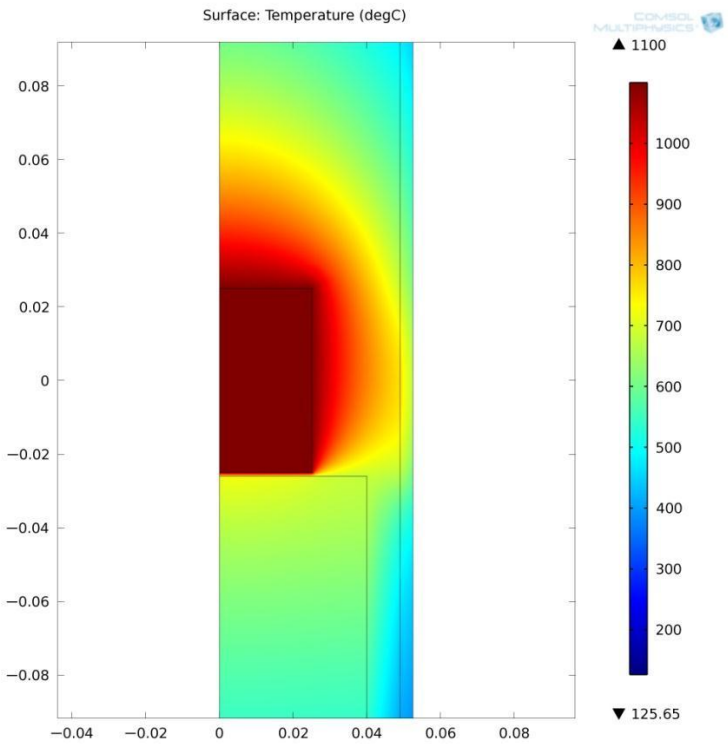

Figure 4.2.13: Simplified thermodynamic simulation of the original sample holder, zoomed

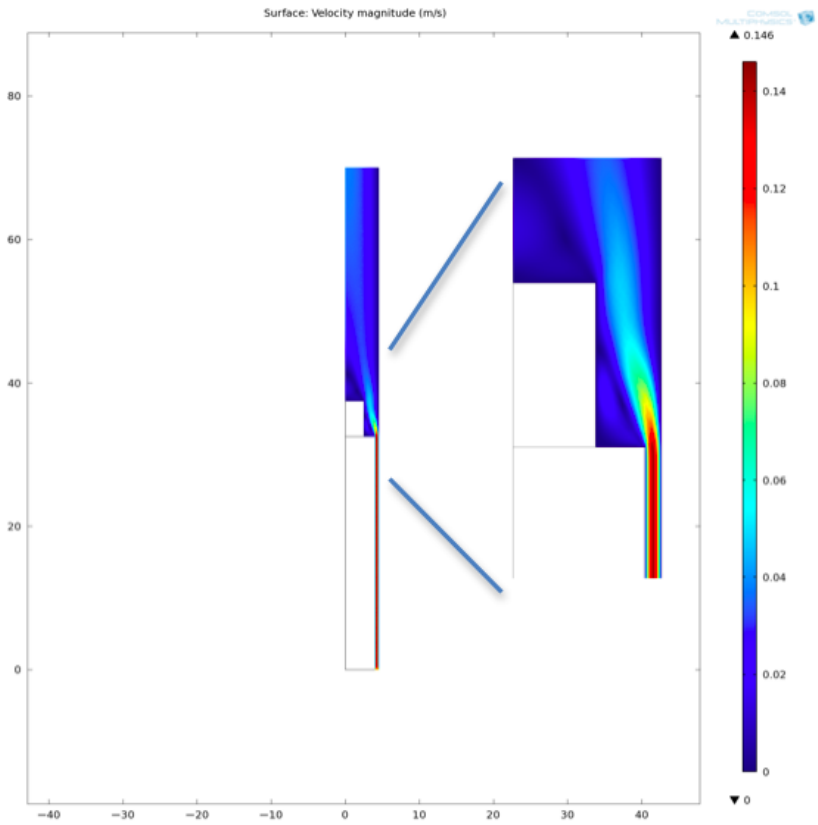

Figure 4.2.14: Fluid dynamic simulation of the original sample holder

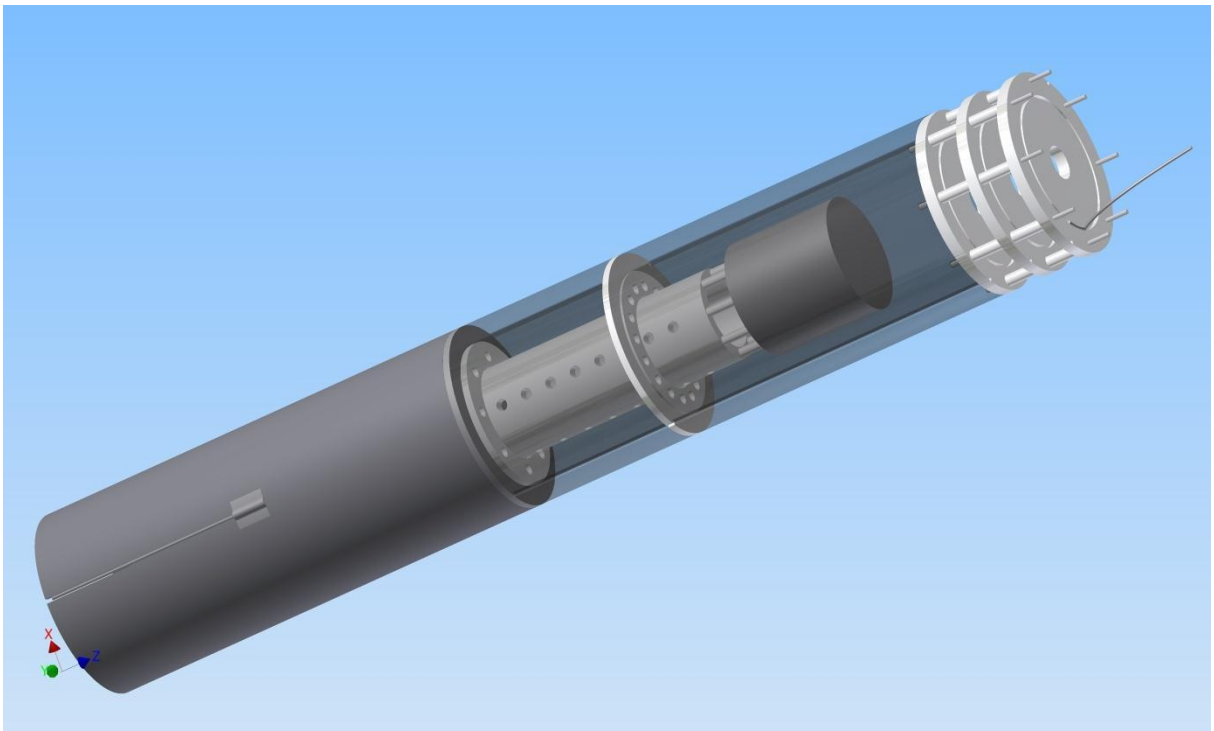

Figure 4.2.15: Overview of the new sample holder with thermal shield (transparent in this picture)

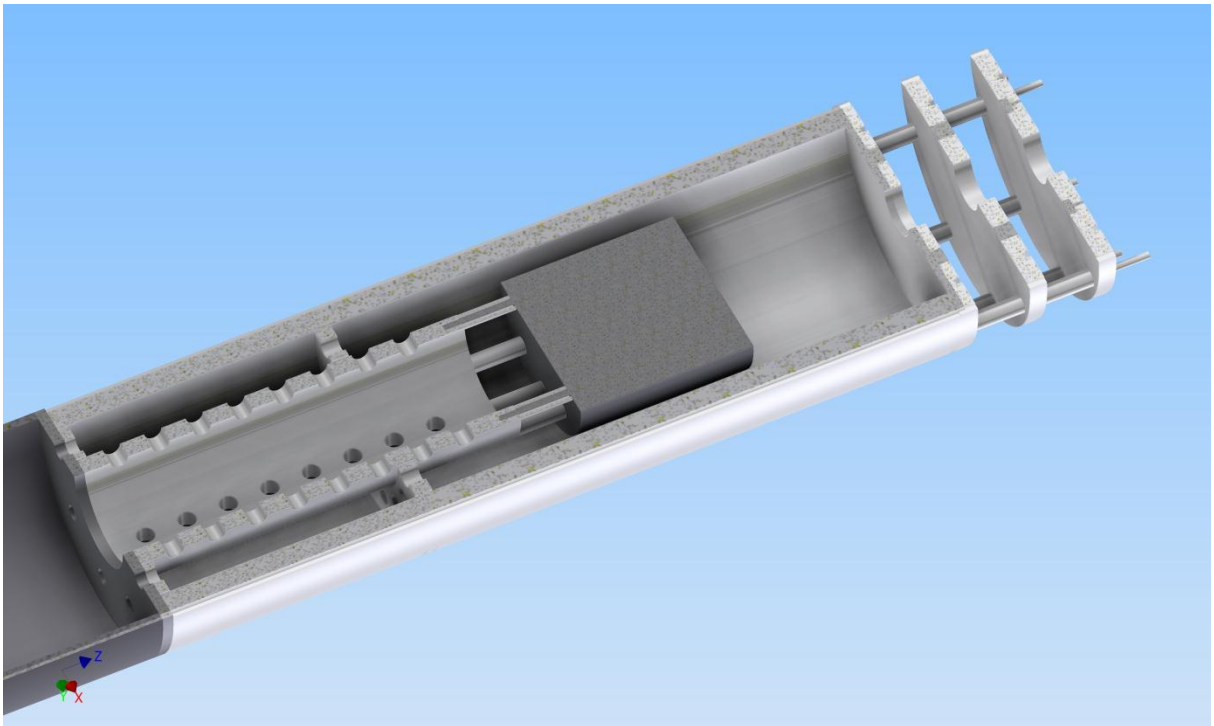

Figure 4.2.16: New sample holder with thermal shield, section view

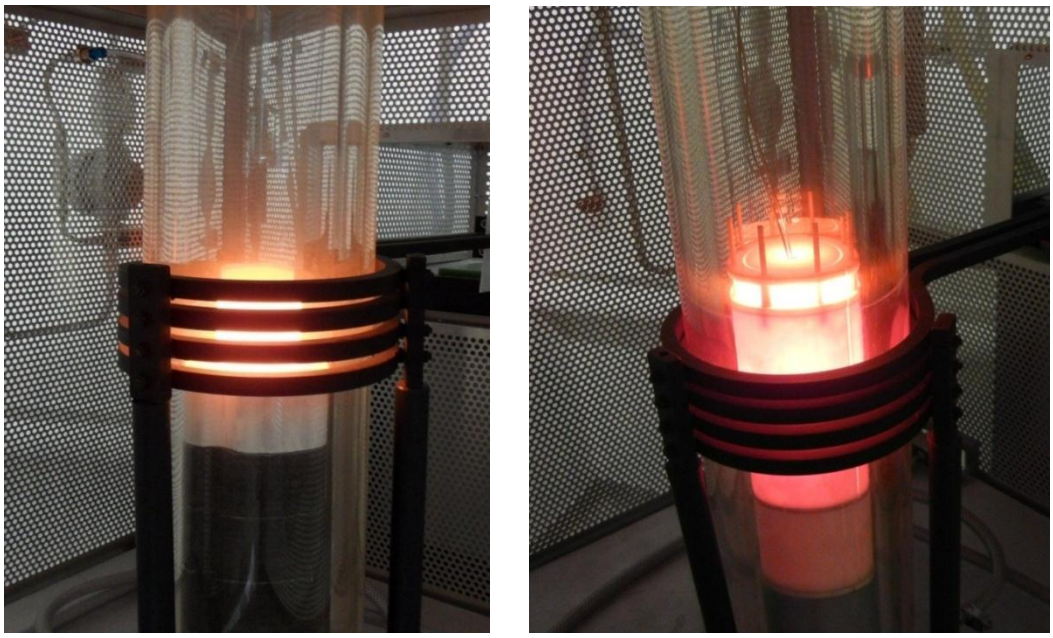

Figure 4.2.17.a-b: Comparison between the old (left) and new (right) sample holder, during operation in the oven

4.2.3 Performance of experiments

In the following, the experiments performed with the induction oven facility are presented. As discussed in section 3.2.2, only massive samples have been considered.[4] One of the scopes of the experiments here described was to measure the on-line gaseous emissions occurring during a thermal treatment under argon, in the way to understand whether oxidant species are already embedded in virgin nuclear graphite. The intention is to give a contribution to the understanding of the reactions taking place and to the removal mechanisms of some species. Further purpose of the here presented experiments was to get closer to an industrial treatment facility, in particular by investigating massive samples with a weight in the order of few hundreds of grams. Up to now, only small samples have been studied (up to few grams) and the question that is naturally rising is: are the small specimens representative of the actual behaviour of bigger massive samples that will be hypothetically implied in an industrial-scale process in the next future? And moreover: is the behaviour the same for massive big and small samples?

Choice of the operational parameters

The choice of some operational parameters is discussed in this section, resulting from consideration based on former experiences.

A short analysis of the most significant previous experiences is reported in this section, in order to choose the best conditions for an efficient removal of volatile/mobile radionuclides.

- Sample influence: massive samples experienced higher fractional releases of C-14 than powder samples [1]. The milling was supposed to increase the surface area of 14C-not enriched graphite, leading to considerable mass losses and low radiocarbon release in relation to C-12 release. The tritium release as well showed to be lower: it is likely that the isotope exchange with humidity released part of the tritium in the ambient air. Following these considerations, the selected sample resulted in a massive one with much higher weight. This also provides a much better chance to characterize the chemical compounds, which are released from the sample during thermal treatment.
- Temperature: Tritium showed to be removed more effectively at high temperatures, with a fractional release increasing at higher temperatures [1,2,8]. Radiocarbon, on the other hand, showed to be not dependent on the temperature but rather on a slight oxidation of the surfaces, since it is believed to be concentrated the more in the outer and inner surface of the porous graphite samples. Therefore, the chosen treatment temperature resulted in 1300 °C, following the results obtained in former experiments.
- Atmosphere: concerning Tritium, the most effective removal was obtained by using inert gases. Radiocarbon showed to be removed in higher fraction with argon and water steam (65 kPa). However, addition of reactive gases showed an increase on the release together with a higher oxidation of the graphite matrix. A selective oxidation could be the best option to remove as much radiocarbon as possible without important mass losses. For that reason the argon represents a good choice, also for radiocarbon release.

[4] The reason of this choice is explained in section 4.2.2.1

In conclusion, the process parameters have been identified as following: 1300°C under inert gas (argon).
Concerning the inert gas choice, hypothetically speaking, there would not be any difference in choosing argon or nitrogen. Considering that nitrogen is one of the precursors of interest and taking into account that nitrogen could react with the graphite surface, the only alternative resulted in the argon. But some
In figs. 4.2.9-13 some former experimental results [1,2,8] are reported to give a clearer view of the discussion reported above. Different graphite grades were investigated and showed typically different total fractional releases. However, similar parameters during thermal treatment resulted in similar radionuclides release behaviour, even with different removal efficiencies.
To clarify the concept it is considered an example: looking at 14C release in Fig. 4.2.18, massive samples of Merlin and AVR graphite under argon at 1060 °C show a similar steep release; in the case of AVR the release is limited,[5] but it is believed that the reason of that is the lacking of oxides, already consumed in the first treatment step, which would allow more radiocarbon to be extracted. On the other hand, since the treatment was performed under inert gas, assuming a non-homogeneous distribution of 14C and hypothesizing a higher concentration on the grain boundaries, it follows that the oxidising species were probably already embedded in the material itself. Some results pointing in that direction can be observed in Fig. 4.2.20: a high release of ^{14}C occurs in the first minutes of the treatment, then the release ceases. Following this line of thoughts, Florjan [8] performed repeatedly a similar experiment (Fig. 4.2.18), exposing the sample to the ambient air between four successive treatments on the same sample: it was observed a lower but proportional release of 14C as in the first experiment, leading to the conclusion that a slight oxidation of the graphite surfaces was probably the best treatment.[6] Proving the existence of oxidizing species inside the graphite is one of the aims of the present work. In addition, the form of released radiocarbon is also important: the possible options are CO_2, CO and small particles of carbon. During the treatment it is likely to observe all these emissions, but their temperature of occurrence and the timing are probably different, as it will be elucidated in section 5.2.

[5] Up to 20% with mass loss in the order of 1%
[6] The atmosphere was not completely inert in that case since the oven was opened in order to insert the sample. However a slight oxidation is still supported as the probable responsible for a good yield of C-14 removal

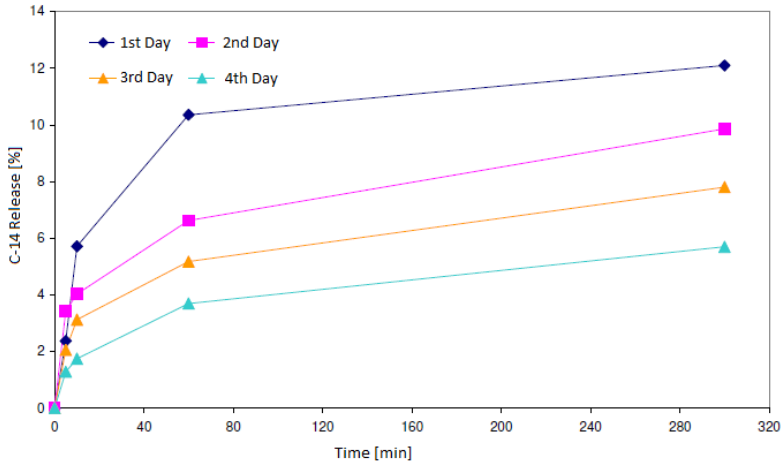

Figure 4.2.18: ^{14}C release vs. time during former thermal treatments [8]

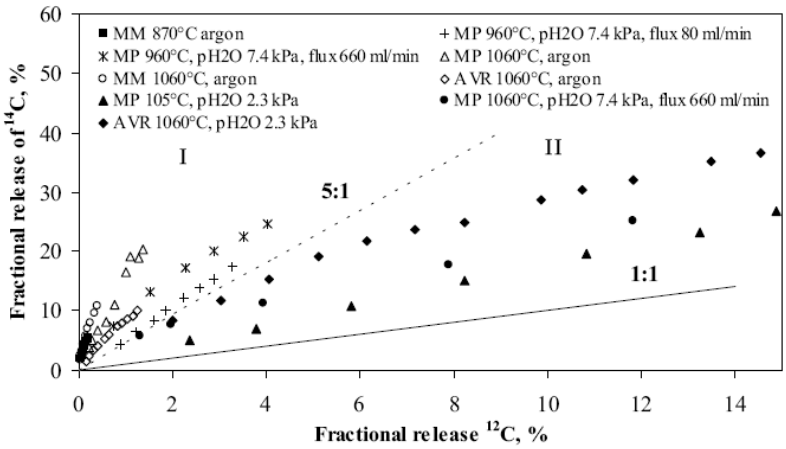

Figure 4.2.19: ^{14}C release vs. ^{12}C release during former thermal treatments [2]

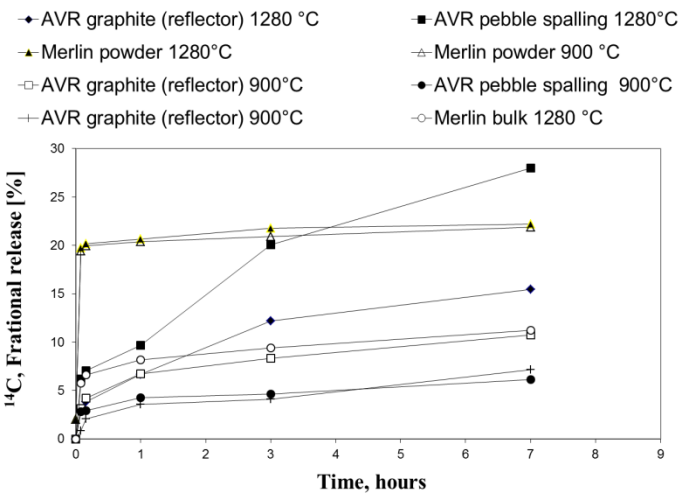

Figure 4.2.20: ^{14}C release vs. time during former thermal treatments under nitrogen [8]

Considering tritium release, similar observation can be done, even though the release mechanism is totally different compared to ^{14}C. The best results obtained point to a total fractional release of tritium up to more than 90% at 1280 °C, much higher than the one at 1060 °C (43%). Furthermore, in Fig. 4.2.21 it can be seen a similar steep increase on the tritium release during the first treatment step, leading to hypothesize desorption of tritium and hydrogen from the surface sites. The expected chemical forms of tritium being released are HT and HTO. Linking it to the virgin graphite experiments and assuming the hypothesis that tritium behaves in the same way as the non-radioactive H_2 and H_2O, a similar release should be experienced, probably with higher amounts of water.

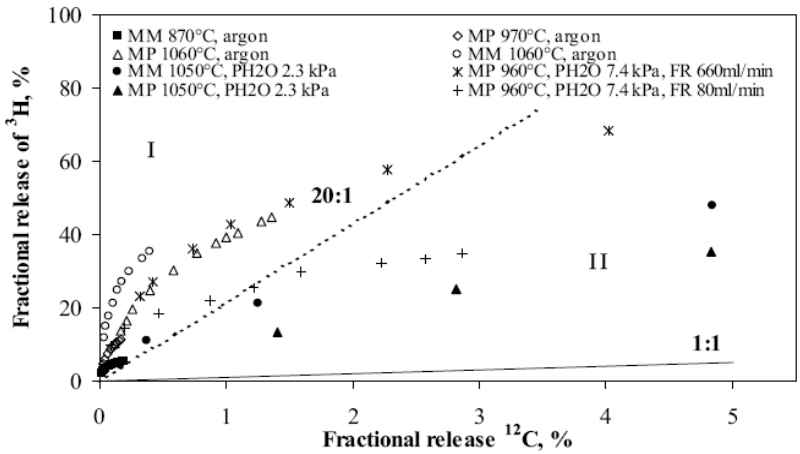

Figure 4.2.21: ^{3}H release vs. ^{12}C release during former thermal treatments under different conditions [2]

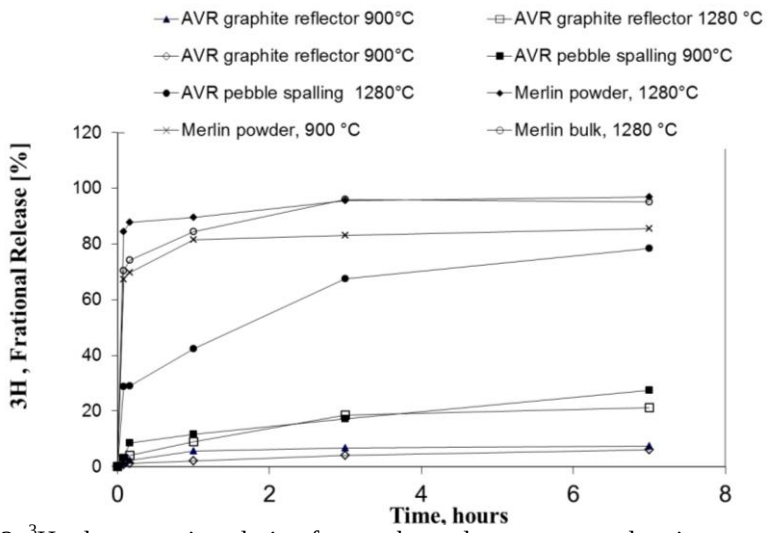

Figure 4.2.22: ^{3}H release vs. time during former thermal treatments under nitrogen atmosphere [8]

Overview of the experiments with the Induction Oven

Following the choice of the operational parameters, several experiments were performed with different timing, in order to have a double check about on-line emissions and mass loss dependence on the treatment time. It has to be reminded that, among other parameters, the mass loss is one of the determining factors for the feasibility of an industrial process, more than an indication of removal of some radionuclides (C-14). The first experiment ("MAVR 1") was performed before the improvement on the oven´s boundary conditions, so it was repeated ("MAVR 2") in order to check the reliability of the on-line emissions. The experiment “MAVR 3” was similar than the formers, but a shorter treatment time was chosen. A second experiment after intermediate air exposure was the “MAVR 3T”, performed to verify the treatments effects on the same “pre-treated” material. In the end, a special case is represented by “MAVR FT”: an involuntary communication problem occurred between the temperature probe and the control unit of the induction oven: it resulted in a very high heating rate, leading to interesting results.

Sample	MAVR 1	MAVR 2	MAVR 3	MAVR 3T	MAVR FT
Dimensions [mm]	Ø50H50	Ø50H50	Ø50H50	Ø50H50	Ø50H50
Initial Weight	172.0615 g ± 0.1 mg	169.5858 g ± 0.1 mg	169.9510 g ± 0.1 mg	169.7626 g ± 0.1 mg	169.5867 g ± 0.1 mg
Final Weight	171.8554 g ± 0.1 mg	169.3782 g ± 0.1 mg	169.7645 g ± 0.1 mg	169.6984 g ± 0.1 mg	169.5171 g ± 0.1 mg
Mass Loss	206.1 mg± 0.1 mg (0.12 %)	207.5 mg± 0.1 mg (0.122 %)	186.5 mg±0.1 mg (0.11 %)	64.2 mg ± 0.1 mg (0.038 %)	69.6 mg ± 0.1 mg (0.041 %)
Argon flow	7 l/h	7 l/h	7 l/h	7 l/h	7 l/h
Relative Pressure	1 bar	1 bar	1 bar	1 bar	1 bar
Heating/cooling rate	about 5° C/min	about 5° C/min	about 5° C/min	about 5° C/min	about 1000° C/min
Max Temp.	1300 °C	1300 °C	1300 °C	1300 °C	about 1300 °C
Holding time at High Temp.	19.4 hours	20.8 hours	6 hours	6 hours	few minutes

Table 4.2.1: Overview of the massive samples used in the most significant experiments with the Induction Oven Facility

5. Experimental Results

5.1 Small Scale Facility at FZJ

5.1.1 Tritium release

The amount of tritium released from Merlin and AVR graphite at different temperatures in inert atmosphere (argon, T. Podruzhina) is shown in Figure 10. The thermal treatment in nitrogen atmosphere at different temperatures (M. Florjan) is shown in Figure 5.1.1.

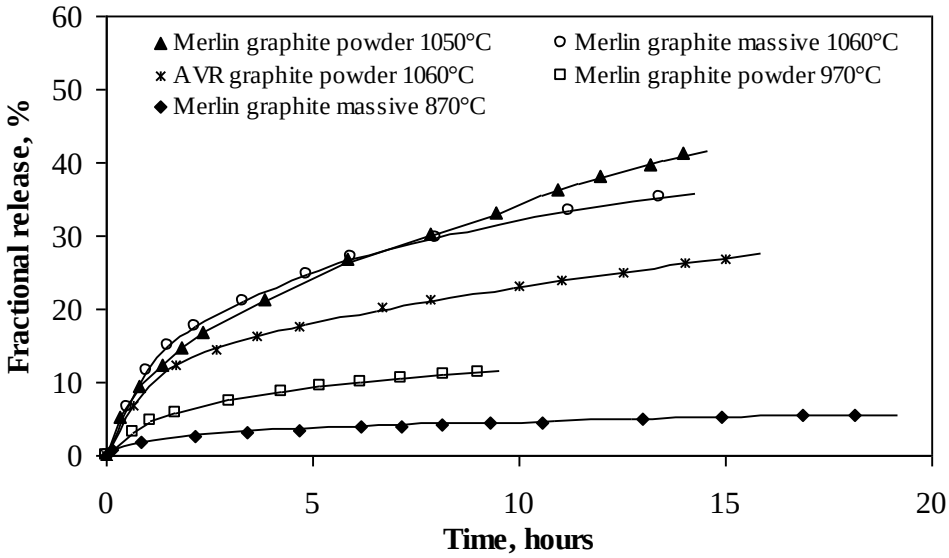

Figure 5.1.1: Tritium release in argon atmosphere [2]

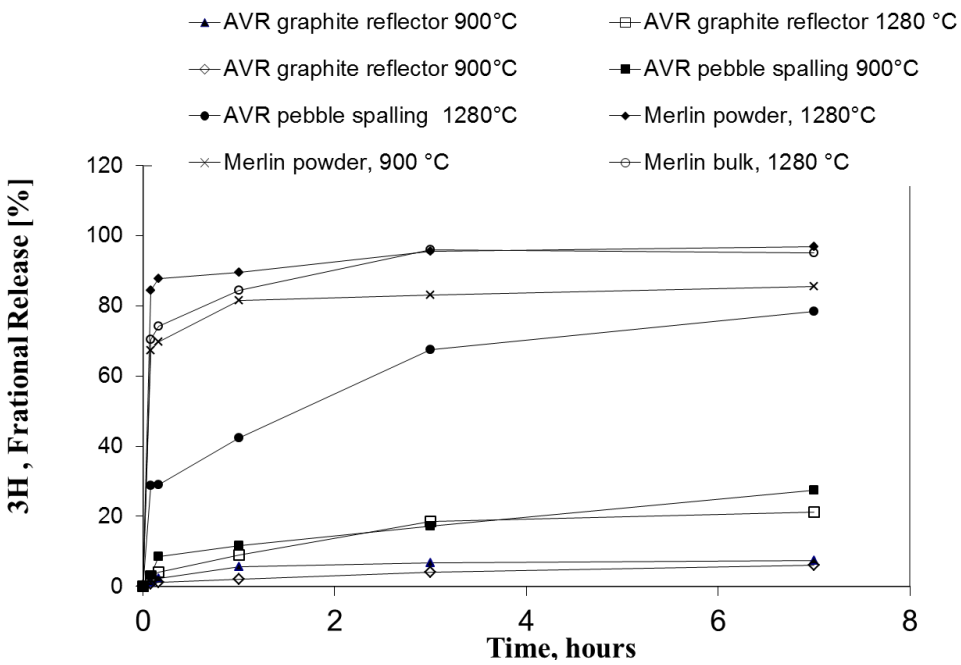

Figure 5.1.2: Tritium release in nitrogen atmosphere [8]

During all experiments two different release stages were observed. In the beginning tritium released faster: this corresponds to the region of the release curves with high ascending slope (see Fig. 5.1.2). There is a very marked slope in the beginning of the test results of M. Florjan: this was observed in the release curves of AVR pebble spalling at 1280 °C, of Merlin powder both at 900 °C and 800 °C and also of Merlin bulk at 1280 °C. M. Florjan also found very high tritium releases at 1280 °C: over 90% of tritium was released under inert atmosphere. T. Podruzhina only measured tritium releases up to 1060 °C, in order not to damage the quartz reaction tube, and found a maximum release of tritium around 40%. The tritium release seems to increase in inert atmosphere with the increasing temperature, up to 1280 °C in the present case. In M. Florjan's tests, only one Merlin powder sample tested at 900 °C showed deviation of a release of about 80% (compare curves in Fig. 5.1.2).

This can indicate that desorption of ^{3}H from active sites, situated on the surface, occurred. On the second stage the release became moderated with time and showed a linear character.

Two types of Merlin graphite´s samples, powder and massive, were investigated with a temperature of 1060 °C. It can be seen that the amount of released ^{3}H was almost the same for both samples. Therefore it can be considered that tritium release from the graphite sample was not limited by in-pore diffusion. The increase of ^{3}H release from powder sample in comparison with massive sample after 9 hours can be explained by oxygen ingress into the system, which caused oxidation of graphite sample and increase of released tritium.
T. Podruzhina obtained the maximum value of tritium removal from Merlin graphite powder at 1050 °C. It amounted to 43% after 15 hours. It seems that this value is reached because of air ingression after 9 h, noticeable due to the ascending slope of the release curve after 9 h (see Fig. 5.1.1).
M. Florjan reached up to 90% tritium release after 7 h treatment at 1280 °C. Reduction of the temperature caused a decrease in ^{3}H release. At 970 °C the released amount of tritium was about 10% after 9 hours of treatment.

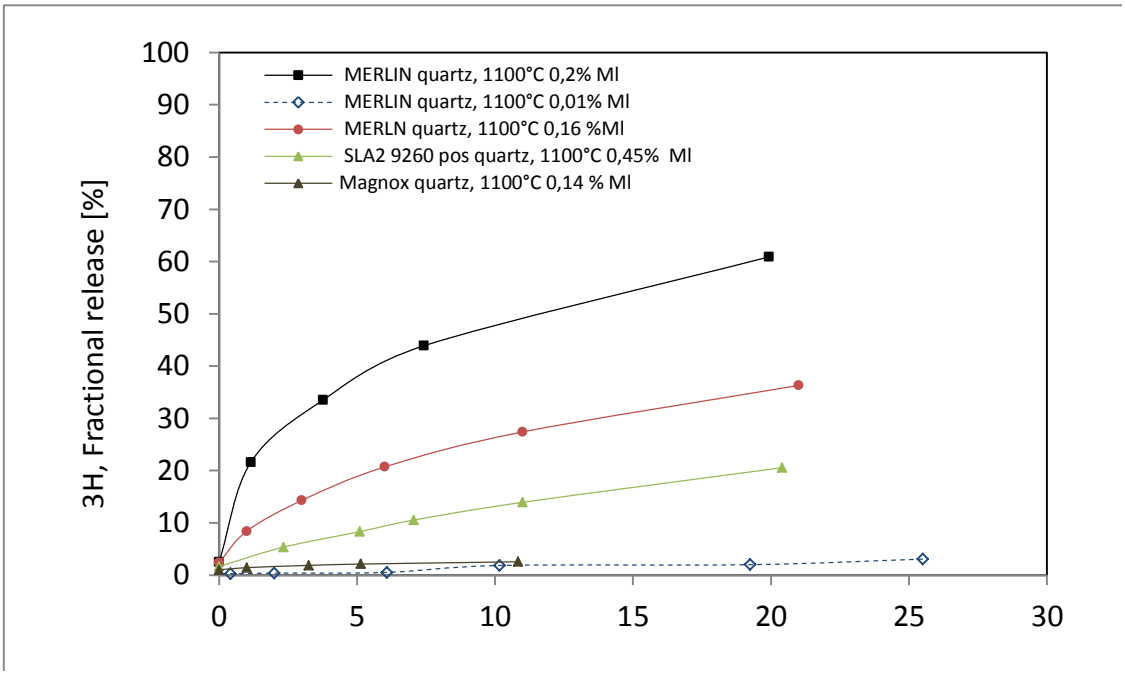

Figure 5.1.3: ^{3}H release from graphite bulk samples in nitrogen, quartz tube (K. Baginski)

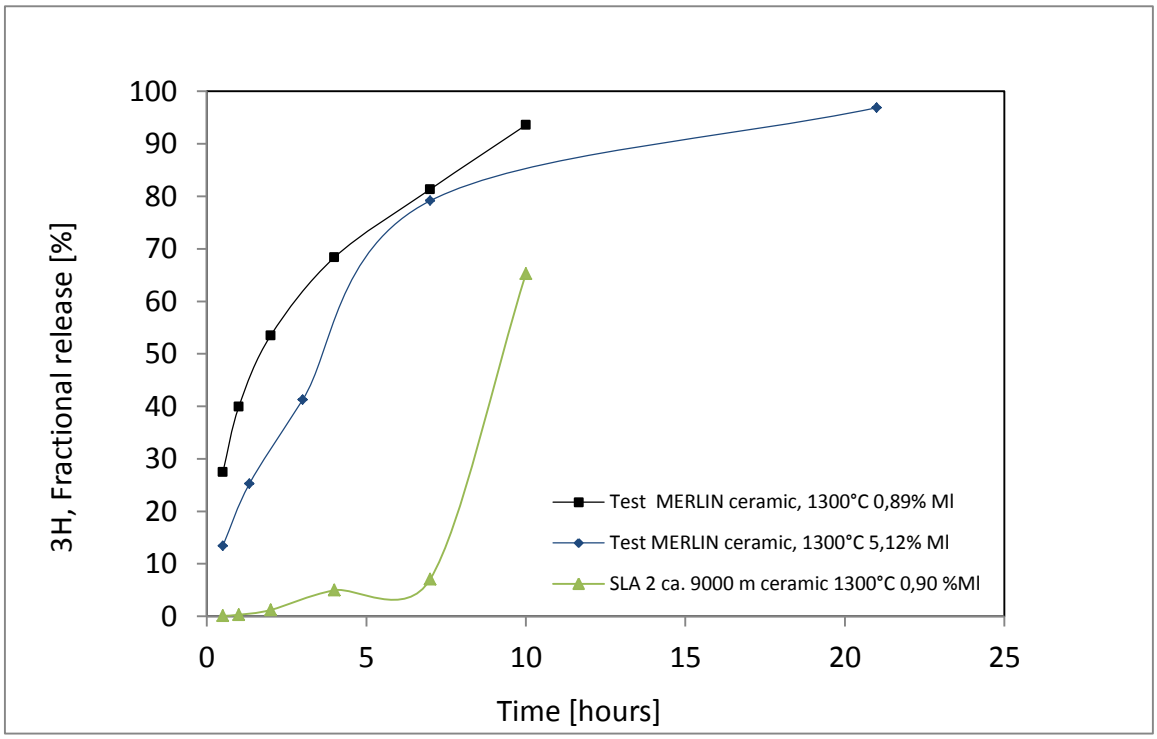

Figure 5.1.4: ^{3}H release from graphite bulk samples in nitrogen, ceramic tube (K. Baginski)

The end values for tritium release of K. Baginski at 1300°C in the ceramic tube and M. Florjan are comparable (> 90%), although the curve shape in the beginning of the experiment looks different. The slope in the beginning of M. Florjans curves ascend very fast in comparison with the curves of T. Podruzhina and K. Baginski. M Florjan used a ceramic tube inlay with metal clamps at the tube, so it is possible that there was a higher amount of oxygen ingress at the beginning of the test, so the high ascent of the release curves in the beginning of the tests could be linked with a corrosion phenomenon. Especially regarding powder tests, powder has a high specific surface compared to massive samples, so it is reasonable to expect higher reaction rates for the reaction with oxygen.

For what concerns AVR graphite, the amount of evolved tritium at the same temperature (1060 °C) was approximately 27%. This difference can be explained with the different operational conditions for these materials. In the AVR, gas-cooled reactor, the average gas-outlet temperature was about 950 °C [22, 23], whereas in Merlin reactor, light water was used both as moderator and coolant. The operational temperature of thermal columns was ambient in this case [28].

It is reported in a number of publications that the mobility of hydrogen molecules in undamaged graphite is rather slow [24,25,26]. In AVR the operational temperatures are rather high and some of the defects caused by neutron irradiation can be annealed. The other reason can be referred to the fact that at high temperature conditions of AVR tritium diffuses inside graphite crystal [24,27].

5.1.2 Radiocarbon release

Radiocarbon release from T. Podruzhina is given in Figure 5.1.5. The maximum value was obtained for Merlin graphite at 1050 °C and amounts to 20%. The release of radiocarbon is slightly higher in the initial period of time. This possibly represents the elimination of ^{14}C in the composition of oxygen complexes from the graphite surface, which can be easily eliminated by heating. The other possibility can be an interaction of carbon with adsorbed oxygen. A drastic increase of ^{14}C release in this experiment after 9 hours of heating was referred to oxygen ingress as it was mentioned above. One can see that oxidation of graphite increased the radiocarbon release twice despite the mass loss of the sample was not significant (1.36%).

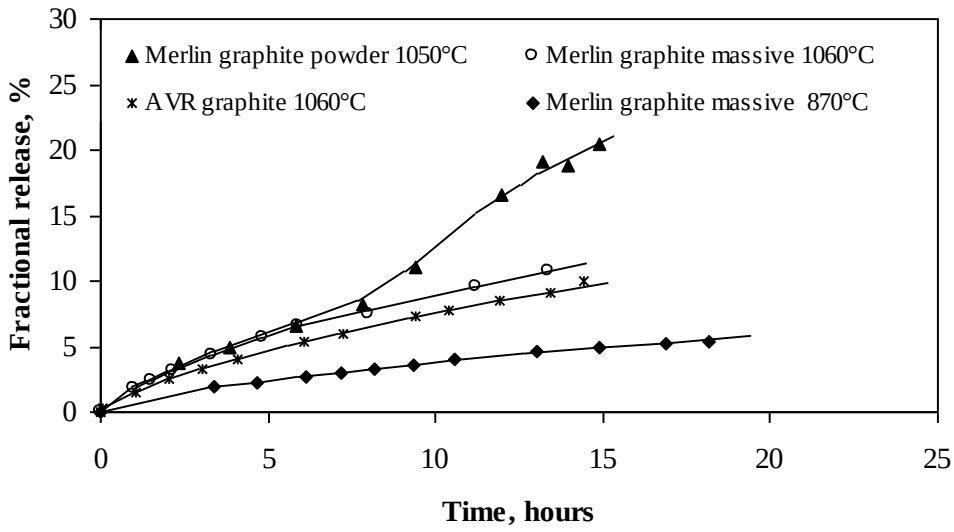

Figure 5.1.5: ^{14}C release from AVR and Merlin graphite in argon (T. Podruzhina)

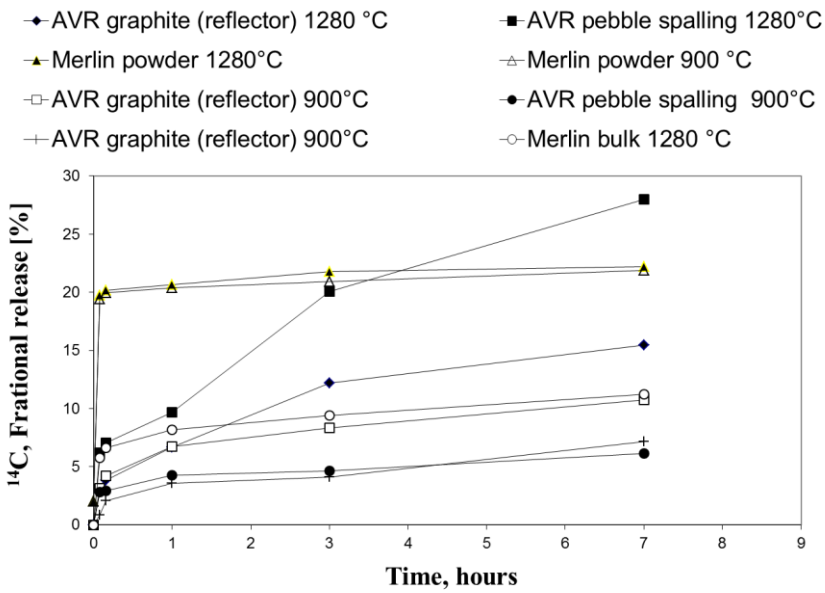

Figure 5.1.6: ^{14}C release from AVR and Merlin graphite in nitrogen (M. Florjan)

The total fractional release of ^{14}C is lower than the one for tritium because location of these radionuclides in graphite matrix is different. Also the reaction mechanisms for radionuclide release are different: while the release of ^{14}C can't be influenced in high amounts by increasing treatment temperature, the release of tritium seems to be supported by using temperatures from 1100 °C.

The AVR pebble spalling sample and the merlin powder samples of M. Florjan show deviation about 20% to 27% ^{14}C release at the test comparing to the tests of T. Podruzhina. M. Florjan found very high release rates of ^{14}C for these samples, probably because pebbles were only surface contaminated. The sample mass loss of T. Podruzhina was negligible and amounted to 0.16-1.36%. The sample mass loss of M. Florjan was even lower.

The latest result of ^{14}C release show figure xx and figure xx1from K. Baginski. It is visible that the temperature increase and /or the oxygen increase (more oxygen ingress with the use of the ceramic test tube) leads to more ^{14}C- release.

The results show the whole content of ^{14}C in washing bottles 3, 4, 7 and 8. We have to verify if there is a reliable separation of ^{14}C coming from CO_2 and ^{14}C coming from CO, this means ^{14}C found in the washing bottles before the catalyst or after the catalyst.

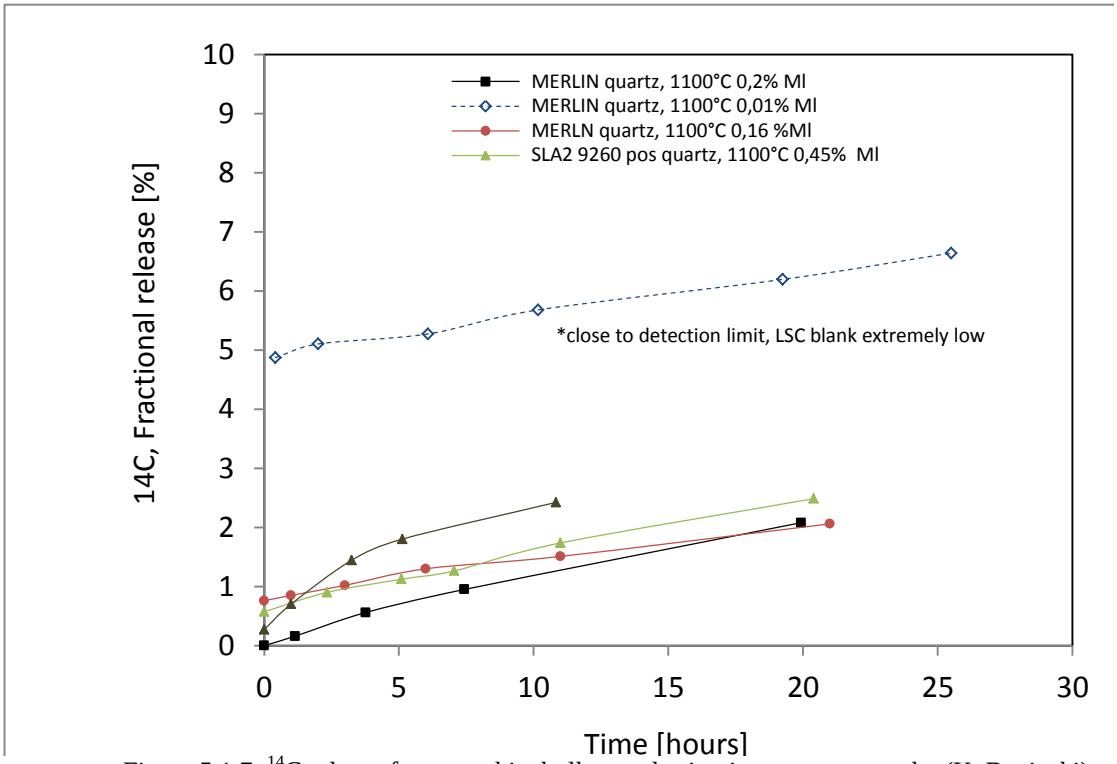

Figure 5.1.7: ^{14}C release from graphite bulk samples in nitrogen, quartz tube (K. Baginski)

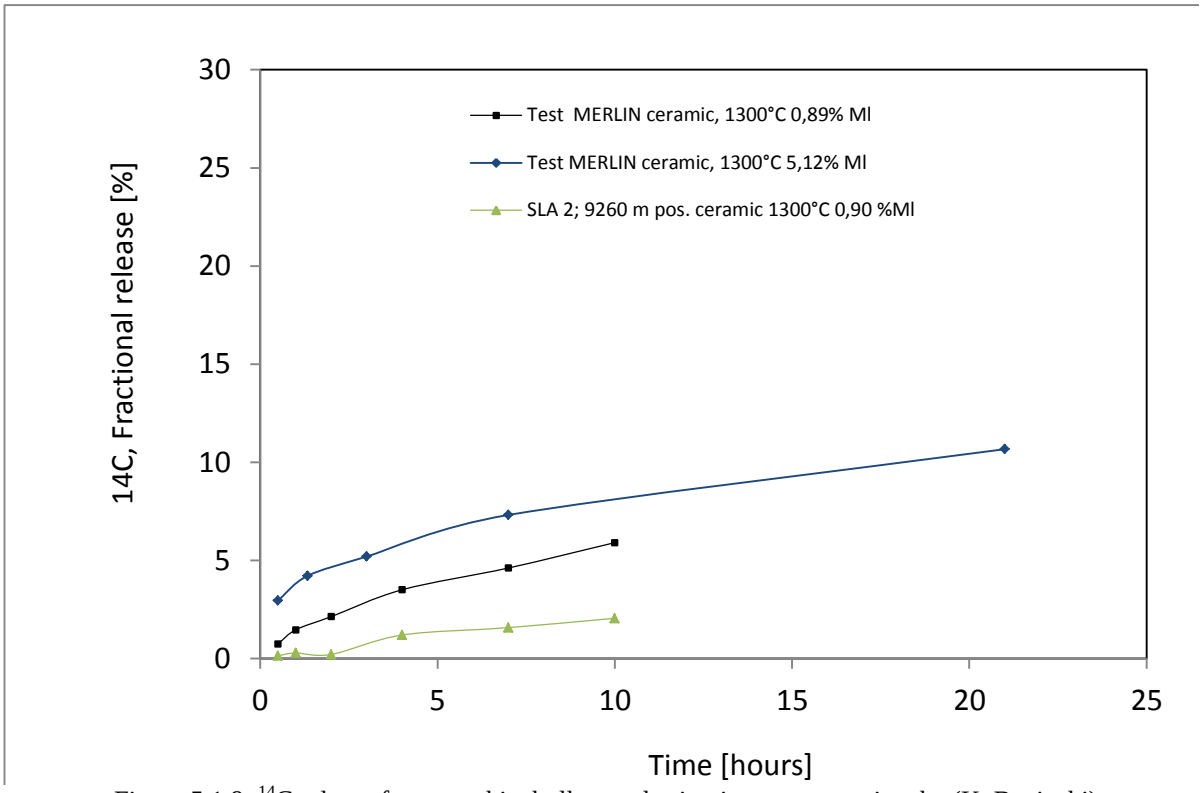

Figure 5.1.8: ^{14}C release from graphite bulk samples in nitrogen, ceramic tube (K. Baginski)

5.1.2 Calculation method of ^{3}H and ^{14}C release

The amount of radionuclides in graphite is very inhomogeneous and depends on the sample location during operation, reactor type, operation temperature etc. It is questionable how a so-called representative sample can be generated. Unfortunately, the determination of the whole amount of ^{14}C and ^{3}H from one graphite sample of one sort of graphite does not provide accurate results. This becomes also a challenge for testing the measurement uncertainty of the thermal treatment equipment: with regards to uncertainty, a representative sample with a known amount of radionuclides has to be treated; moreover, the results of two samples, one sample located next to another, result differ and the radiation history is often not exactly fixed. In several cases, clear documents for reactors that started operating 50-60 years ago are not available, so the amount of radionuclides are only estimations with high uncertainties.

It follows that, for the determination of the whole amount of ^{14}C and ^{3}H of a graphite sample in the presented work, the treatment test is firstly performed with a piece of graphite taken from a larger graphite body by core drilling. For the treatment test the drilled sample is inserted in the oven and the test is done in the described way (with quartz or with ceramic tube as test tube). The beta–emitting nuclides ^{14}C and ^{3}H are separated by the treatment process. The gaseous reaction products CO_2 and H_2O were captured in the corresponding washing solutions. HTO steam was captured in the bottles with 0,1 M nitric acid due to its liquefying , CO_2 was captured in the bottles with 4 M sodium hydroxide solution as sodium carbonate. The copper oxide catalyst is installed to oxidize HT and CO to obtain CO and CO_2.

At defined time steps (for example after 1hour, 2 hours, 4 hours, 9 hours, 20 hours), 1,5 ml of washing solution were taken off the washing bottles. The washing bottles developed at the FZJ glass manufacture have two outlet valves, one below the other, so that the test can be continued during sample taking. The liquid samples were prepared for liquid scintillation counting (LSC) measurement and here the counts of each sample can be calculated to a value for release of ^{14}C and ^{3}H at every time step. All time steps are added, so that the whole values for release are given.

The content of ^{14}C and ^{3}H which was not released from the sample during the treatment process is determined by the incineration of the remaining sample with pure oxygen as flow gas. Therefore a more simple apparatus is used because, in order to retain the radionuclides of the whole sample, more capturing liquid is necessary and the liquids with the whole content of ^{14}C and ^{3}H are only interesting for LSC-measurement. In the same way like as for the treatment test the beta –ray emitting nuclides ^{14}C and ^{3}H were separated. The gaseous reaction products CO_2 and H_2O (also HTO) were captured in washing solutions. HTO was captured in the bottles with 0,1 M nitric acid due to its liquefying in the first bottle, CO_2 was captured in the bottles with 4 M sodium hydroxide solution as sodium carbonate in the second bottle. In the third bottle are only radionuclides captured when the washing solution is saturated. By using pure oxygen for incineration no copper oxide catalyst is necessary. Figure 5.1.9 shows the apparatus for sample incineration.

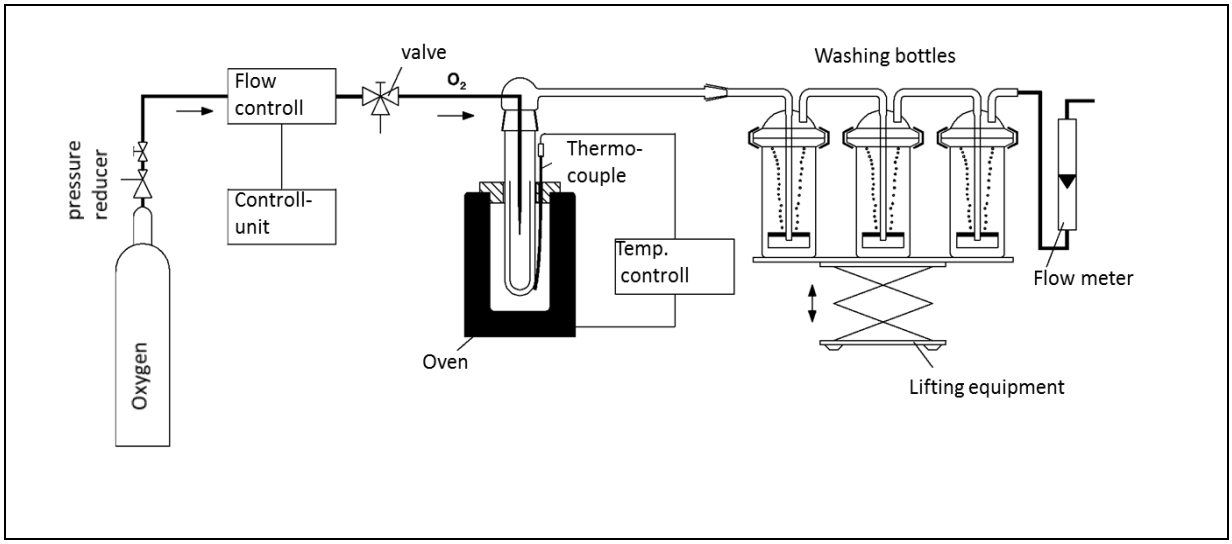

Figure 5.1.9: Incineration scheme of radioactive graphite samples

5.2 Induction Furnace at FZJ

The purpose of the investigations performed with virgin materials was to contribute on the understanding of some removal mechanisms, especially the ones connected with the precursors of the relevant activation products and oxidizing species adsorbed and/or originally embedded in the graphite structure during manufacturing. In particular, assuming the hypothesis that the governing physical-chemical removal mechanisms for impurities are the same for virgin and i-graphite, several thermal treatments have been applied to virgin samples of AVR graphite. After having identified the main radionuclides precursors, together with their possible origin and location, several investigations have been focused on the thermal treatment effects on such species.

In particular, massive samples tested in an induction oven showed on-line emissions during thermal treatments which were not observable with small ones, used in a thermo gravimetric analyser: methane and sulphur dioxide in small quantities have been measured.

The intention of thermal treatments was to operate under argon atmosphere, in order to measure the outgases and to connect their release with the embedded species and with temperature. Perfectly inert conditions were not achievable with any of the used equipment, but the comparison of multiple on-line measurements allowed to reveal the effective presence of oxidizing species and different volatile chemical compounds in the graphite structure. Their release, in particular, has been proven to occur during the first steps of the treatment.

Several comparisons of the emissions, measured with a Thermo Gravimetric Analyser (TGA) and the induction oven (see figs. 5.2.1-4), with results obtained in the past (figs. Par. 4.2.3.1) allowed to link the removal of some nuclides with the measured outgases. More in detail, water (steam) was found to be released from the sample even at relatively high temperatures, during the initial treatment step: tritium release curves observed in the past have been confirmed by such observation, leading to the conclusion that a considerable of it is probably released in form of water.

It seems to be confirmed that the removal of radiocarbon occurs because of a slight oxidation of the graphite surfaces, assuming its superficial enrichment. During the initial heating step, a well-defined peak of CO_2 was measured in all the experiments at relatively low temperatures, followed by a marked peak of CO at higher temperatures. In previous experiments it was observed a steep initial release even under inert atmosphere, linked to a partial oxidation probably caused by embedded oxidizing species: that hypothesis has been confirmed.

Methane was observed to be released from massive samples, resulting from the pyrolysis of embedded hydrocarbons, during the heating up step: it is probable that during treatments of i-graphite small amounts of tritium and radiocarbon will be released in form of methane, in all the possible combinations.

At last, sulphur was measured as SO_2 in small quantities, mostly during the high temperature step, probably due to a small income of oxygen: since it is one of the precursors of ^{36}Cl, its removal before implying graphite in a NPP could result in lower activation products.

A repeated thermal treatment on the same sample showed considerably lower emissions in the first steps, together with a reduced mass loss, compared to the one measured in the first treatment. This observation confirms the effective presence of many chemical species inside the graphite matrix, main responsible of the gaseous emissions during treatments under inert gases. On the other hand, the lower amounts of outgases can be linked to a probable improved behaviour of the thermally treated i-graphite under repository conditions. Further studies on i-graphite could confirm such hypothesis.

Concerning other radionuclides, in particular ^{36}Cl and ^{41}Ca, few studies have been established in the past. Considering the respective main precursors, i.e. ^{35}Cl and ^{40}Ca, some investigations with SIMS have been performed, focusing also on other species like nitrogen, the main precursor of ^{14}C (see figs. 5.2.5-7). The results confirmed an effective removal of some species from the first micrometers in depth from the sample surface, with high efficiencies for chlorine (up to 70%), and lower removal efficiencies for nitrogen. Nitrogen removal was confirmed also by XPS analysis, but future investigations are necessary to prove what has been measured here.
For what concerns calcium, its migration from the graphite bulk to the surface was observed through SEM, XPS, XRF and SIMS. Most of the calcium on the surface was found to be bound with oxygen through XRF and SIMS analyses. However, part of the calcium coming from the sample was found also on the bottom part of the sample holder, with a completely different structure, together with sulphur. It is probable that calcium, after having migrated to the sample surface, reacted with oxygen and also sulphur, forming at least two different compounds with different melting points. It has been confirmed by visual inspections with SEM analyses. Calcium was found on the sample surface in higher amounts after longer exposures to high temperatures.
Superficial structure changes and impurity migration have been observed via Scanning Electron Microscope analyses, with a marked effect on the structure when oxygen was used in the process gases.
In conclusion, high temperature thermal treatments revealed to affect graphite in many ways, removing many impurities and causing the migration of others. The presence of oxidizing species, originally embedded but also chemisorbed on the graphite surfaces, has been proven. The connection with previous experiments has confirmed some observations and hypothesis, in particular correlated with the removal mechanism of radiocarbon and tritium.
A more detailed paper about high temperature thermal treatments on virgin AVR graphite is reported in Deliv. 4.2.1-a.

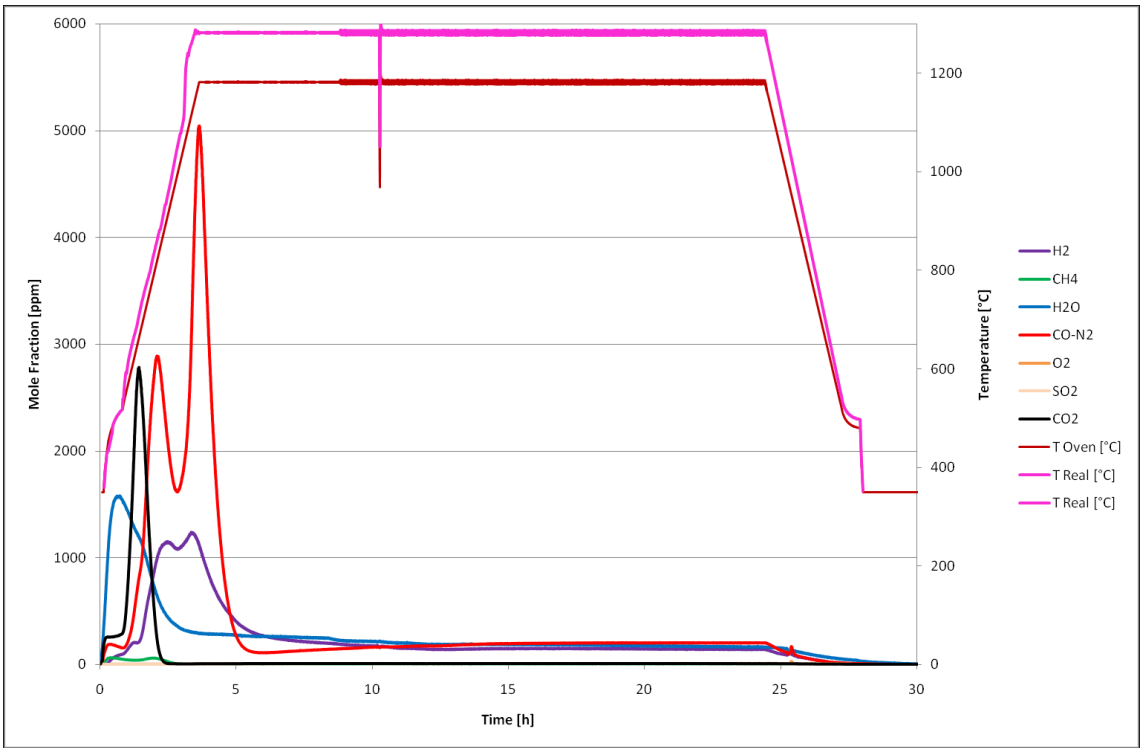

Figure 5.2.1: On-line gaseous emissions from AVR graphite, Induction Oven, sample "MAVR 2", linear plot

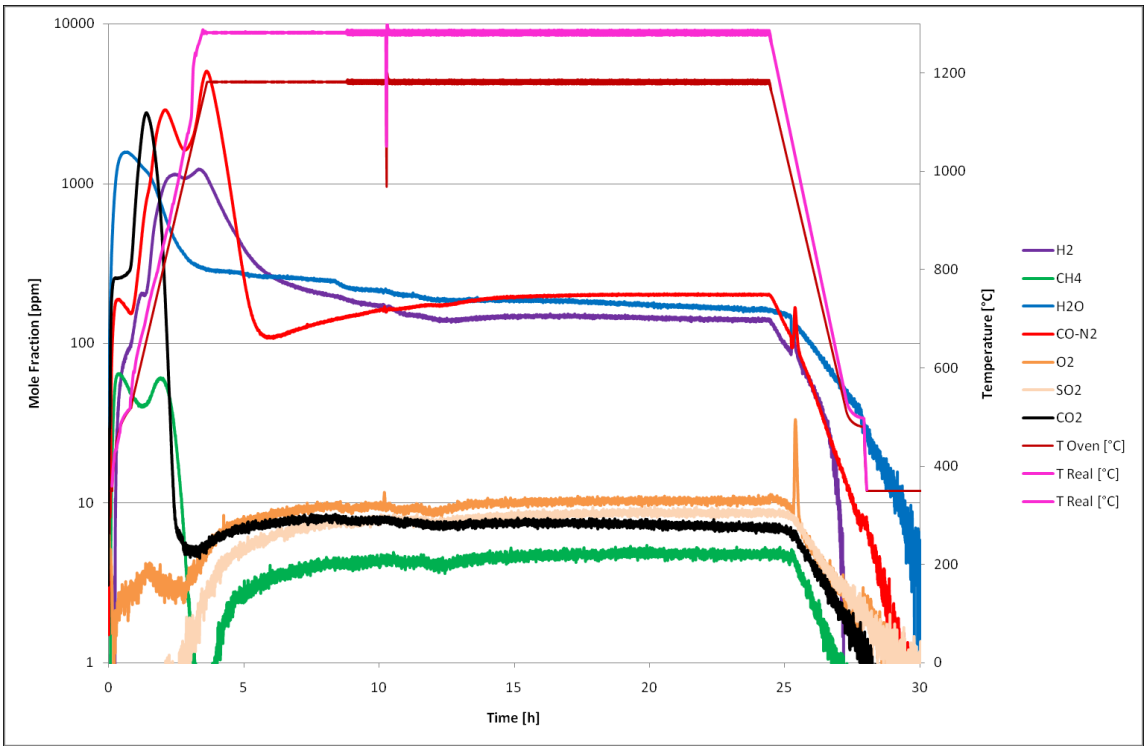

Figure 5.2.2: On-line gaseous emissions from AVR graphite, massive sample "AVR 2", semi-log plot

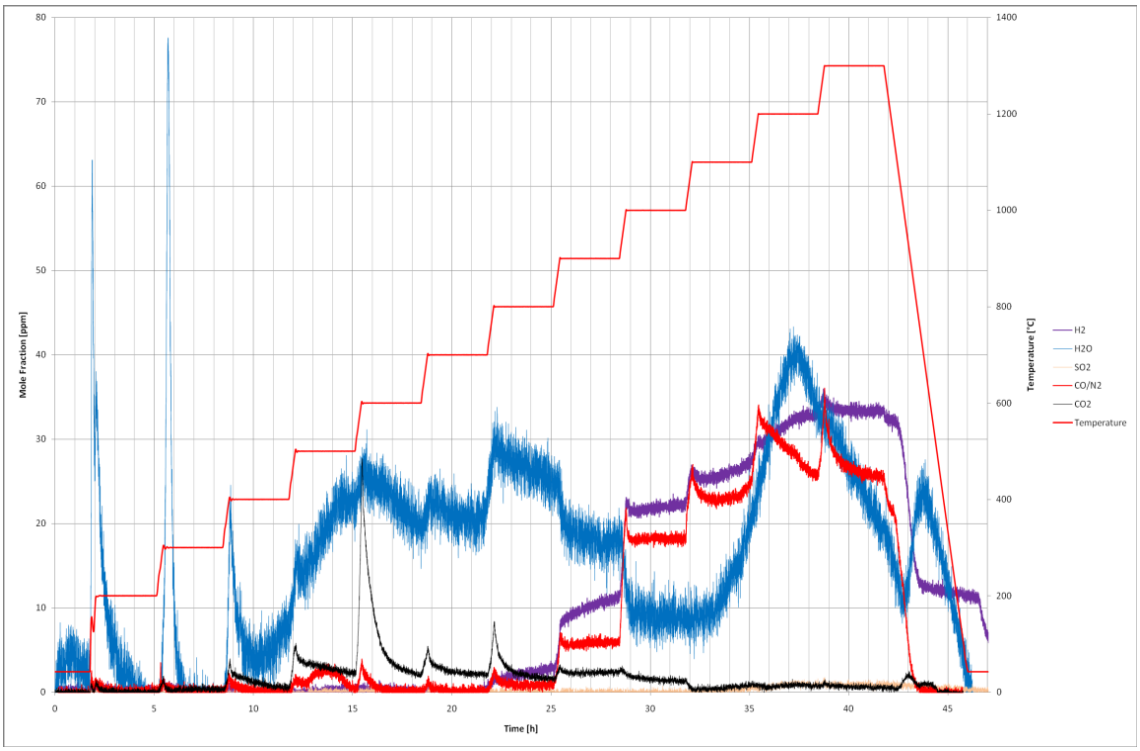

Figure 5.2.3: On-line gaseous emissions from AVR graphite, TGA, sample "CR 01", linear plot

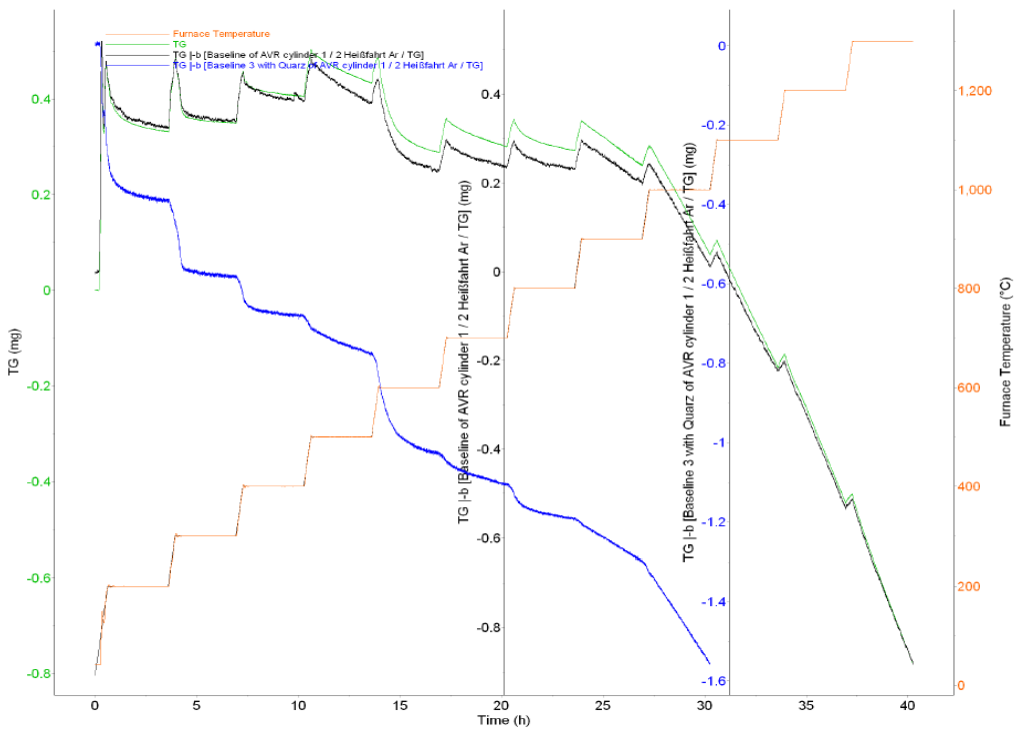

Figure 5.2.4: On-line weight measurement of AVR graphite, TGA, sample "CR 01", Thermo Gravimetric Analyser

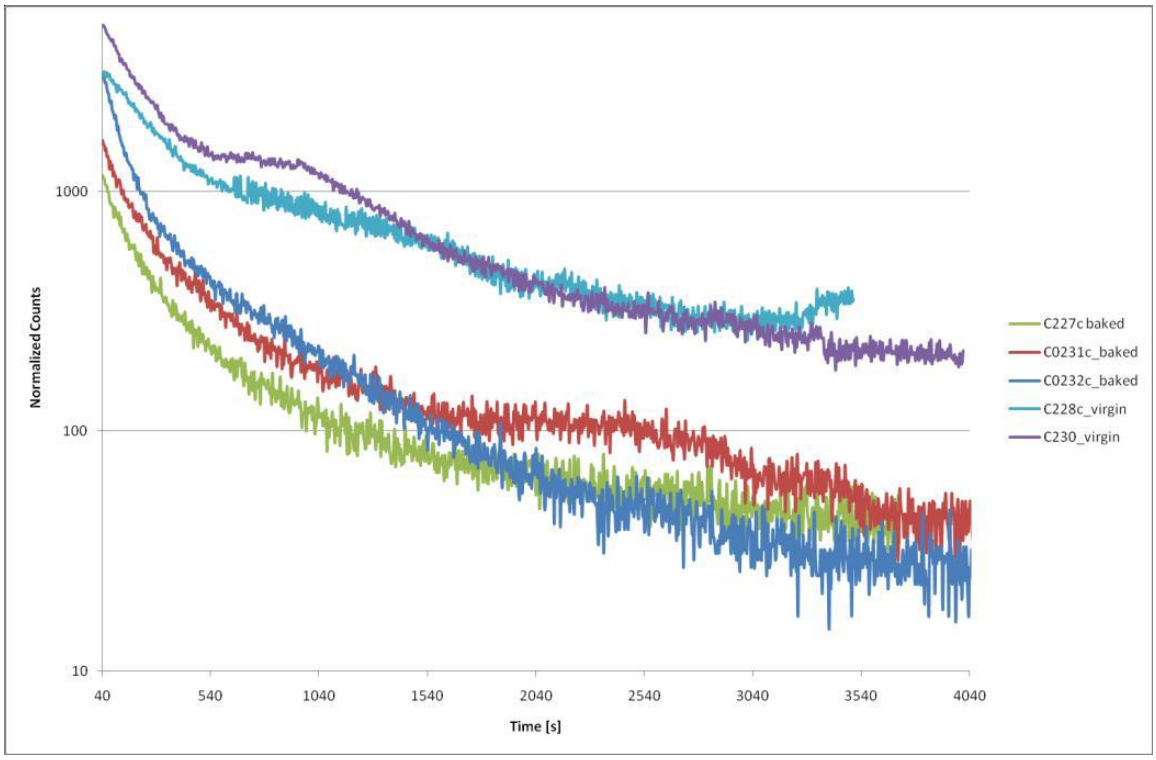

Figure 5.2.5: Comparison among normalized SIMS depth profiles of chlorine as Cl-, before and after thermal treatment, semilog plot

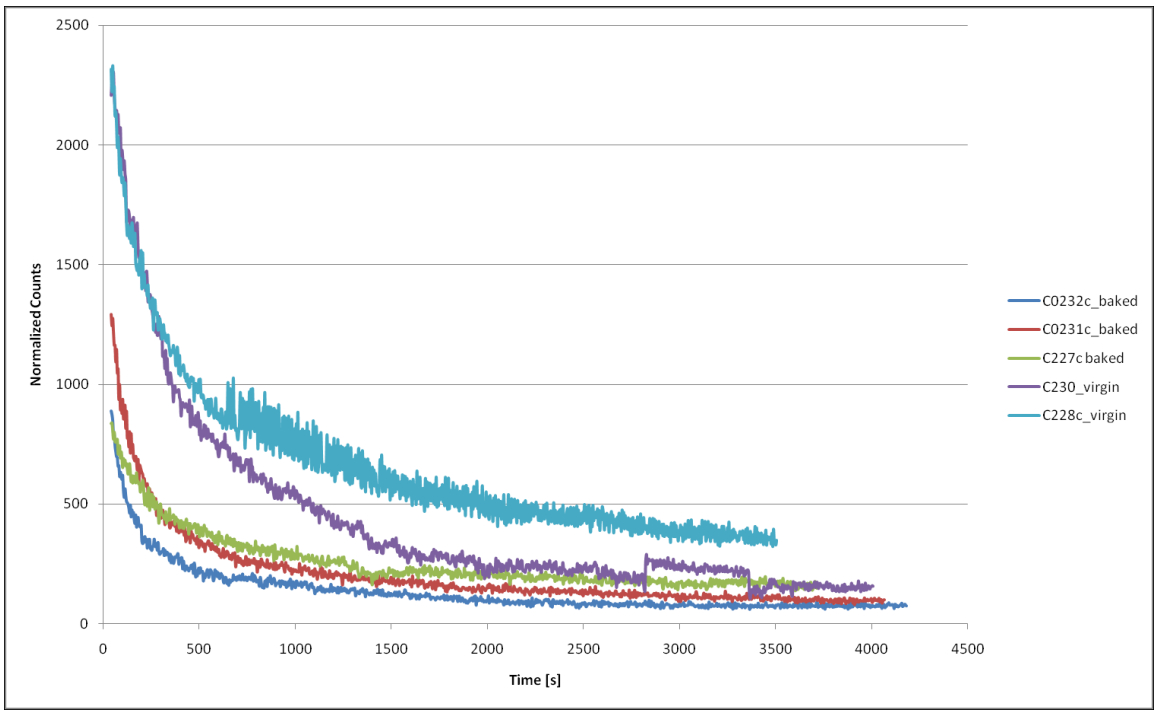

Figure 5.2.6: Comparison among normalized SIMS depth profiles of nitrogen as CN-, before and after thermal treatment, linear plot

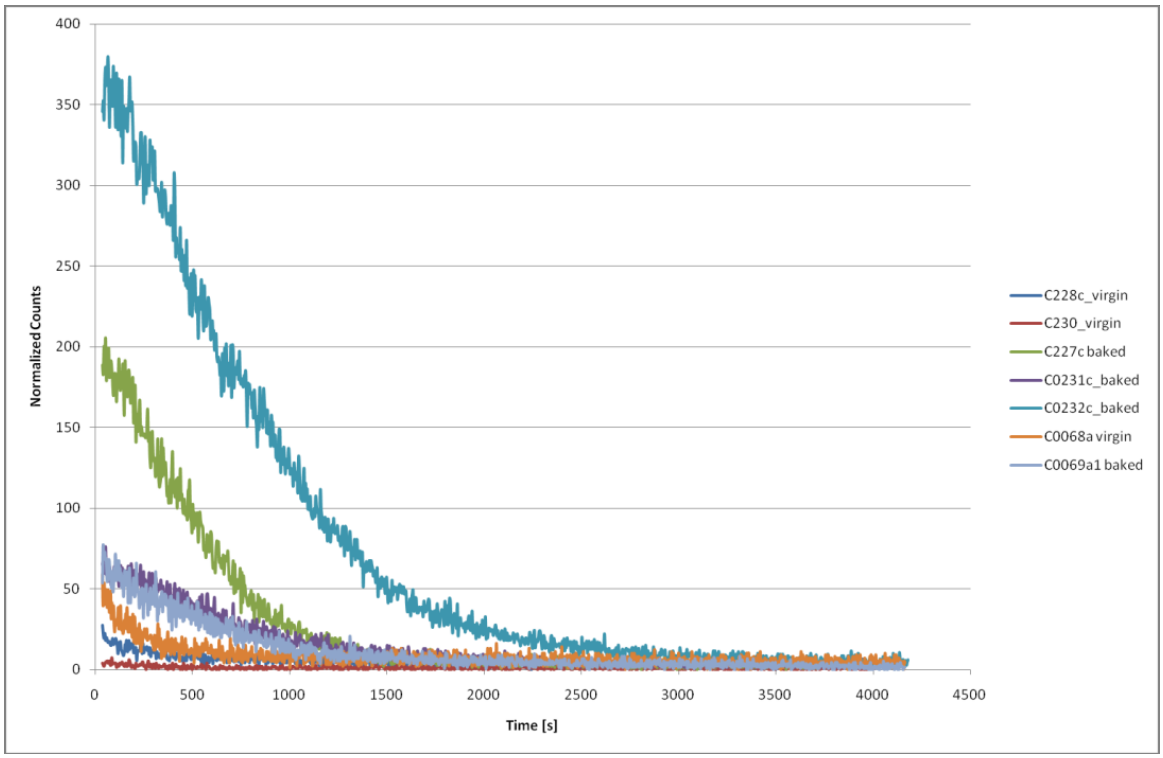

Figure 5.2.7: Comparison among normalized SIMS depth profiles of calcium as CaO-, before and after thermal treatment, linear plot

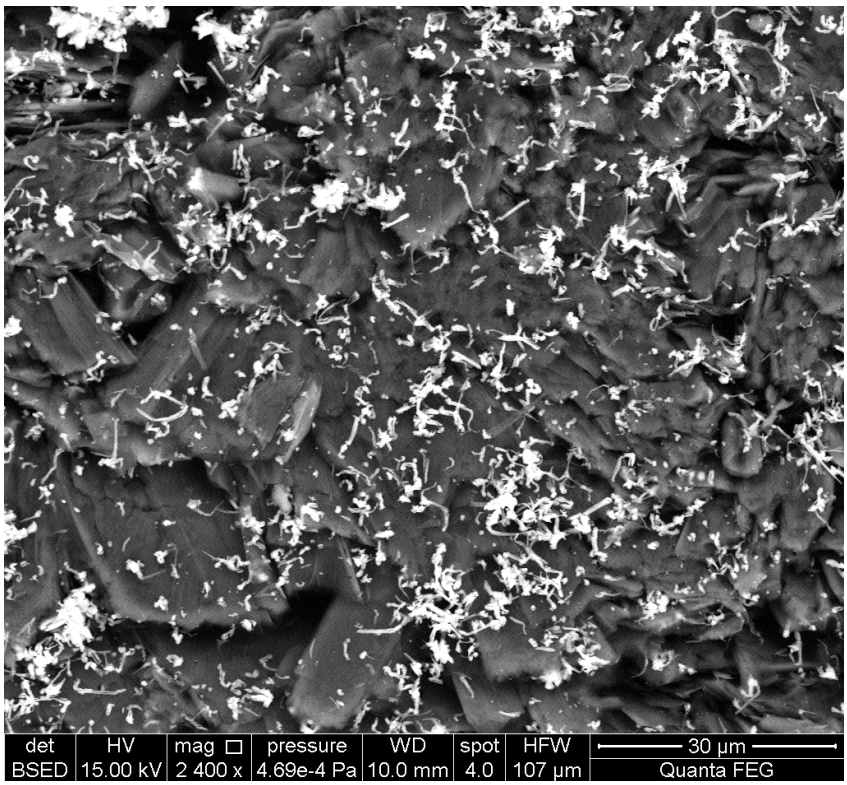

Figure 5.2.8: Overview of AVR graphite surface, treated in experiment "AVR square 1", mag. 2400x

6. Decontamination Factors

The decontamination factor is a well-defined parameter in the engineering science, defined by the ratio of initial specific radioactivity to final specific radioactivity resulting from a separation process [29]. The assessment of decontamination factors follows the rule: 1000 and above is excellent; 10 and below is poor [30].
In other words, the decontamination factor is a value higher than 1. "1" means that no decontamination has occurred. The reciprocal of the decontamination factor is the residual relative specific activity.

Decontamination factors determined at FZJ are summarised in Appendix 1.

Sometimes it is advantageous to define an enrichment factor: it is the ratio of radionuclide release to mass loss. The definition makes sense to decide if there is a real selective release process or if the graphite matrix is only consumed.

The enrichment factors determined at FZJ are summarised in Appendix 2.

Considering the decontamination factors, it is remarkable how they are very low for ^{14}C. This means that the largest part of ^{14}C is strongly bound within the graphite matrix. This is in accordance with the findings reported in Deliverable CW-D-3.3.2. Therefore, it can be concluded that graphite is a very good "retainer" for most of the ^{14}C-content. This finding is particularly important for the waste management of irradiated graphite.

In the following sections the decontamination factors for H-3 and C-14 will be elucidated for every graphite grade/type investigated in FZJ.

6.1. Decontamination Factors for Merlin Graphite

Table 6.1.1 reports an overview of the DF (Decontamination Factors) achieved by thermal treatment under inert gas with Merlin graphite.

Sample	Irradiation Conditions		Treat. Gas	Treat. T [°C]	Treating Time [h]		Mass Loss [%]	DF H-3	DF C-14
	Cool. Gas	T [°C]			Heating	Isothermal			
Merlin V4	Air	Room Temp.	N_2+0.14 % O_2	1300	0	10	0.89	15.4	1.05
Merlin V8	Air	Room Temp.	N_2+x% O_2	1300	0	21	5.12	30.4	1.06
Merlin V9	Air	Room Temp.	Pure N_2	1100	3.75	20	0.20	2.55	1.02
Merlin V10	Air	Room Temp.	Pure N_2	1100	3.75	25.5	0.01	1.01	1.03
Merlin V11	Air	Room Temp.	Pure N_2	1100	3.75	20.5	0.16	1.57	1.02
Merlin V14	Air	Room Temp.	N_2+0.1% O_2	750	2.5	5	0.22	1.01	1.01
Merlin V17	Air	Room Temp.	N_2+0.3% O_2	900	3	5	1.62	1.41	1.14
Merlin V18	Air	Room Temp.	N_2+0.3% O_2	900	3	5	2.72	1.46	1.03

Table 6.1.1: Overview of the performed thermal treatment experiments with Merlin graphite in “inert” atmosphere.

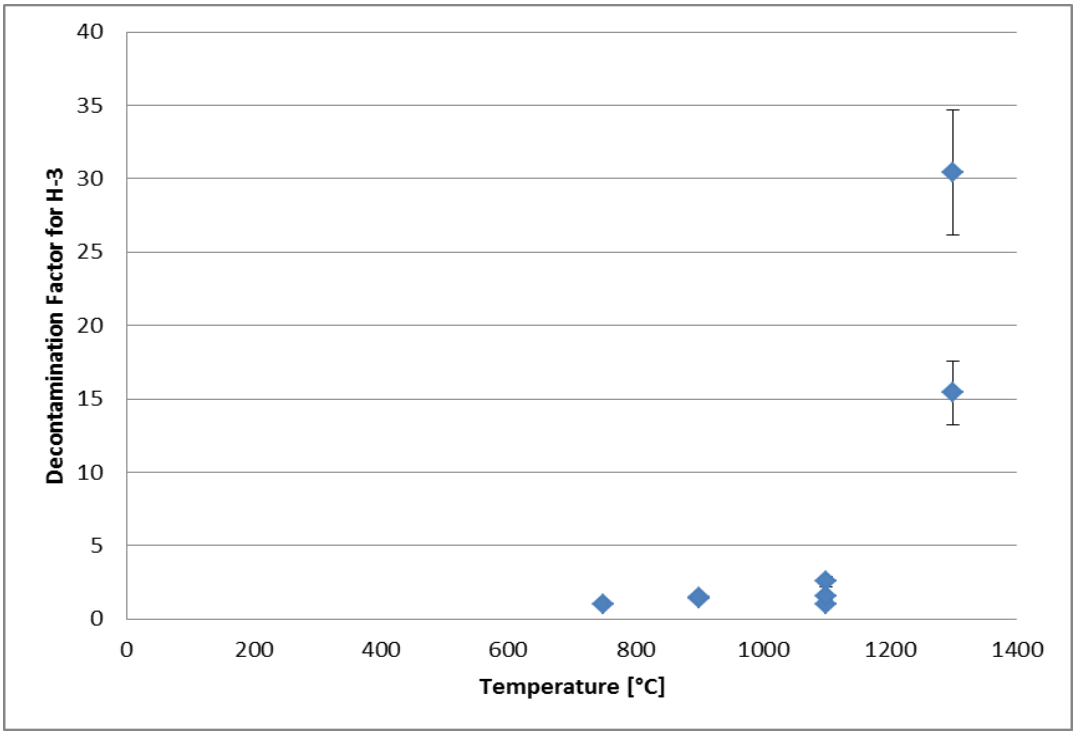

Figure 6.1.1: Decontamination factors of H-3 for Merlin graphite in function of the isothermal treatment temperature

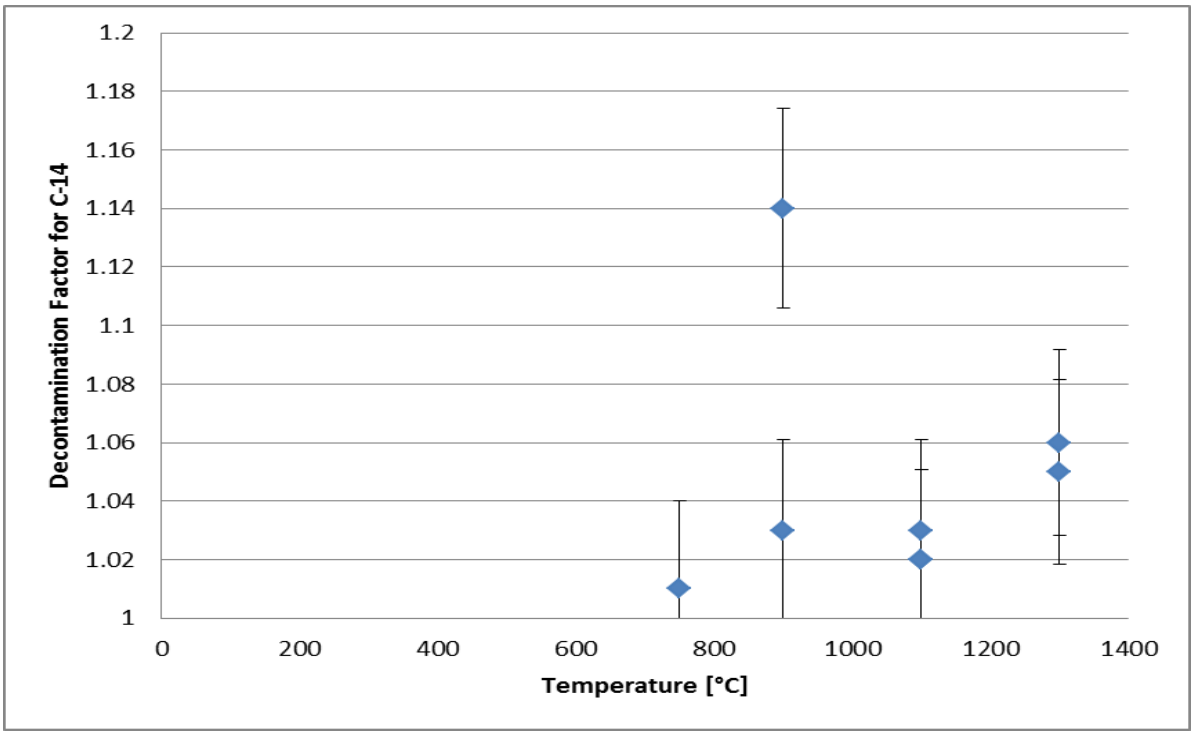

Figure 6.1.2: Decontamination factors of C-14 for Merlin graphite in function of the isothermal treatment temperature

The uncertainties on the decontamination factors have been estimated, starting from the calibration of the LSC equipment with H-3 and C-14 standards, by performing repeated measures.

In Table 6.1.1 it can be noticed that several experiments revealed traces of oxygen in the treatment gases, obtaining de facto a not-ideal inert atmosphere. In a practical situation, an inert atmosphere is really difficult to establish. On the other hand, the presence of small amounts of oxygen could or could not affect significantly the results: the higher the oxygen concentration, the higher the mass loss. In a certain way, “high” or “low” amounts of oxygen are relative so, in general, a threshold cannot be pre-fixed. Experimental results provided in D-4.3.6 revealed that a concentration of 1% O_2 in the adduct gases resulted in high mass losses (>10%), depending on treatment time, temperature and graphite grade. A high mass loss is not preferable for several reasons:

- High mass losses reveal high removal of C-12, which is diluting the removed fraction of C-14; since the most used method for C-14 capture is a precipitation as a carbonate, a high dilution of radiocarbon is producing a higher volume of total “not-concentrated” waste at the end of the process; similar considerations are feasible for isotopic separation. In fact, the intention of a thermal treatment is to remove “selectively” the volatile radionuclides, as much as possible, limiting the corrosion of the graphite matrix.
- Considering, for example, a direct disposal of the graphite, purified from the mobile radionuclides through a thermal treatment, a high mass loss would result in the impairment of the structural characteristics of the interested specimen, leading to easier structural failures and consequently escape of radionuclides.

Following the above-mentioned considerations, a mass loss threshold for an industrial thermal purification process could be fixed to 5%, but it is strongly depending on every single case, so it cannot be assumed as a general constrain. Nevertheless, the mass loss is an important factor that is revealing up to which extent an inert experiment can be considered such.
Another important consideration about the presence of oxygen (or other oxidising agents as water) stands on its effect on the efficiency of radionuclide removal: it is strongly bound with the driving mechanism of H-3 and C-14 removal (more details in chapter 7).
The analysis of the release of H-3 with the temperature can be performed through the Fig. 6.1.1. Not considering in detail, for the moment, the oxygen effect, the Tritium removal shows a raising trend with the treatment temperature (see Fig. 6.1.1). Linking this observation to the identified driving mechanism for Tritium removal, modelled by Atsumi et al [31] and underlined in Chapter 7, high removal efficiencies (and then Decontamination Factors) are expected for temperatures higher than 1200 °C: from this point, the higher the temperature, the shorted is the time necessary to obtain the same results. This finding is in accordance to the Deuterium implantation and thermal treatment investigations performed by N. Toulhoat, N. Moncoffre and Y. Pipon (IPNL-University of Lyon). Hypothetically, it seems to be possible to remove nearly 100% of H-3 in a selective and efficient way from Merlin graphite (a DF of 30 corresponds to a fractional release of about 97%). One has to be careful before generalising this statement for all the different graphite grades and histories.
For what concerns C-14, the temperature shows smaller effects on its removal (not considering the single point out of the trend), as it can be observed in Fig. 6.1.2. The driving mechanisms for C-14 removal are elucidated in Chapter 7. It seems that the higher the temperature, the hgher the C-14 removal. However, the analysis of the DFs cannot provide a clear statement on the temperature effect on Radiocarbon removal, due to the fact that in many cases oxygen was present in the adduct gases and, moreover, the activity uncertainties must be considered. Despite that, an evident fact that needs to be highlighted is the following: low DFs, and consequently low fractional removals of C-14, have been experienced in all the experiments in “inert” gas. Starting from that and considering, in addition, the mass losses, a complete decontamination of Merlin graphite from C-14 is not achievable. The reasons behind this statement cover a wide range of considerations, starting from the origin of the radiocarbon contamination, its distribution inside the graphite matrix, its chemical bonds, the irradiation and storage history, etc. Some preliminary elucidations are reported in D-3.3.2, but more investigations are necessary on different graphite in order to come to a more complete understanding.

6.2. Decontamination Factors for SLA2 Graphite

Sample	Irradiation Conditions		Treat. Gas	Treat. T [°C]	Treating Time [h]		Mass Loss [%]	DF H-3	DF C-14
	Cool. Gas	T [°C]			Heating	Isothermal			
SLA2 9260 V7	CO2	258.5	N_2+0.14 % O_2	1300	0	10.5	0.91	2.87	1.02
SLA2 9260 V19	CO2	258.5	N_2+0.3 % O_2	900	3	5	2.43	1.02	1.03
SLA2 5120 FH1	CO2	391.5	Ar	1000	about 3	40	1.07	1.42	1.02
SLA2 1680 R2	CO2	443	Ar	1000	3.25	10	0.32	1.03	1.01

Table 6.2.1: Overview of the performed thermal treatment experiments with SLA2 graphite in “inert” atmosphere

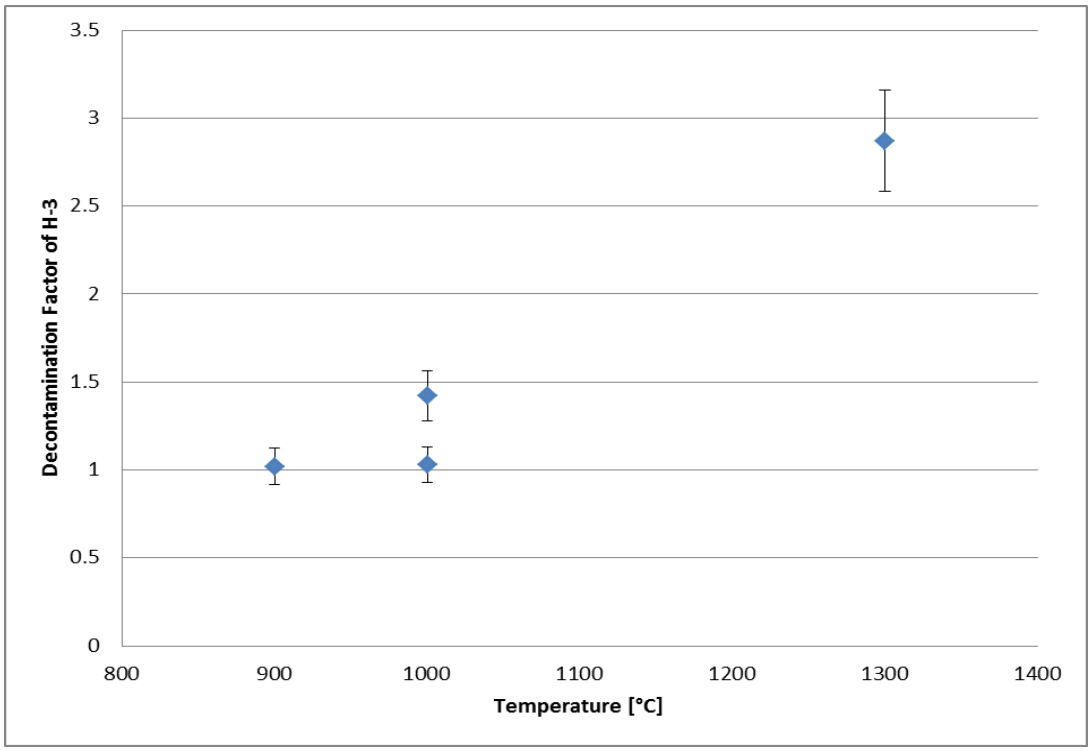

Figure 6.2.1: Decontamination factors of H-3 for SLA2 graphite in function of the isothermal treatment temperature

Similarly to what has been underlined in Section 6.1, obtaining a real inert gas experiment is a challenge. Few Saint Laurent A2 samples were analysed due to several unforeseen problems

with the laboratory equipment. In any case, not only for the case of Saint Laurent Graphite, a statistical evaluation is most of the times difficult to establish due to:

- Small availability of samples
- Consistent amount of variables affecting the results
- Time-consuming procedures and analyses

Despite that, the analysis of Table 6.2.1 and, more in detail, of Figure 6.2.1, reveal an atypical behaviour under inert gas experiments, compared to the one experienced with Merlin graphite. In particular, despite the presence of oxygen in the adduct gases which resulted in mass losses up to 2.43%, the fractional removal (and consequently DF) of H-3 showed to be really low. As observed for Merlin graphite, the trend of H-3-release is a raising function with the temperature, but the efficiency in this case is very small (fractional removals up to 65% at 1300 °C after 10.5 h treatment).

In order to explain this fact, the historical background of the samples has to be taken into account. It is considered a sample from height 1680 mm, irradiation temperature of 443 °C, SLA2 sleeve, irradiation atmosphere CO_2. Even though the neutron fluence experienced by the specimen was not the highest, since it was positioned in the lower part of the reactor core, a radiolytic corrosion took place anyway: a direct measurement of that can be performed through the density analyses of the different samples. Even though the values in Table 6.2.2 are not representative of all the graphite from the same position due to the fact that the measurements were performed with few and small samples, a significant mass loss during operation can be noticed: ~11%. Up to now, the effects of radiolytic corrosion with regards to Tritium (or Radiocarbon) removal have not been investigated. Up to some extent, this phenomenon can be correlated with the effect of oxygen in the adduct gases during a thermal treatment: there is an effect on H-3 removal (better explained in Chapter 7), but it is much weaker than the temperature effect. In the case of radiolytic corrosion, instead, the effect could be relevant even at relatively low temperatures (not sufficient otherwise to remove Tritium), due to the fact that all the open - even micro - pores are filled with CO_2: under neutron irradiation, the corrosion process may occur even in the bulk of the graphite in a “chemical-neutron irradiation regime”, removing a significant part of the mobile Tritium. It is believed, then, linking to the model of Atsumi [31], that the H-3 fraction still present in the graphite at the end of the UNGG reactor´s life is the most immobile one, with the highest activation energy for its removal due to its interlayer/interstitial position (about 4.6 eV, according to Atsumi [31]) . Consequently, a thermal treatment in inert gas with higher temperatures is necessary to decontaminate the graphite from Tritium in this special case. No data is available for temperatures higher than 1300°C, due to the fact that the available equipment was not designed to work at higher temperatures.

Density of Virgin SLA2 sample	Density of SLA2 h.1680mm sample	Density of SLA2 h.5120mm sample
~1.69 g/cc	~1.61 g/cc	~1.51 g/cc

Table 6.2.2: Comparison among sample densities before and after irradiation in the reactor core. Indicative values.

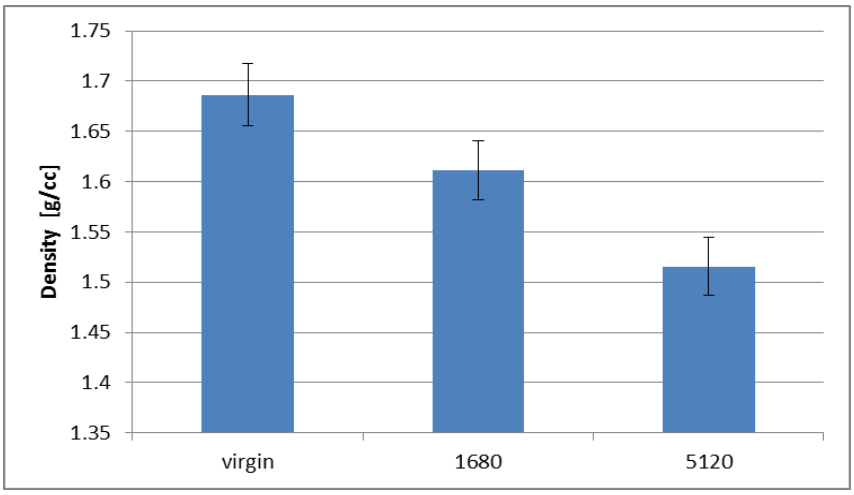

Figure 6.2.2: Comparison among sample densities before and after irradiation in the reactor core at vertical position 1680 mm and 5120 mm, SLA2 sleeve graphite. Indicative values.

For what concerns C-14, temperature shows nearly null effects on its removal (see Fig. 6.2.3). In the case of UNGG graphite, considering that a significant corrosion has been already experienced during reactor operation, it is believed that most of the mobile C-14, probably coming mainly from the neutron activation of N-14, has been already released due to radiolytic corrosion. Consequently the remaining part, supposed to be originated mainly from C-13 (see D-3.3.2 for more details), is probably the most stable fraction, really difficult to remove without oxidising the graphite bulk. In fact, the fractional removal of C-14 showed to be close to the value of the mass loss: by considering the uncertainties on the activity measurements and on the mass determination, it is plausible to state that C-14 is released in all cases lower than 5:1, which is for every carbon atom 5 radiocarbon atoms are released, in a poorly enriched way compared to H-3. This fact indicates that probably C-14 is in a major fraction homogeneously distributed inside the graphite and it is difficult to establish a selective way of removal. Further studies are advisable in order to correlate the removal fractions with the different positions of the samples in the reactor and, consequently, to better discriminate the effects of different variables (irradiation temperature, radiolytic corrosion, neutron fluence, etc.).

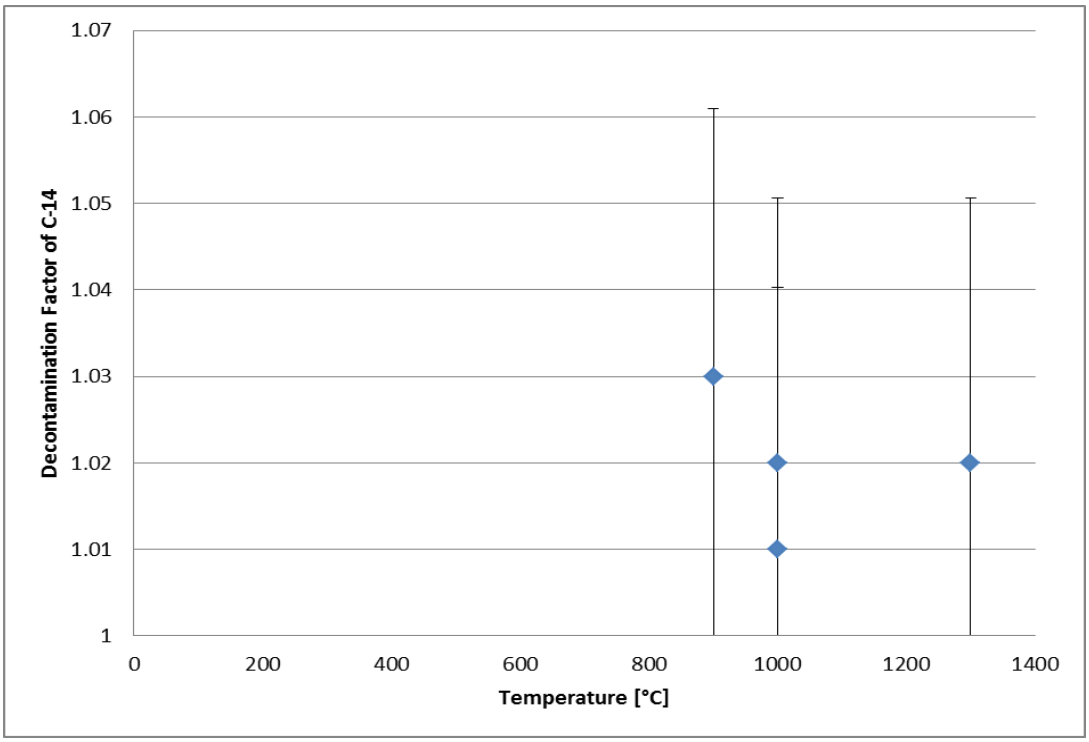

Figure 6.2.3: Decontamination factors of C-14 for SLA2 graphite in function of the isothermal treatment temperature

6.3. Decontamination Factors for Oldbury 2 Graphite

Sample	Irradiation Conditions		Treat. Gas	Treat. T [°C]	Treating Time [h]		Mass Loss [%]	DF H-3	DF C-14
	Cool. Gas	T [°C]			Heating	Isothermal			
Magnox V13	CO2	270	Pure N2	1100	3.75	11	0.14	1.02	1.02
Magnox V15	CO2	270	N_2+0.1 % O_2	900	3	5	0.7	1.05	2.34
Magnox V16	CO2	270	N_2+0.3 % O_2	900	3	5	3.9	1.06	1.1

Table 6.3.1: Overview of the performed thermal treatment experiments with Oldbury 2 graphite in "inert" atmosphere

A similar behaviour to the SLA2 graphite has been experienced with the Oldbury 2 graphite. The Tritium release is quite limited (see Fig. 6.3.1 and Tab. 6.3.1): a possible explanation of such behaviour is similar to the considerations performed for SLA2 graphite. Some preliminary calculations of the mass loss during operation revealed up to 40% mass loss; in other words, a strong corrosion took place during operation and it is reasonable to expect a significant removal in-situ of C-14 and possibly H-3. No detailed studies are available in order to better understand the effect of radiolytic corrosion with regards to H-3 and C-14 removal. In the case

of C-14 removal, not considering the single point out of the trend in Fig. 6.3.2, the decontamination factor is insignificant. The point out of the trend could represent a case of surface contamination: thermal treatments with small presence of oxidants in the adduct gases showed an excellent removal of surface contamination. The history of the graphite samples, inside the reactor but not only, is a decisive factor in order to understand the behaviour under thermal treatment first and storage conditions later.

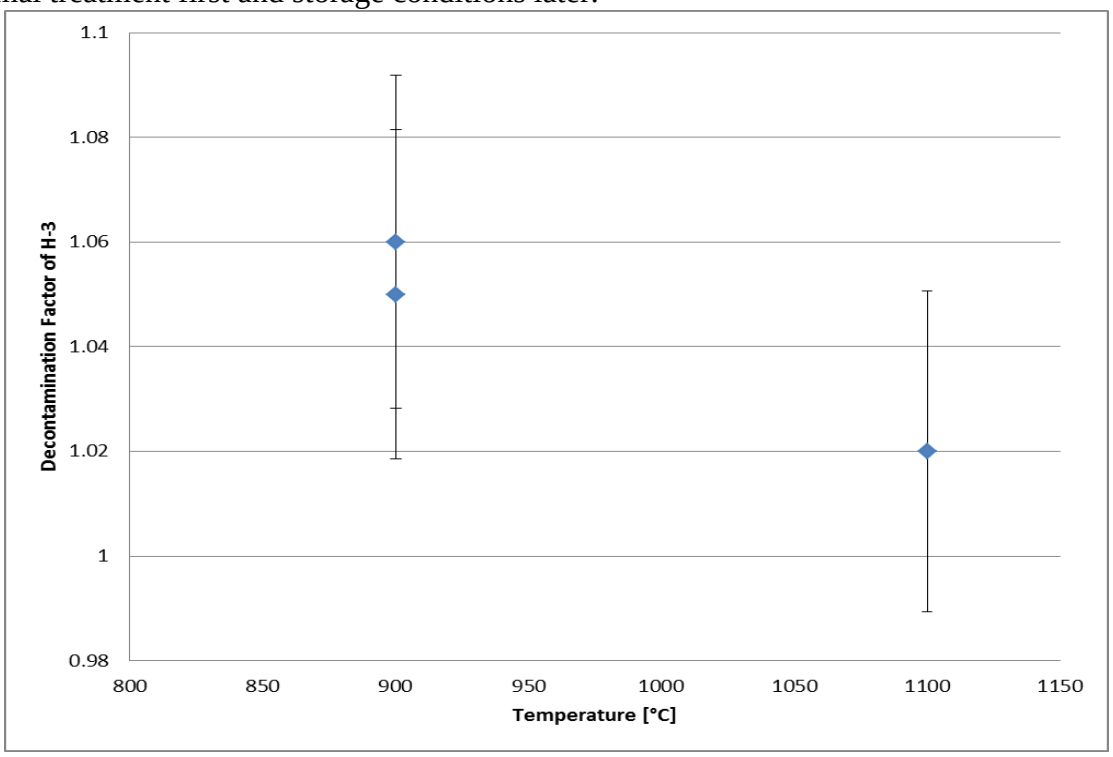

Figure 6.3.1: Decontamination factors of H-3 for Oldbury 2 graphite in function of the isothermal treatment temperature

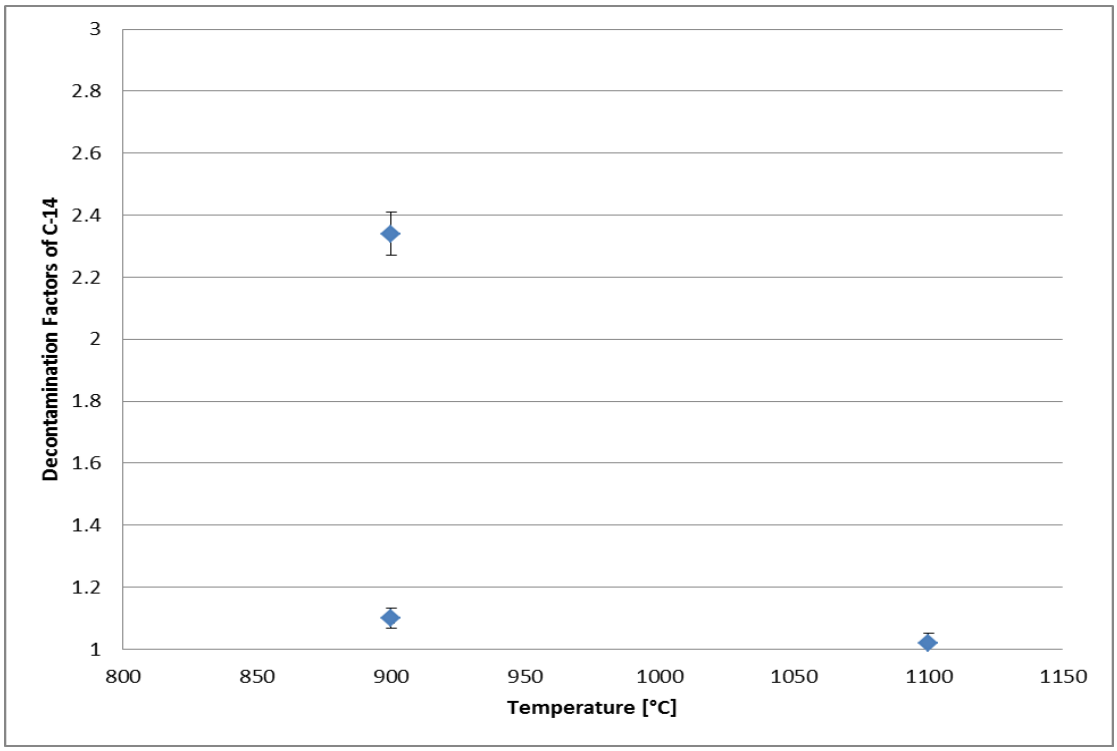

Figure 6.3.2: Decontamination factors of C-14 for Oldbury 2 graphite in function of the isothermal treatment temperature

6.4. Decontamination Factors for AVR Graphite

Sample	Irradiation Conditions		Treat. Gas	Treat. T [°C]	Treating Time [h]		Mass Loss [%]	DF H-3	DF C-14
	Cool. Gas	T [°C]			Heating	Isothermal			
AVR Powder	He	Unkn. – Medium to High	Ar	1060	-	15	1.24	1.4	1.1
R3, AVR Refl.	He	Unkn. – Medium to High	N2	900	-	7	0.60*	1.08	1.12
R5, AVR Refl.	He	Unkn. – Medium to High	N2	900	-	7	1.3*	1.06	1.08
R4, AVR Refl.	He	Unkn. – Medium to High	N2	1280	-	7	1.6*	1.28	1.18
R9, AVR Refl.	He	Unkn. – Medium to High	N2	1280	-	7	2.3*	5.56	1.26

Table 6.4.1: Overview of the performed thermal treatment experiments with AVR graphite in "inert" atmosphere. (* mass losses are only estimated due to the particular method applied, without removing the sample from the treatment chamber)

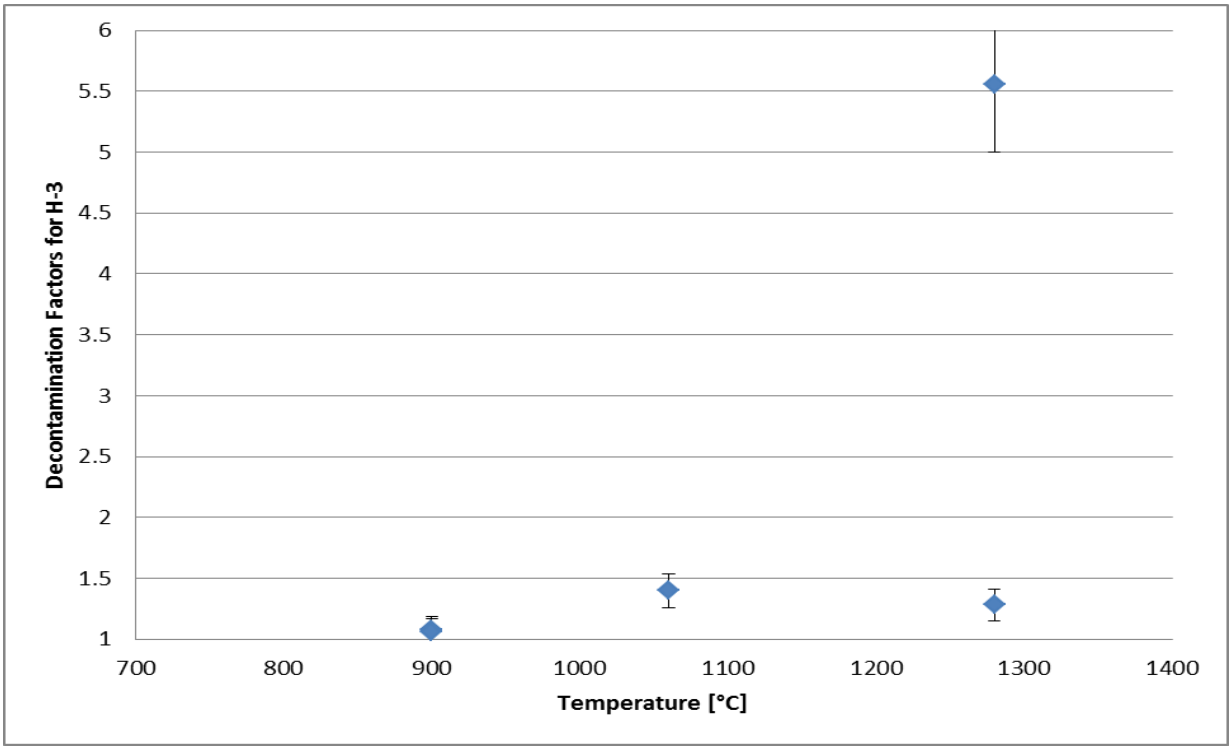

Figure 6.4.1: Decontamination factors of H-3 for AVR graphite in function of the isothermal treatment temperature

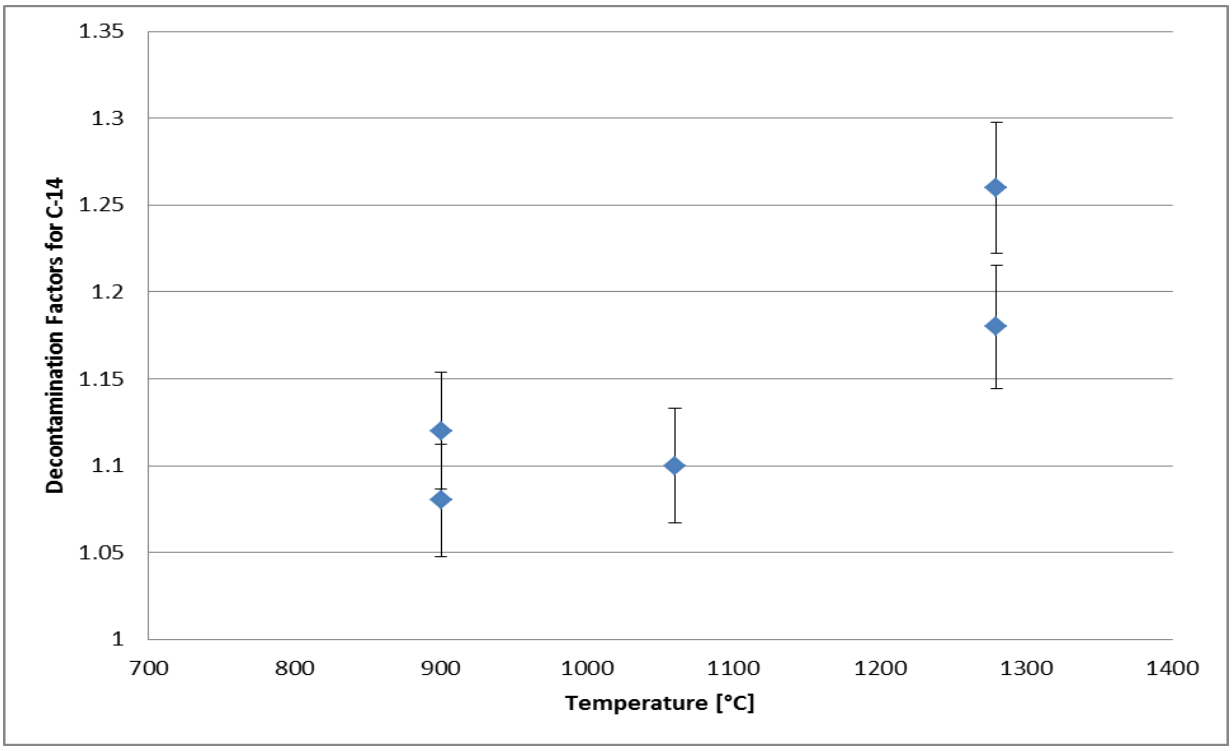

Figure 6.4.2: Decontamination factors of C-14 for AVR graphite in function of the isothermal treatment temperature

In the case of AVR graphite, a particular behaviour in a middle way between Merlin and UNGG/Magnox graphite is observed. For example, tritium is removed up to 27% (DF=1.4) after 15 hours of treatment at 1060°C: this difference can be explained by the different operational conditions. The average gas-outlet temperature of the AVR was about 950°C [36], in Merlin reactor the operational temperature of thermal columns was the ambient one and in the UNGG/Magnox reactor the temperature was in the middle, depending on the sample´s position in the core, up to 446°C. Nevertheless, in Fig. 6.4.1 it is possible to observe that a raising trend of Tritium release with the temperature is still present, even though the removed fraction is much lower than the one in the case of Merlin graphite. Also in the present case, the traceability of the samples represented a problem, so the temperature and neutron dose is not known precisely.
Concerning the C-14 release, observable in Fig. 6.4.2 it can be underlined, also for the AVR graphite case, that only a small fraction of radiocarbon can be removed with a continuous, single step, thermal treatment under inert gas.

6.5 Removal of other radionuclides

In the present work we focused mainly on H-3 and C-14 but it has not to be neglected that other radionuclides, as Cl-36, are very mobile in the environment, so a selective removal would be preferred. The problem related to Cl-36 is its very low specific activity (10-100 Bq/g in general): experiments performed with samples in the order of 1 g result in very low activities and Cl-36 beta spectra showed to be comparable with the background, with the equipment used at FZJ. However, several SIMS analyses (some of them are reported in D-3.3.2) performed on virgin massive samples revealed the effectiveness of a thermal treatment in inert atmosphere, with a Cl-37 and Cl-35 removal up to 70% and 90% respectively in the particular case of Saint Laurent A2 graphite. Similar results were obtained with virgin AVR graphite. The link between virgin and irradiated graphite goes through many influencing factors: final remarks cannot be done at the present state, but the above-described results give a hint about Chlorine behaviour under thermal treatment. However, the temperature-dependent removed fraction still needs to be deeper investigated. Other authors reported removal up to 30% for implanted Cl-37 on graphite, with a peak around 350°C followed by a shoulder at 450 °C [51]; it was reported, through XPS analyses, that the removed part was mainly the inorganic Chlorine (as HCl) [52]. It is hypothesised that, depending on the temperature, neutron fluence and operational conditions, part of the most labile Cl-36 is probably removed during operation.
Other non-volatile radionuclides, like Co-60, Eu-154/155, Ba-133, Cs-134/137 showed to be retained in an excellent way in SLA2 graphite during thermal treatment. In general, considering also other nuclear graphite, the only isotope that showed a partial removal at temperatures higher than 1000°C was Cs-(137), with a fractional removal up to 20-35%, depending on the case.

6.6 Overview of Decontamination Factors for Different Graphite

A summary view of the different decontamination factors for H-3 and C-14 related to the different graphite (AVR, Merlin, Oldbury 2, SLA2) can be observed in Figs. 6.6.1 and 6.6.2a-b. In general, it is possible to observe higher Tritium releases than Radiocarbon ones, due to the driving mechanisms that are governing the respective removals. A total removal of Tritium is theoretically achievable, but it strongly depends on the history of the graphite in question: for example, an inert gas treatment at 1300°C for 10 hours could remove nearly the total amount of H-3 from Merlin graphite, a lower fraction (less than half) from the AVR graphite and small percentage from SLA2 and Oldbury 2 graphite (compare Fig. 6.6.1). Even excluding the point out of the trend in Fig. 6.6.2-a, there is not a clear dependence of C-14 removal with temperature but, in general, a low fractional release can be expected in all cases. The point out of the trend in the case of Oldbury 2 could be explained with a surface contamination of the sample, as it has been proven with some autoradiographic analyses: a surface contamination is relatively easy to remove since that specific location is the first one being attached by any oxidising agent present as impurity in the adduct gases during thermal treatments. It has to be underlined that, despite the small oxygen ingress during the thermal treatment, the release of tritium seems to be not significantly affected, since the temperature dependence is quite clear, linking the Tritium behaviour to a diffusion-like process [31]; on the other hand, the release of radiocarbon is strongly bound with the presence of oxidising agents in the treatment gas: it is probable that the difficulties identified on controlling the experimental boundary conditions have influenced the Radiocarbon removal results. From this point of view, mass losses lower

than 0.5-1% could be a good quality indicator for the effective tightness of the equipment during the treatments.

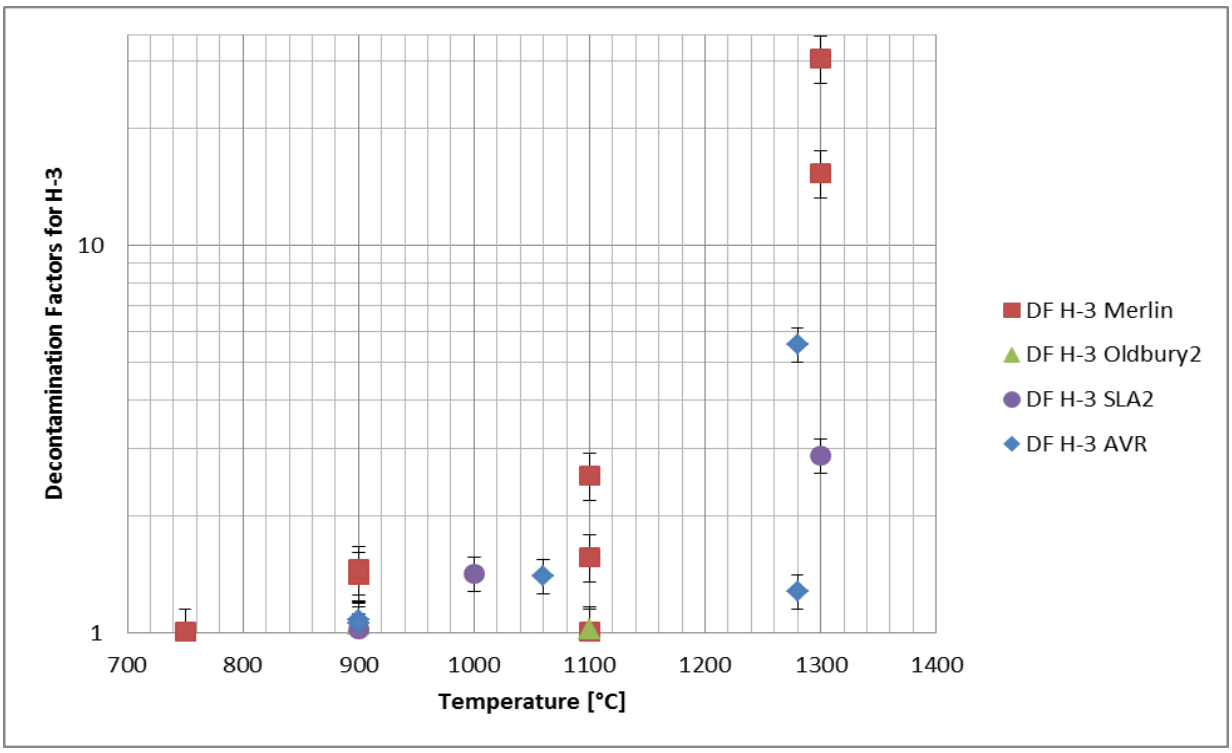

Figure 6.6.1: Decontamination factors of H-3 for different graphite in function of the isothermal treatment temperature

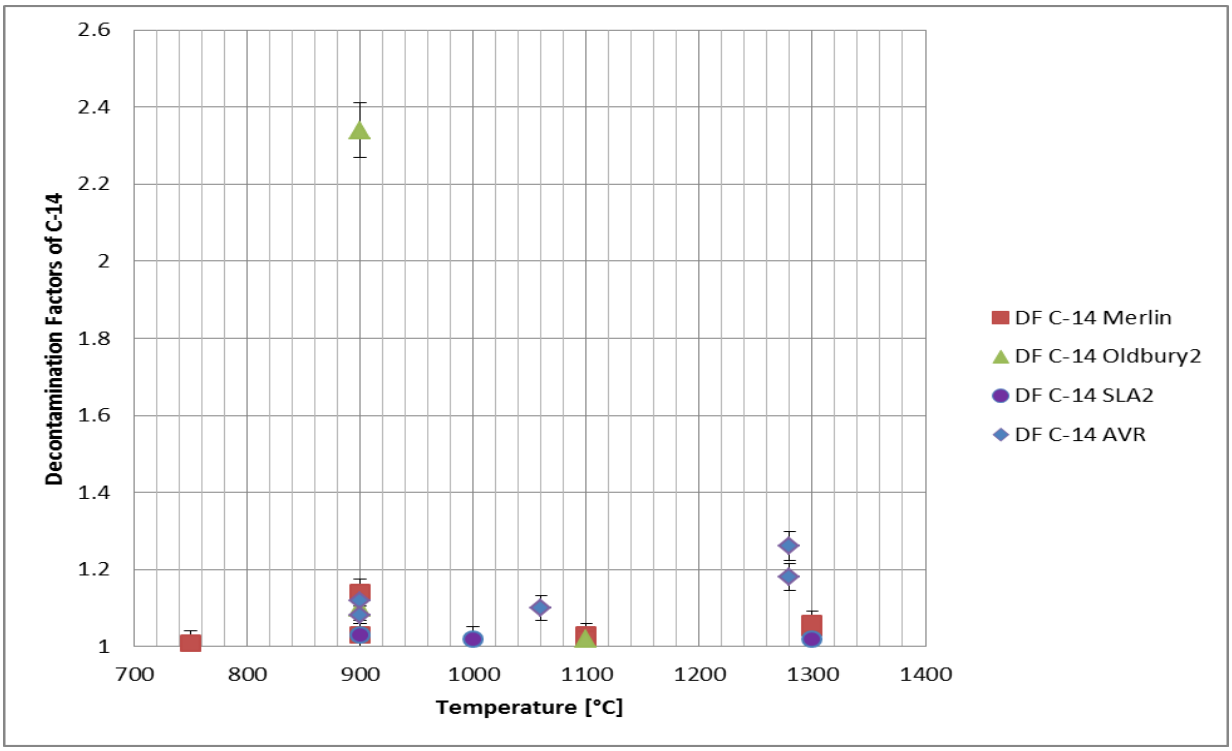

Figure 6.6.2-a: Decontamination factors of C-14 for different graphite in function of the isothermal treatment temperature

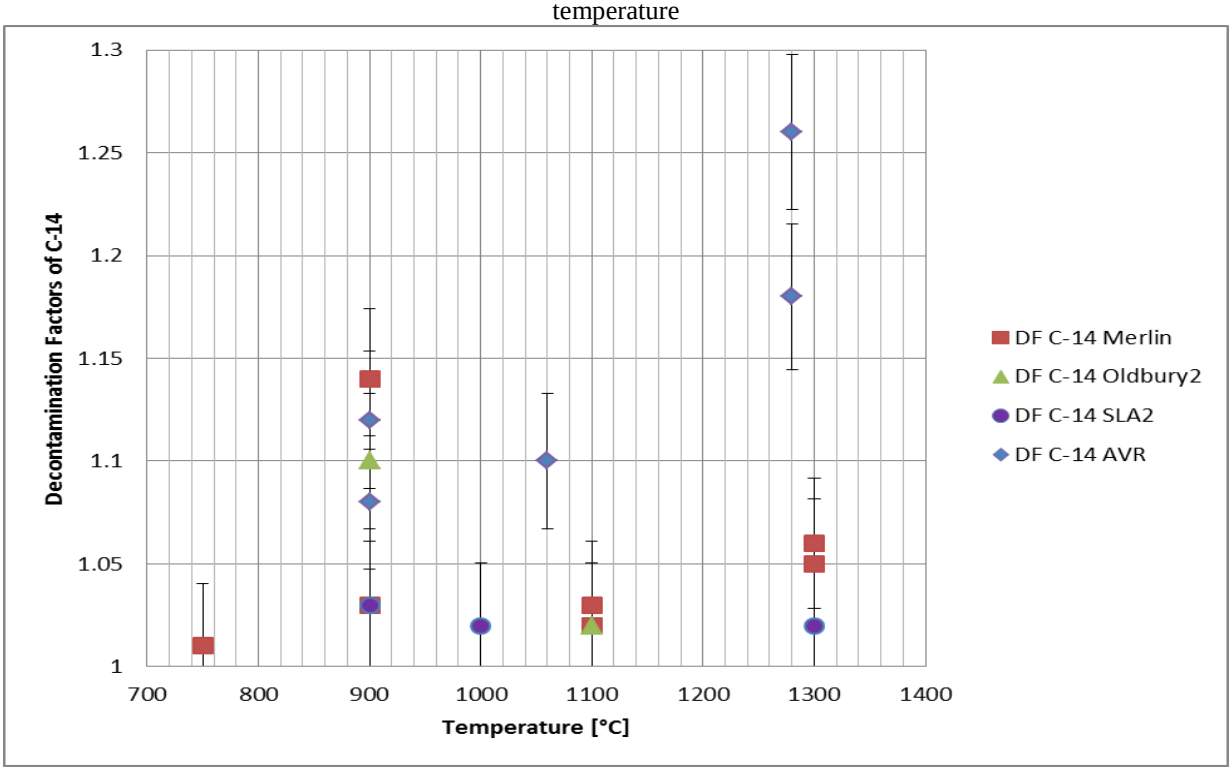

Figure 6.6.2-b: Decontamination factors of C-14 for different graphite in function of the isothermal treatment temperature

7. Interpretation of Results

7.1 Release Mechanisms and Kinetics

Treatment of neutron-irradiated nuclear graphite is not only a possibility for industrial waste management but also a possibility to study the binding relations and the release mechanisms of radionuclides in neutron-irradiated nuclear graphite. With this information, industrial processes for nuclear waste management can be developed.
A suitable method to study the binding relations and the release mechanisms of radionuclides in neutron-irradiated nuclear graphite is a thermal treatment in inert gases. The use of inert gases inhibits the oxidation of the graphite matrix: only pyrolysis processes or reactions of adsorbed gases can occur. Therefore, the release kinetics of radionuclides from neutron-irradiated nuclear graphite can be investigated.

7.1.1 Release of Tritium

7.1.1.1 Background

A theoretical model of Katayama [41] showed that tritium trapped on the graphite surface of a small particle (with diameter in the order of um) can be removed rapidly even at room temperature, through isotopic exchange reaction with water steam. In the model, even a water partial pressure of 10 Pa could be sufficient to obtain the same removal factors as in the case of a thermal treatment at 900 °C with 100 Pa hydrogen stream. However, tritium trapped the graphite showed to be released only at temperatures higher than 1000 K.
The high mobility of trapped tritium, occurring only at high temperatures, has been discussed previously in another theoretical model from Fromherz at al. [40]
Atsumi et al.[41] developed and validated a model to describe the behaviour of hydrogen in graphite, before and after neutron irradiation, represented in a schematic way in Fig. 7.1.1.

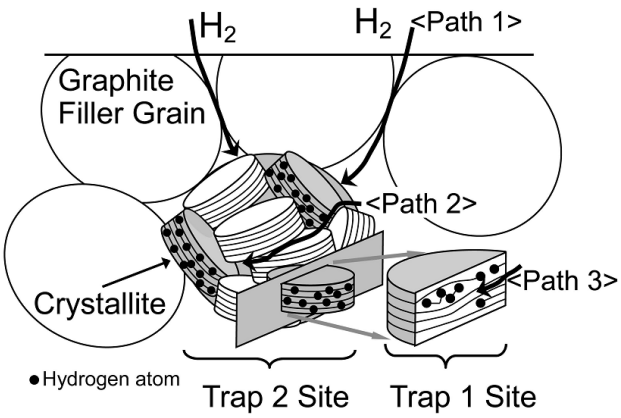

Figure 7.1.1: Model of Atsumi for Hydrogen trapping sites and transport in graphite [31,42]

The model identifies two trapping sites for hydrogen in graphite: interstitial cluster loop edge sites (trap 1) with an enthalpy of 4.6 eV and carbon dangling bonds at edge surfaces of crystallites (trap 2) with an adsorption enthalpy of 2.6 eV. The trap 2 is predominant in unirradiated graphite and it represents normally 80% of the total. In addition, neutron

irradiation showed to increase hydrogen retention up to 100 times more than that in unirradiated graphite, with a prominence of trap 1 sites.[31]
Concerning the hydrogen absorption mechanism, similar but reversed than the desorption one, at the initial stage hydrogen can reach a graphite filler grain through open pores (path 1 in Fig. 7.1.1); then the molecules dissociate into atoms and migrate into a filler grain along graphite crystallites in a sequence of trapping and detrapping (path 2 in Fig. 7.1.1); this stage can be reproduced as a diffusion-controlled process. The last stage of hydrogen migration should be an intercalate diffusion between graphite lamella (path 3): this stage is controlled by the detrapping reactions at trap 2. Trap 1 sites revealed experimentally to be more stable than trap 2, during high temperatures thermal treatments (1550 °C). On the other hand, the desorption process should be controlled by detrapping from Traps 1 and 2, due to a higher energy of trapping (2.6 and 4.6 eV respectively) than the activation energy of diffusion (about 1.3 eV) [44]. More in detail, some Thermal Desorption Spectra of hydrogen from graphite showed two peaks, respectively at 735 K and 1220 K: such results could be interpreted with a diffusion-controlled process. However, the fundamental process of desorption for both peaks would be recombination but, due to the long path to the surface, hydrogen will be successively trapped and detrapped, resulting in an apparent diffusion as the dominant process of desorption.[43]
Even though TDS spectra showed two peaks, it is believed they are actually three: the desorption of hydrogen with an activation energy of 1.3 eV is assumed to be a recombination-controlled process. [43]
In conclusion, three kinds of desorption processes are representative of hydrogen desorption in graphite.
Many experiments on different graphite grades [1,2] showed that tritium release is, in general, increasing with the temperature. In particular, Fachinger et al.[1] observed a fast initial release of tritium under thermal treatment in argon atmosphere, connected with the desorption from the active superficial sites: tritium desorption was not limited by diffusion in pores; however it was supposed that higher temperatures would have resulted in higher fractional releases. Tritium release from graphite started from 800 °C, increasing with temperature.
From the previous theoretical and experimental findings, it seems that tritium can be released by implying high temperatures.

7.1.1.2 Merlin Graphite

In Figure 7.1.2 the release of tritium from Merlin graphite in inert gases at different temperatures is shown. Several massive graphite samples from the thermal column of the Jülich Material Test Reactor “Merlin” were used (trepanned plug specimens; diameter: 8 mm, length: 37…50 mm, mass: 3-4 g). One can see that the release of tritium depends on the treatment temperature. At 1300 °C, 93.6% of the tritium inventory of the graphite sample was removed within about 10 hours, whereas the mass loss of the graphite matrix was negligible (< 1%).

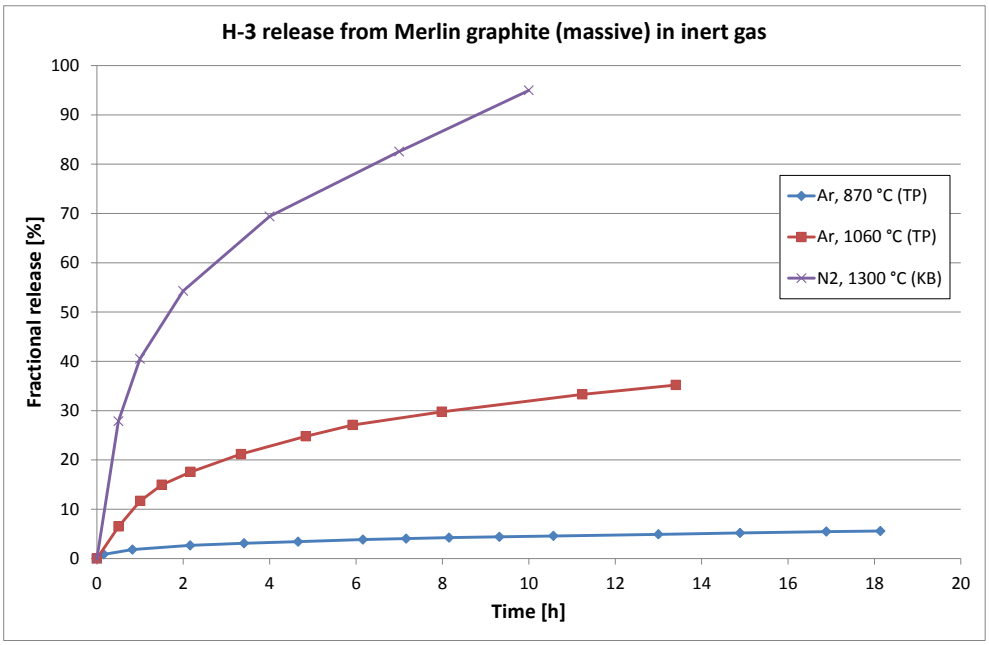

Figure 7.1.2: Release of tritium in inert gases at different temperatures

The release of tritiated water (HTO) from Merlin graphite in nitrogen at 1100 °C plotted as diffusion reaction is shown in Figure 7.1.3. The fit of the data points is a straight line with a correlation factor of 0.9933. This is an indication of a predominant apparent diffusion reaction; it can be explained with a molecular migration process, as stated by Atsumi, in which hydrogen migrates along graphite crystallites in a sequence of trapping and detrapping process: this stage can be reproduced as a diffusion-controlled process [31].

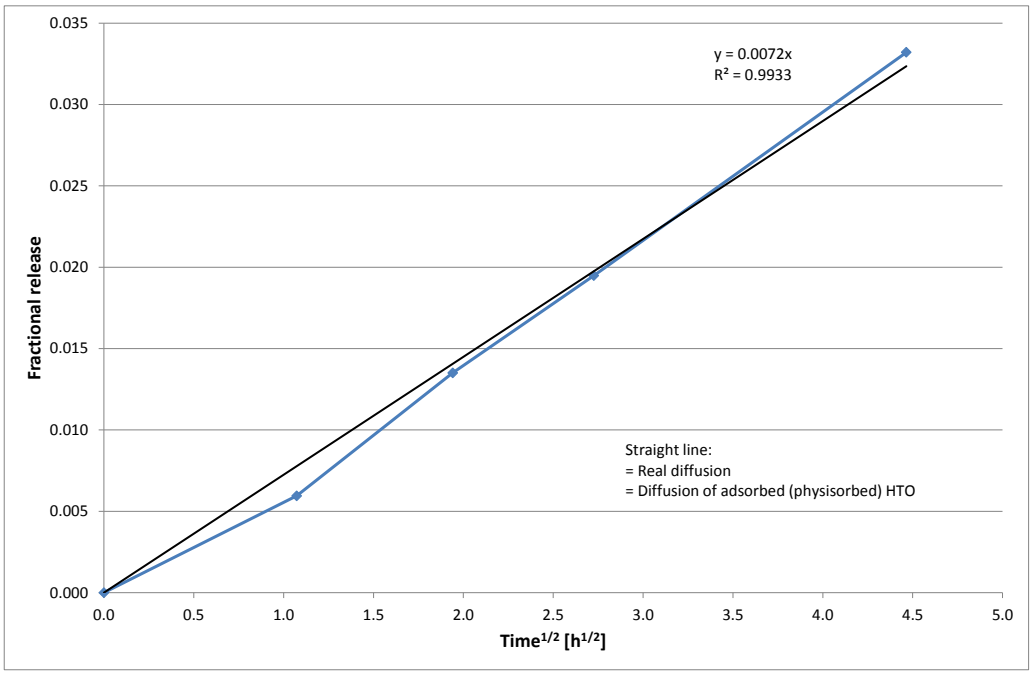

Figure 7.1.3: Release of HTO from Merlin graphite in nitrogen at 1100 °C plotted as diffusion reaction

The release of tritiated hydrogen (HT) from Merlin graphite in nitrogen at 1100 °C seems to be mainly a diffusion reaction. This can be seen in Figure 7.1.4. The fit of the data points is only scarcely a straight line with a correlation factor of 0.9646. There are other reactions behind the diffusion reaction. Such a reaction could be the formation of HT from pyrolysis processes. Anyway, the predominant reaction is an apparent diffusion because the tests performed for first or second order reactions provided worse results, as can be seen in Figures 7.1.6 and 7.1.6. Atsumi [33] and Denisov [34] reported that most of the hydrogen is released out at temperatures around 1400 K (1127 °C), in agreement with what has been observed here.

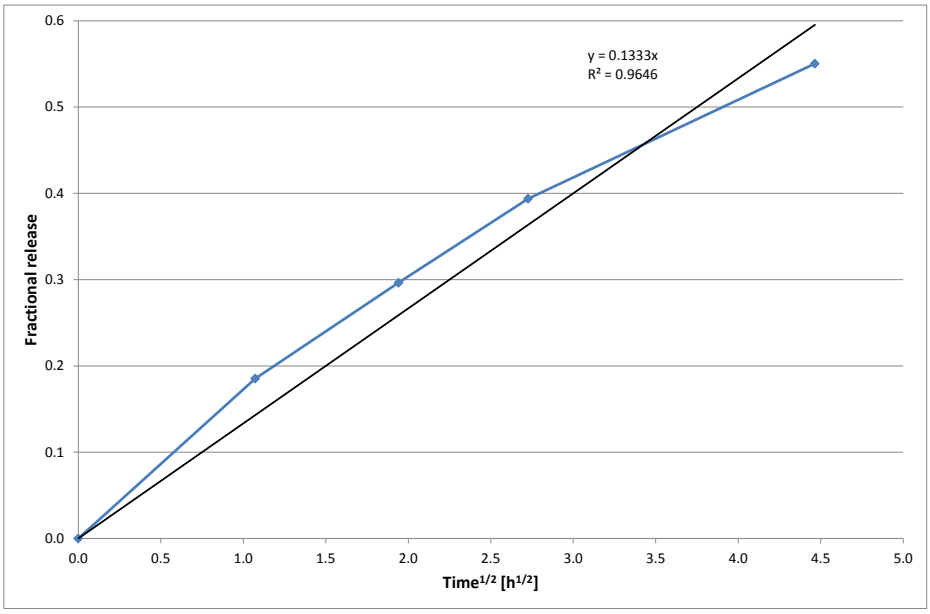

Figure 7.1.4: Release of HT from Merlin graphite in nitrogen at 1100 °C plotted as diffusion reaction

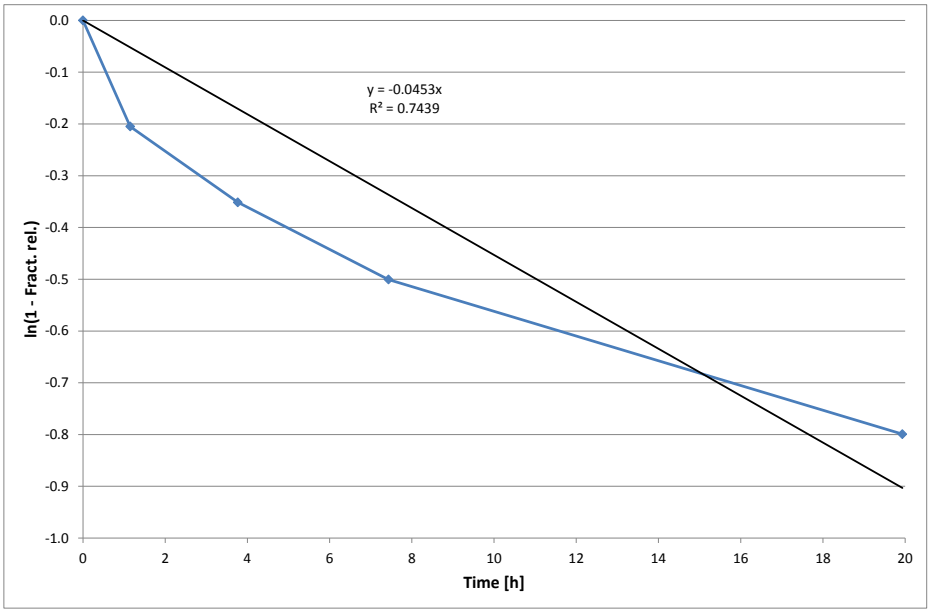

Figure 7.1.5: Release of HT from Merlin graphite in nitrogen at 1100 °C plotted as first order reaction

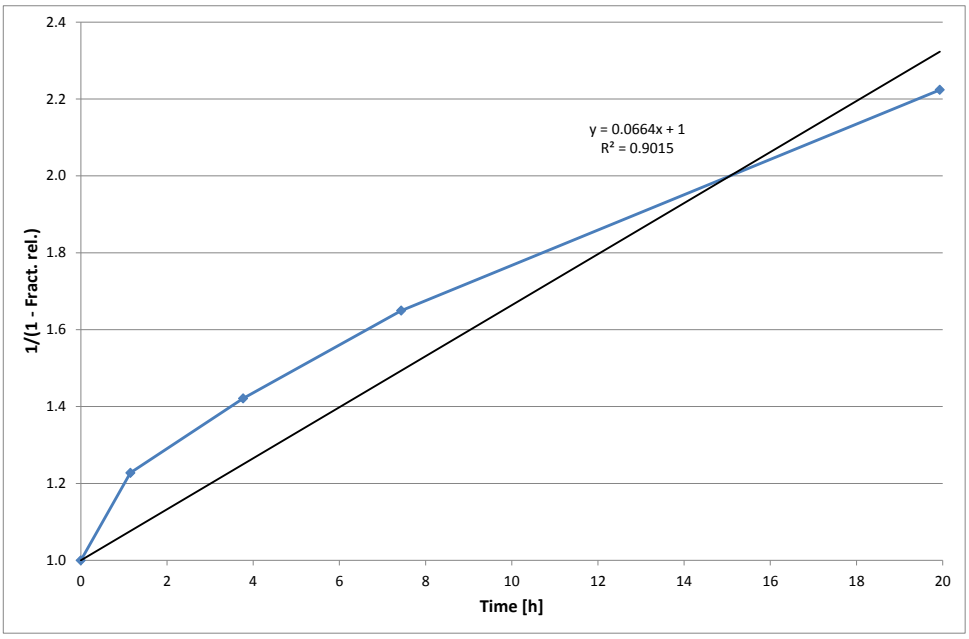

Figure 7.1.6: Release of HT from Merlin graphite in nitrogen at 1100 °C plotted as second order reaction

The Tritium release kinetics, so, best corresponds to a diffusion reaction, in accordance with the modelled release mechanism previously described. A first order or a second order reaction is not applicable. However, the graph for a diffusion reaction (fractional release vs. square root time) is not linear, as can be seen in Figures 7.1.3 and 7.1.4. It is reasonable to assume that diffusion is not the only reaction which is taking place and leading to a release of tritium. As tritium must be bound within the graphite matrix in a certain way, additional energy is necessary to remove it from its binding places. Such additional reactions could be: desorption of tritiated water (HTO) and pyrolysis of tritiated hydrocarbons (C─T or C─OT). In addition, the presence of small amounts of oxygen in the adduct gases could favour the oxidation of HT to HTO. An indication that there are different reactions is given by the observed inversion of the release ratios of HT and HTO: at 866 °C the release of HTO is predominant whereas at 1063 °C the release of HT is predominant. This behaviour is comprehensible by considering that at lower temperatures more HTO is released because desorption requires less energy and that at higher temperatures more HT is released because pyrolysis requires more energy. However, the dependence of HTO/HT ratio with temperature needs more investigations to be confirmed, depending also on the graphite grade.

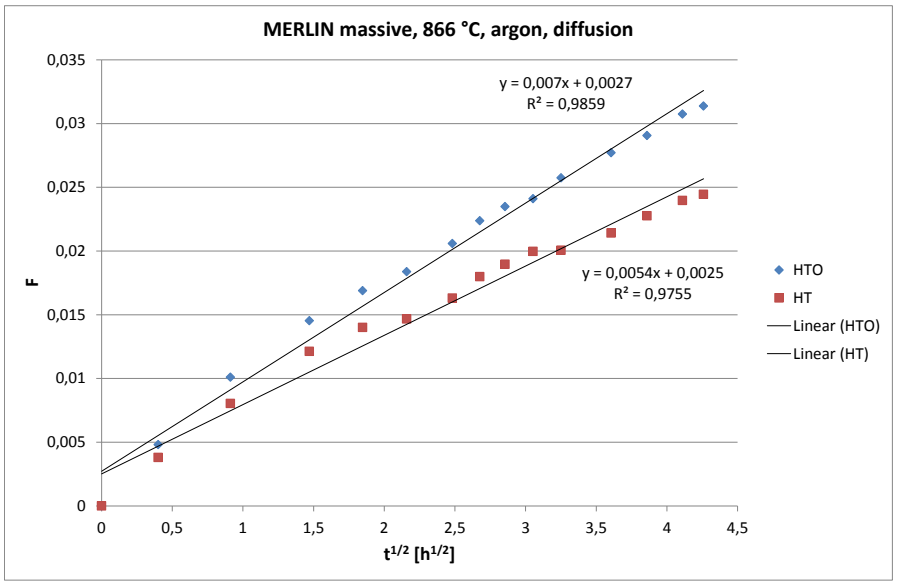

Figure 7.1.7: Release of tritium in argon at 866 °C plotted as diffusion reaction.

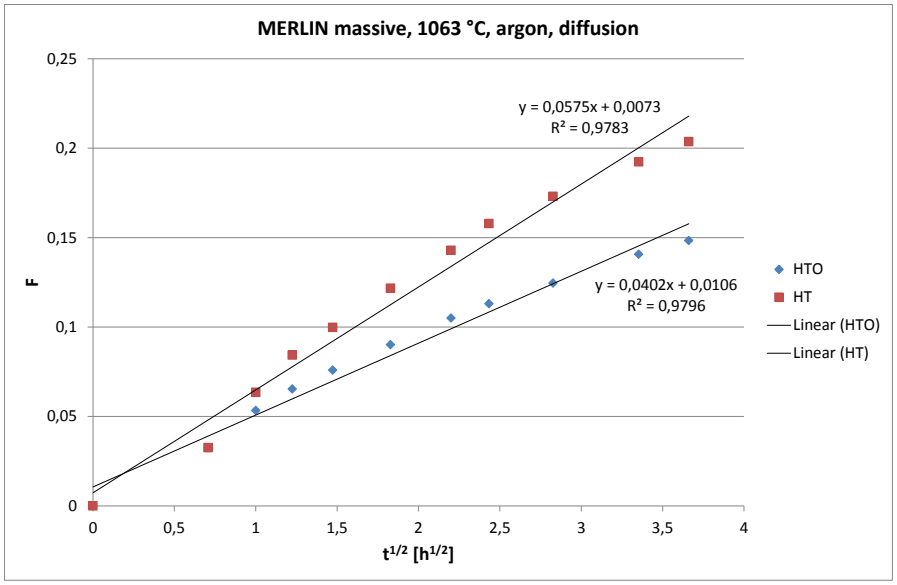

Figure 7.1.8: Release of tritium in argon at 1063 °C plotted as diffusion reaction.

The data from Figures 7.1.7 and 7.1.8 can be used to estimate the activation energy for the apparent diffusion reaction (diffusion plus desorption or pyrolysis). Diffusion is described by the following equation:

$$\frac{\partial c}{\partial t} = D\Delta c \tag{7.2}$$

where D is the diffusion coefficient. The solution of the differential equation presuming spherical pore geometry results in

$$F = \sqrt{\frac{36D't}{\pi}} \tag{7.3}$$

where F is the fractional release of the diffusing material and D' the reduced diffusion coefficient ($D' = D/R^2$, R = diffusion radius). The reduced diffusion coefficient is controlled by temperature according to

$$D' = D'_0 \cdot e^{-\frac{E_D}{k_B T}} \tag{7.4}$$

where E_D is the activation energy for diffusion and k_B the Boltzmann constant. Determining the reduced diffusion coefficient for two temperatures, the activation energy can be calculated by

$$E_D = k_B \cdot \frac{T_1 \cdot T_2}{T_2 - T_1} \cdot \ln\left(\frac{D'_2}{D'_1}\right) \tag{7.5}$$

The tritium releases plotted in Figures 7.1.7 and 7.1.8 are divided into the chemical forms HT and HTO. Therefore, activation energies can be calculated for the release of HT and HTO. The apparent activation energy for the release of tritium as HT amounts to 3.15 eV and as HTO to 2.33 eV. The average amounts to 2.74 eV. This value is in good agreement with Fischer et al. [7] which found 2.78 eV. On the other hand, Atsumi [31] found 2.6 eV. In addition, Atsumi [32] stated that the cristallite-boundary diffusion activation energy of 1.3 eV can be considered only when the trapping effect can be negligible, i.e. when the hydrogen is not significantly trapped e.g. at the edge surfaces of cristallites. The difference between HT and HTO could be explained by different desorption/formation energies of these diffusing species: HTO is possibly only adsorbed on the surface of the graphite particles whereas HT must be formed by pyrolysis. In general, desorption energies are lower than pyrolysis energies. However, more investigations are necessary to better understand whether Tritium is released initially as HT and then partially oxidized to HTO or HT and HTO are formed directly at the sample side, without further significant secondary reactions.

7.1.1.3 AVR graphite

In the AVR the operational temperatures were rather high (outlet temperature of 950°C[45]) and some of the defects caused by neutron irradiation could be annealed. It is reported in a number of publications that the mobility of hydrogen molecules in undamaged graphite is rather slow [7, 37, 38]. The other reason may be related to the fact that under the high temperature conditions of AVR tritium diffuses inside graphite grains [39, 7], so the fraction that is still present in the graphite is more difficult to be removed due to its more stable nature. Another factor that could influence the more difficult removal of H-3 is the neutron fluence: the higher it is the more are the interstitials/inter-layer H-3 atoms, more stable than the ones laying on the grains boundary (see model of Atsumi [31] for more details). A first calculation of the diffusion coefficient of H-3 for some cases is reported in Table 7.1.1: it can be observed how D is much lower in the AVR case than in the Merlin graphite.

Type of graphite	Temperature, °C	Diffusion coefficient D, cm^2/s^{-1}
Merlin	870	5.70E-14
Merlin	970	7.40E-13
Merlin	1060	6.19E-12
AVR	1060	1.70E-12

Table 7.1.1: Diffusion coefficients of H-3 at different temperatures for Merlin and AVR graphite [2]

7.1.1.4 Saint Laurent A2 and Oldbury2 graphite

The identification of the driving release mechanisms from the SLA2 and Oldbury2 graphite is much more complex than in the previous cases: the number of variables affecting the graphite behaviour under thermal treatment is considerable, so it is difficult to separate the different effects and histories (temperature, neutron fluence, radiolytic corrosion, etc.). It has to be underlined that the CO2-cooled graphite has already experienced significant mass losses (up to 40%) during the reactor operation, leading to the removal of the most mobile fractions of both H-3 and C-14. For this reason, it is believed, following the results of the experiments performed in FZJ, that the most stable H-3 (as interstitials for example) and the most stable C-14 (coming probably from the activation of C-13) are embedded in the graphite matrix in a quite stable way, much more than in the other cases here reported.

The release of HTO and HT from Magnox Oldbury 2 graphite in nitrogen at 1100 °C plotted as diffusion reaction is shown in Figures 7.1.9 and 7.1.10, respectively. In both cases, the fit of the data points is a straight line with a correlation factor of 0.9978 and 0.9954, respectively. These release reactions are clearly diffusion reactions.

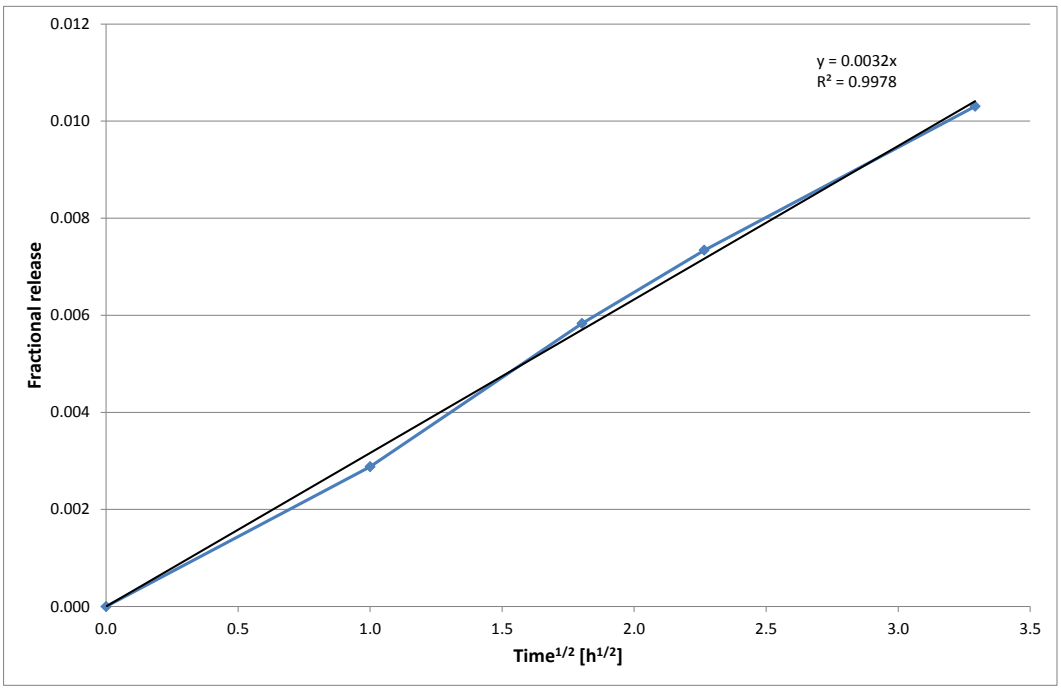

Figure 7.1.9: Release of HTO from Magnox Oldbury 2 graphite in nitrogen at 1100 °C plotted as diffusion reaction.

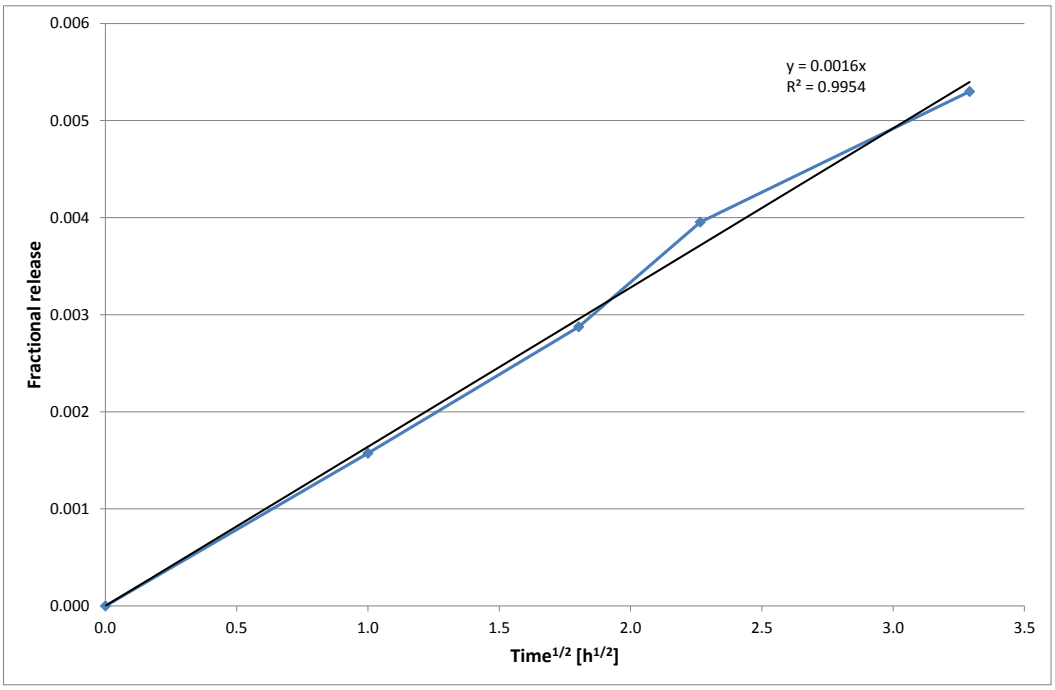

Figure 7.1.10: Release of HT from Magnox Oldbury 2 graphite in nitrogen at 1100 °C plotted as diffusion reaction

7.1.1.5 Effects of Small Amounts of Oxygen on Tritium Removal

As reported in the previous sections, obtaining absolute inert conditions is quite difficult. The release mechanism for H-3 seems to fit well with the model of Atsumi [31], i.e. a simil-diffusion driven mechanism. Considering then the additional presence of oxygen, it is interesting to understand the related effects, considering small quantities in the adduct gases (higher quantities of oxygen have been discussed in D-4.3.6). A "standard" experiment is repeated with graphite coming from similar positions of the Merlin reactor´s thermal column: in the first one a relatively low amount of oxygen was introduced (around 1400 ppm), while in the second one a higher amount was adopted (estimated around 3700 ppm). It is reasonable to expect, with equal treatment´s boundary conditions (e.g. temperature, heating rate, gas flow, etc.), higher mass loss with higher oxygen concentrations: it was measured, in fact, a mass loss of 0.9% against 2.43% for the same treatment time. A direct consequence of an enhanced corrosion of the graphite bulk, due to the presence of oxygen, is a lower selectivity on the removal of e.g. Tritium. Nevertheless, not considering the mass loss, taking into account the uncertainty on the measurements, there are small differences on the two curves: this fact can lead to thinking that H-3 removal is not much influenced by the presence of oxygen (see Fig. 7.1.11 for comparison).
Another experiment, performed in previous times in inert gas, showed a sudden ingress of oxygen (of unknown amount) resulting in visible changes in the release curves (see Fig. 5.1.1): the increase in the on-line tritium release curve showed to be small compared to the similar, but pronounced, effect on radiocarbon removal (see Fig. 5.1.5).
In conclusion, it can be stated that small amounts of oxygen in the adduct gases are not effective from the point of view of H-3 removal, considering a continuous thermal treatment

with steady conditions; on the contrary, the increased corrosion of the graphite bulk results in lower enrichment of the removed H-3 and, consequently, in a lower efficiency of the selective extraction process. The driving removal mechanism seems to be in agreement with a diffusion-like one, as modelled by Atsumi [31].

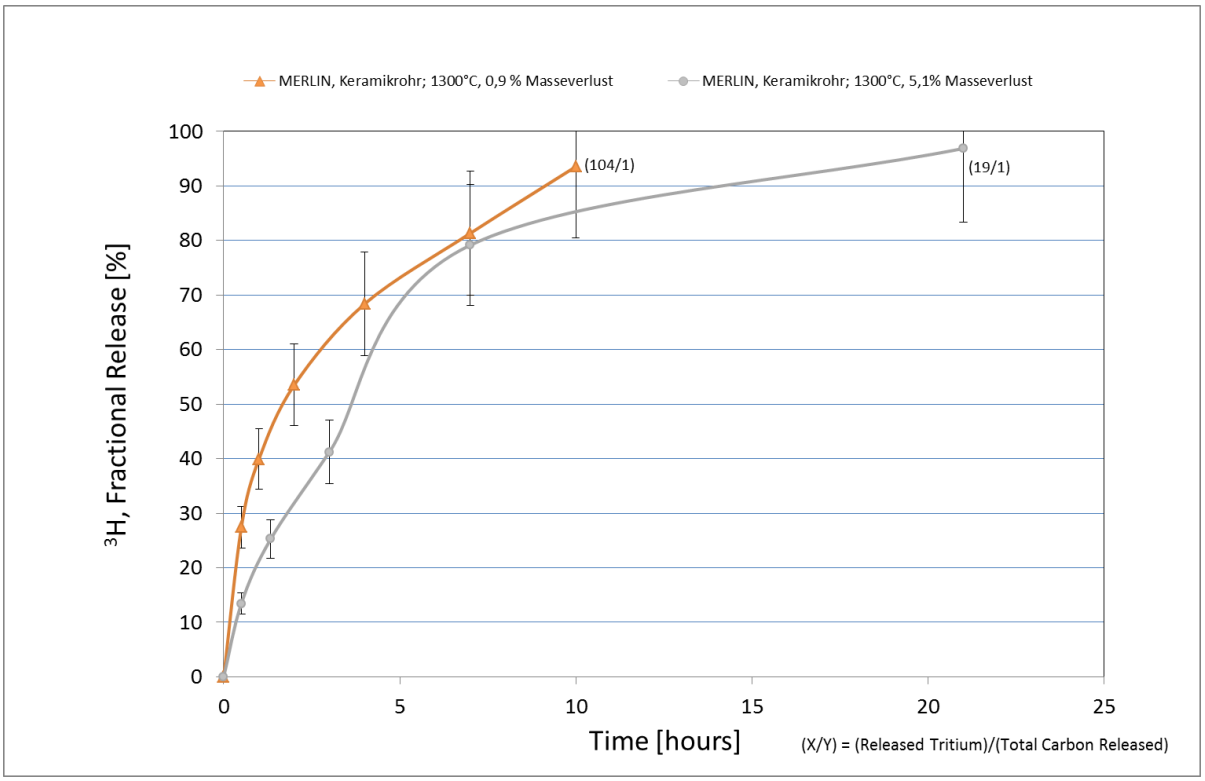

Figure 7.1.11: Comparison among two tritium release curves from similar experiments, with different oxygen amounts in the adduct gases

In conclusion, one of the most promising treatments for tritium removal is implying high temperatures and argon (or nitrogen) atmosphere, to obtain at the same time high fractional releases of tritium and low graphite burn-off.

The removal efficiency is expected to be high for not-corroded graphite, low irradiation temperature and relatively low neutron fluence. As the neutron fluence raise – directly correlable to some activation products as Co-60 – the presence of interstitial atoms increases, leading to higher activation energies for Tritium removal, for example. The temperature during operation is of fundamental importance under many aspects:

- Wigner energy can be prevented/released at medium temperatures, possibly with “roasting” cycles if the operational temperature is too low (e.g. ambient temperature);
- Low operational temperatures do not allow the migration of interstitials, so it can be assumed that most of the tritium will stay in the graphite (Merlin); Medium/high operational temperature will allow annealing of defects and migration of some radionuclides (AVR).
- The presence of radiolytic corrosion heavily influences the graphite behaviour under thermal treatment and consequently under disposal conditions. It is reasonable to expect that the most labile fractions of C-14 and H-3 have been already removed in an enhanced way during reactor

operation (UNGG/Magnox), so further decontamination from volatile radionuclides is possible but more difficult and less efficient compared to the other cases.

7.1.2 Release of Radiocarbon

7.1.2.1 Background

In the past no models have been established for what concerns radiocarbon: only some experimental data is available. The most common encountered problem is the neglected history/nature of the considered graphite: such material, already quite complex, experienced a series of conditions affecting its behaviour under disposal conditions and its radionuclide distribution. Starting from the manufacture, going through the storage history, the operational history inside the reactor and the storage conditions after irradiation, the graphite is experiencing a consistent number of variables affecting its structure, radionuclide distribution and, at the end, behaviour under thermal treatment and under final disposal. For this reason, any nuclear graphite is a unique case. In some cases, similar behaviours are detected under thermal treatment, but this can be liked to similar histories and/or main sources of contamination.
The origin and location of C-14 is out of the scope of the present paper: it is analysed in D-3.3.2.
Takahashi et al. [46] measured, through SIMS analyses, nitrogen (CN-) concentrated mostly near the graphite surface, in the first tens of nm (about 30 nm). Moreover, after a thermal treatment at 400°C, no differences were observed: it was stated that nitrogen is sorbed on the graphite surface in a stable way. The variation of nitrogen concentration in the depth direction suggested that nitrogen molecules cannot penetrate interior of nuclear-grade graphite, protected by scale-like graphite planes, so the nitrogen stays mainly on the surface. C-14 release was estimated to occur from the first superficial nanometer of the graphite surface. It has to be underlined, however, that the investigated samples had very low radioactivity and the experiments were performed at relatively low temperatures. It is expected that highly radioactive graphite, as the AVR one, will show considerable amounts of mobile carbon due both to the old-grade manufacture and radiation damage.
Some experiments have shown that most of the C-14 is located on the outer and inner surfaces of the porous graphite, in the case of AVR and MERLIN graphite.[1]
Thermal treatments of T. Podruzina [2] showed results related to the temperature, the used sample and the utilized gases. The most promising results, concerning AVR reflector graphite, were obtained at 1060 °C in inert atmosphere (argon), with a fractional release $\%^{14}C/\%^{12}C=20$ and mass loss in the order of 1%.

The theoretical implications related to the experimental results will be presented in the following chapters.

7.1.2.2 Merlin Graphite

The release of radiocarbon in inert gas (without ingress of air) seems to be a temperature-dependent diffusion process in which gases like ^{14}CO and $^{14}CO_2$ are released, formed by oxidation of radiocarbon in the pore system. This process is often overlain by a radiocarbon release caused by simple corrosion of the outer layers of the graphite matrix. In particular, this effect occurs when the inert gas contains traces of oxidising gases (e.g. oxygen) due to small leakages of the used furnace (e.g. thermal permeability of the oven tube).

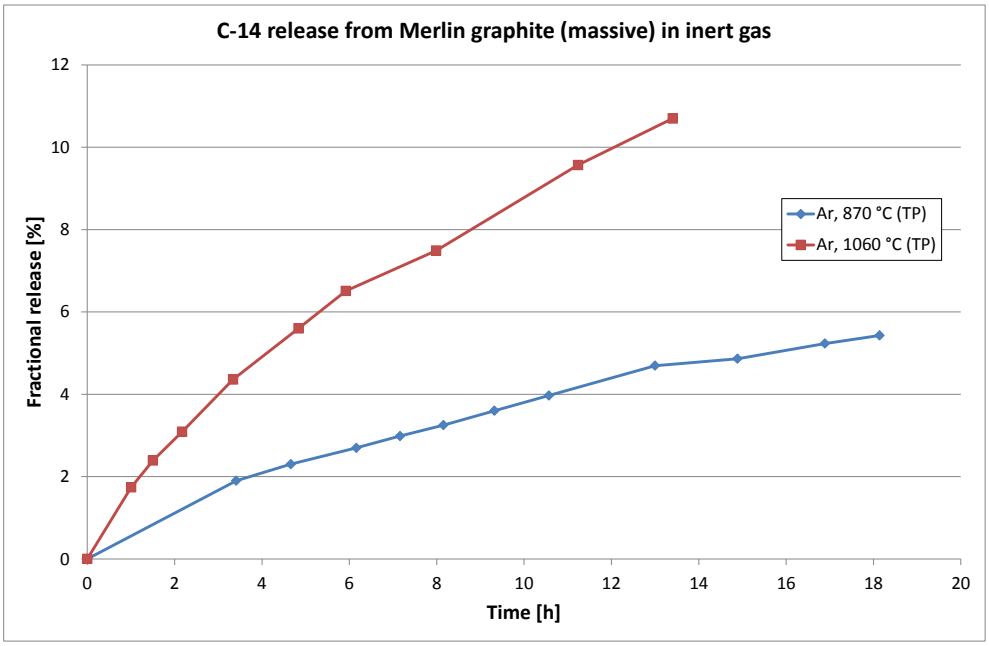

Figure 7.1.12: Release of radiocarbon in inert gas at different temperatures

The release of radiocarbon in inert gas is also dependent on the amount of adsorbed oxidising gases. Several experiments revealed that a simple addition of oxidising gases increases the release of radiocarbon but increases also the corrosion of the graphite matrix, leading to a less effective radiocarbon removal.

The kinetic description of the thermal release of radiocarbon from graphite is derived from two kinds of experiments:

- “Real” inert gas experiments (as shown in Figure 7.1.12) and
- Experiments in which the treatment gas contained a defined (small) amount of oxygen.

Real inert gas experiments give the chance to study the diffusion of radiocarbon through the graphite matrix. The graphical test for a diffusion reaction is made by plotting the fractional release of radiocarbon vs. the square root of time (see Figure 7.1.12). Application of Eq. 7.6–10 results in an apparent activation energy of 1.17 eV.

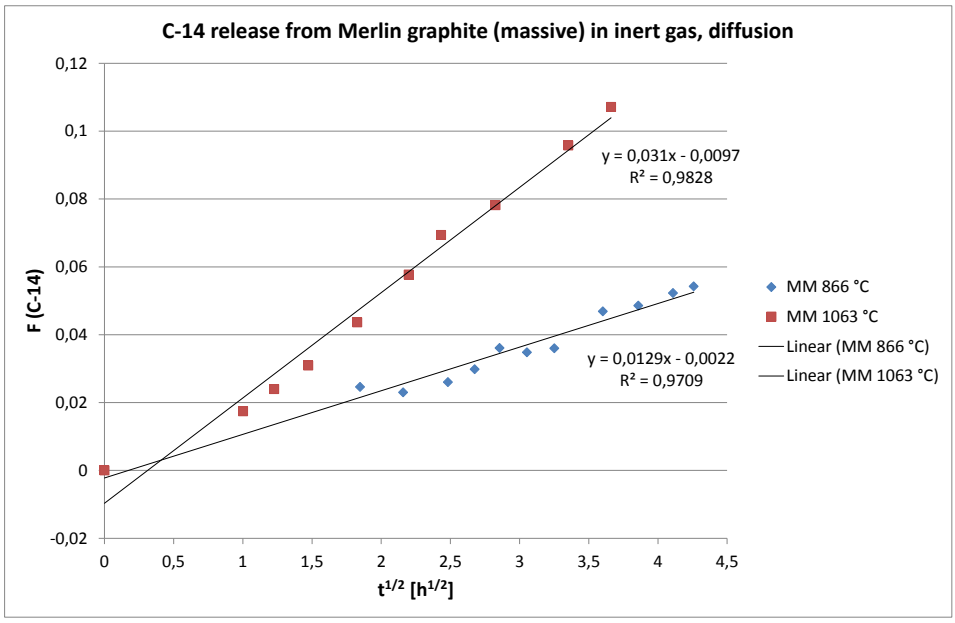

Figure 7.1.13: Release of radiocarbon in inert gas at different temperatures plotted as diffusion reaction

The apparent diffusion activation energy is the sum of the real diffusion activation energy and the formation energy of the diffusing species. To determine the formation energy of the diffusing species, it is necessary to study the oxidation process of the graphite matrix since the release of radiocarbon is related with it. Therefore, experiments were performed with a treatment gas containing a defined amount of oxygen. The results of these experiments are given in Figure 7.1.14. MERLIN graphite was treated with nitrogen + 1% oxygen. Two different temperatures were applied: 700 °C and 900 °C.

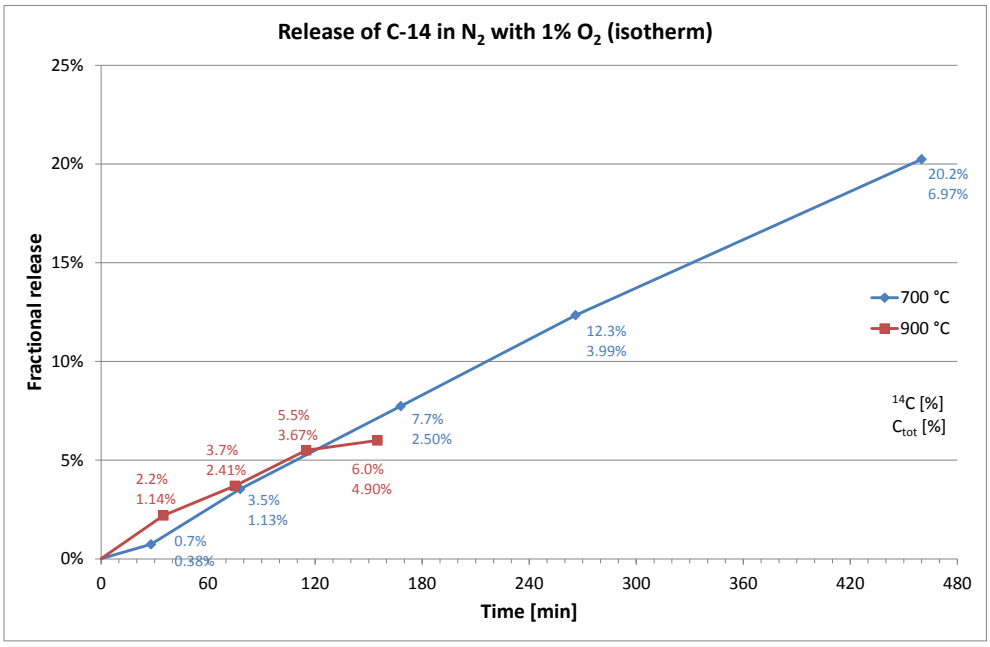

Figure 7.1.14: Release of radiocarbon in nitrogen with 1% oxygen at different temperatures (the upper number gives the % ^{14}C released and the lower number the % carbon consumed)

One can see that the release isotherms are quite linear with time up to a certain point at which the removable part of radiocarbon is consumed and they lie upon each other. In kinetic terms this means that the reaction between radiocarbon and oxygen is of zero order (independent on the concentration of radiocarbon and oxygen) and that the reaction rate is independent on the temperature.
The thermal release of radiocarbon is always coupled with an oxidation of the graphite matrix. To obtain more information about the release mechanism and the release kinetics of radiocarbon, it is necessary to study the oxidation behaviour of the graphite matrix. In Figure 7.1.15 the release of total carbon (all carbon isotopes of graphite) for the above-mentioned experiments with MERLIN graphite is shown. One can see that the reaction mechanism is of zero order again, but there is also – as expected – a temperature dependence of the reaction rate: the higher the temperature the higher the reaction rate.

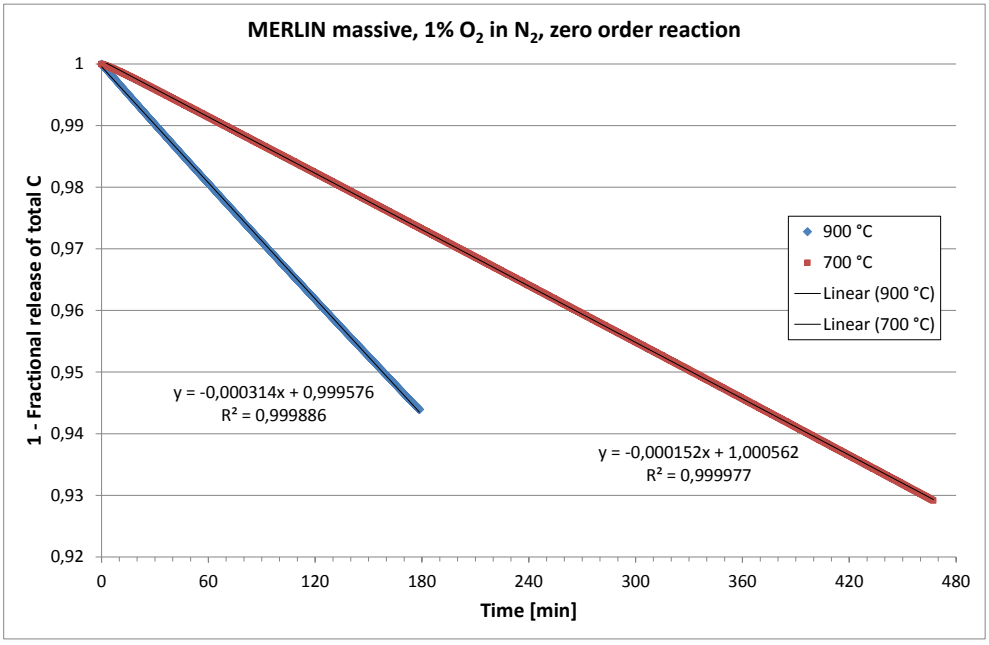

Figure 7.1.15: Release of total carbon in nitrogen with 1% oxygen at different temperatures

With the temperature dependence, the activation energy for the oxidation of the graphite matrix can be calculated. The reaction rate of a zero order reaction is defined by

$$c(\mathrm{A}) = -k \cdot t + c_0(\mathrm{A}) \tag{7.6}$$

A plot of the concentration of the starting material (= 1 − fractional release of total carbon) vs. time should give a straight line with a slope of $-k$ (= reaction rate constant). From the known dependence of the reaction rate constant on the temperature (Arrhenius equation), the activation energy E_A can be calculated:

$$E_\mathrm{A} = R \cdot \frac{T_1 \cdot T_2}{T_2 - T_1} \cdot \ln\left(\frac{k_2}{k_1}\right) \tag{7.10}$$

With Eq. 7.10, it can be calculated an activation energy of 34.4 kJ/mol (= 0.36 eV). With this result the true activation energy for the diffusion of radiocarbon through the graphite matrix can be obtained: a simple subtraction of the activation energy for the oxidation of the graphite matrix from the apparent diffusion activation energy results in Eq. (7.11).

$$1.17\ \text{eV} - 0.36\ \text{eV} = 0.81\ \text{eV} \tag{7.11}$$

An interesting modification of these experiments is a step-by-step process performed by reloading the graphite sample surface with atmospheric oxygen and by repeating the same thermal treatment, as it can be seen in Figure 7.1.16 [8]. Such experiment shows the influence of adsorbed oxygen on the release of radiocarbon and seems to the most promising way to remove C-14 from graphite in a selective way.

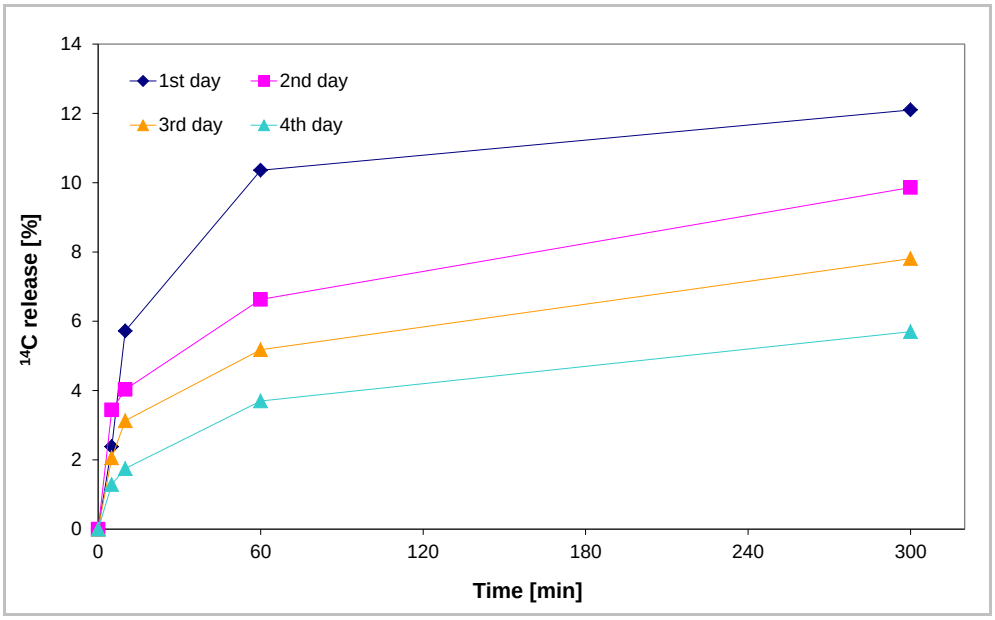

Figure 7.1.16: Repeated thermal treatment at 900 °C under nitrogen atmosphere after intermediate exposure of the sample to air at room temperature for 20 hours (cumulated ^{14}C release: 35.5%, cumulated release of total carbon: 2.7%, ^{14}C enrichment in the gas phase: 13:1) [8]

7.1.2.2 Saint Laurent A2 and Oldbury 2 Graphite

The release of $^{14}CO_2$ and ^{14}CO from Magnox Oldbury 2 graphite in nitrogen at 1100 °C shows also a diffusion character, as can be seen in Figures 7.1.17 and 7.1.18. This implies that both species must be already preformed in the graphite bulk. It is possible that the chemical bonds are already formed. This can be imagined as ^{14}C─O surface complexes like shown in Figure 7.1.19. The formation of volatile compounds such as $^{14}CO_2$ and ^{14}CO is then possible by supplying thermal energy and breaking the ^{12}C─^{14}C bonds. Another option is the presence of small amounts of oxidizing species in the adduct gases: due to the difficulty on the boundary conditions control, it is not possible to separate the two effects in an ideal way. However, it is reasonable to expect that, after some time at high temperature, the pyrolysing process terminates due to the exhaustion of the pyrolysable functional groups for that certain temperature; it follows, then, an oxidation of the graphite due to the traces of oxidisers present in the adduct gases. Looking at Figs. 7.1.17-18 it can be noticed that the fractional releases of Radiocarbon in the case of Oldbury2 graphite are up to 4 times lower than the C-14 releases from Merlin graphite, under the same conditions: it has to be considered, in fact, the history of the graphite. In particular, the radiolytic corrosion occurred under reactor operation is likely to have already removed a significant part of the C-14, since the experienced mass losses at the end of the reactor´s life were up to 40%.

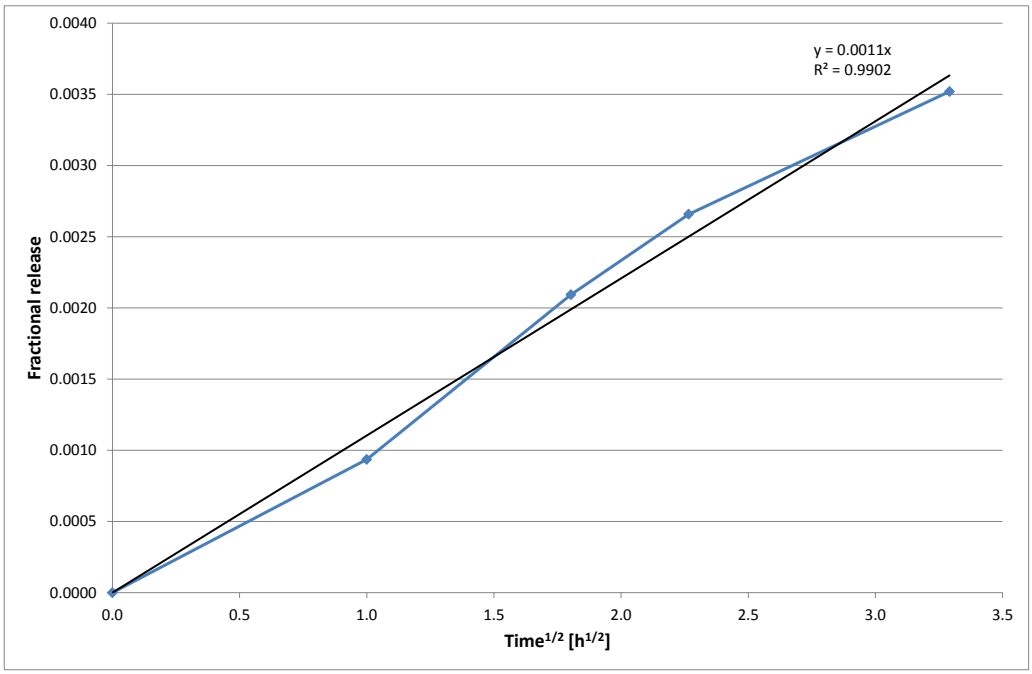

Figure 7.1.17: Release of $^{14}CO_2$ from Magnox Oldbury 2 graphite in nitrogen at 1100 °C plotted as diffusion reaction

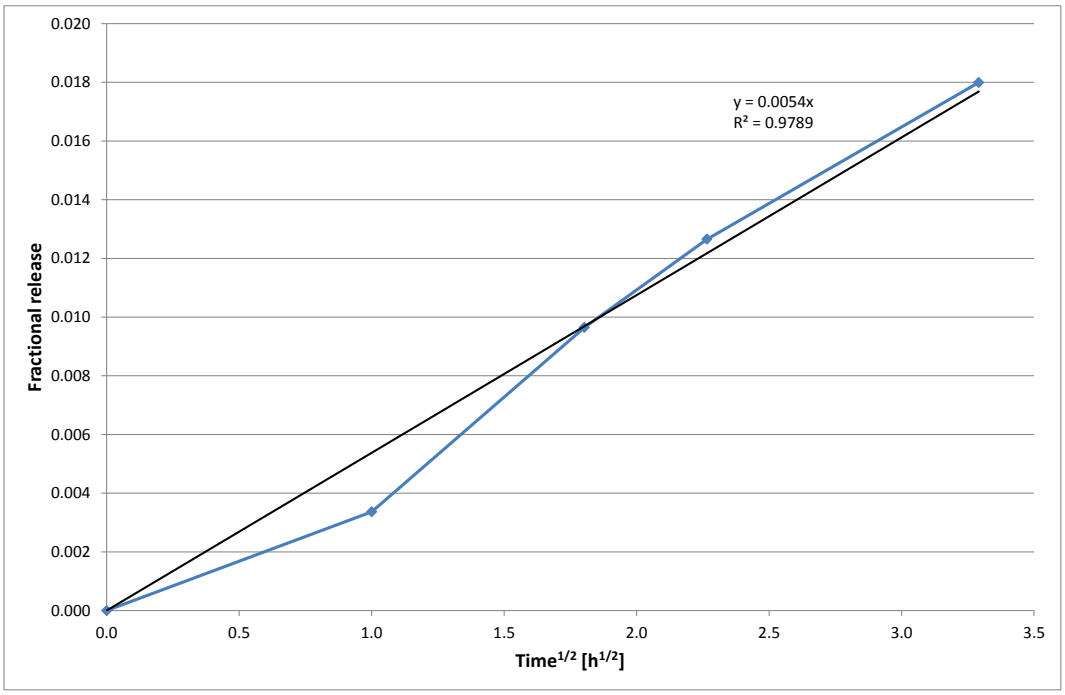

Figure 7.1.18: Release of ^{14}CO from Magnox Oldbury 2 graphite in nitrogen at 1100 °C plotted as diffusion reaction

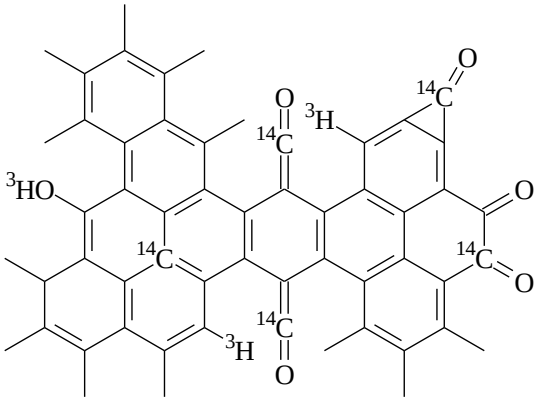

Figure 7.1.19: Model of a graphite surface with ^{3}H and ^{14}C as functional groups (surface complexes)

For what concerns the release of $^{14}CO_2$ and ^{14}CO from Saint Laurent A2 graphite the on-line values are reported in Figs. 7.1.20-21.

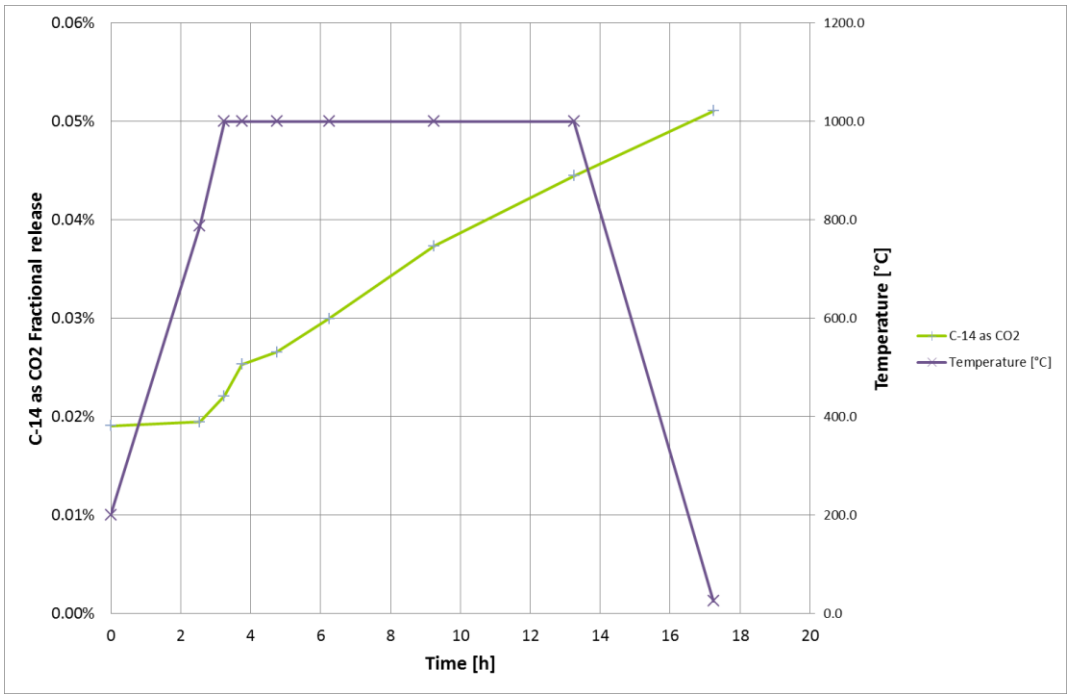

Figure 7.1.20: Release of $^{14}CO_2$ from SLA2 graphite in Argon at 1000 °C (mass loss after 10 h: 0.32%)

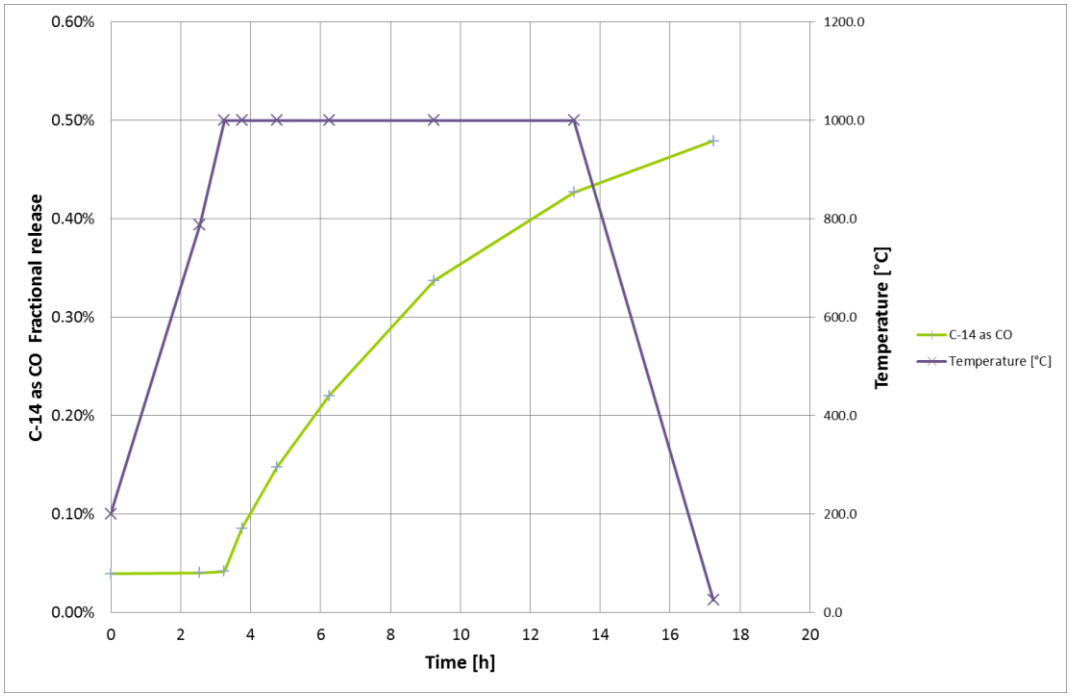

Figure 7.1.21: Release of ^{14}CO from SLA2 graphite in Argon at 1000 °C (mass loss after 10 h: 0.32%)

The hypothesis of a diffusion-dominating phenomenon seems to be validated for $^{14}CO_2$ also in this case (see Fig. 7.1.22). In the case of ^{14}CO the curve fitting is much worse than the previous case (see Fig. 7.1.23): it is reasonable to expect an overlapping of different phenomena, not excluding e.g. secondary reactions (Bouduard reaction, thermal gradient effects on the gas

phase species, etc.). However, the measured values here presented for the Saint Laurent A2 case are affected by significant errors (about 11%) since the removed activity was very low. Future investigations should be performed to check the validity of the present results.

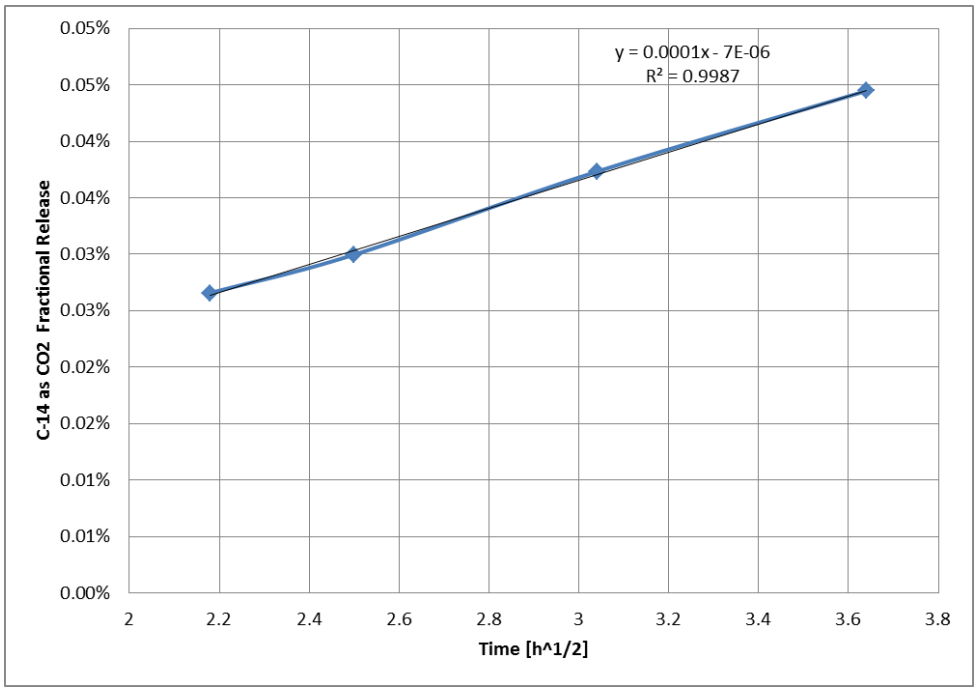

Figure 7.1.22: Release of $^{14}CO_2$ from SLA2 graphite in Argon at 1000 °C, isothermal section plotted as diffusion reaction

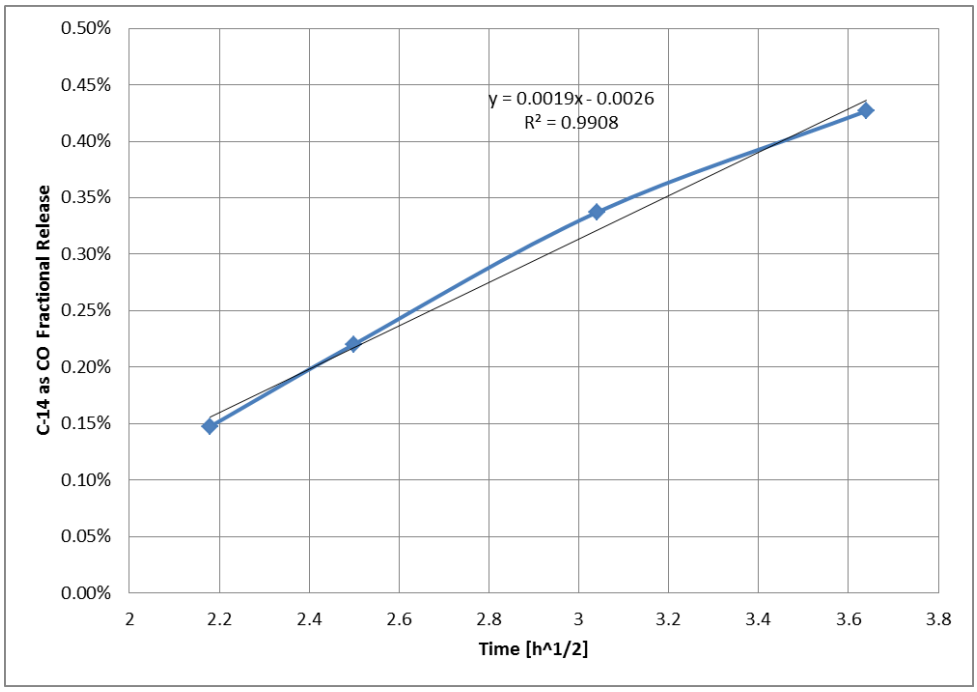

Figure 7.1.23: Release of ^{14}CO from SLA2 graphite in Argon at 1000 °C, isothermal section plotted as diffusion reaction

In conclusion, two phenomena have been identified: diffusion-driven removal of radiocarbon under inert gases and zeroth order reaction of the total carbon under oxidizing atmosphere (1% O_2 in N_2). The removal of radiocarbon, moreover, showed to be correlated with the oxidation of graphite: it is strongly bound with the presence of oxidizing agents, as it can be highlighted by Fig. 5.1.5; on the other hand, the presence of e.g. small amounts of oxygen are increasing at the same time the C-14 release and the mass loss, resulting in a less selective removal.
Following these findings the possible routes for radiocarbon removal are:

- Diffusion of C-14 atoms from interstitials or defects to the outer surface of the graphite matrix;
- Selective removal of C-14 from the enriched layers near to the surfaces by slight oxidation;

The dilemma that has to be faced is dual: considering the diffusion of C-14 under inert gases with only traces of oxidants, the time necessary for a reasonable decontamination is estimated in the order of days or even weeks of thermal treatment, time not reasonable from an industrial point of view. Following the line of thought, the next option would be accelerating the process by providing slight amounts of oxidising gases, in a continuous process at high temperature: the temperature, however, affects in a opposite way the reaction rate (higher with T.) and the established regime (mass-transfer controlled regime at high T.), resulting in a surface decontamination at high temperatures without affecting significantly the bulk material. On the other side, low temperature result in a chemical regime with very low reaction rates and low diffusion coefficients.

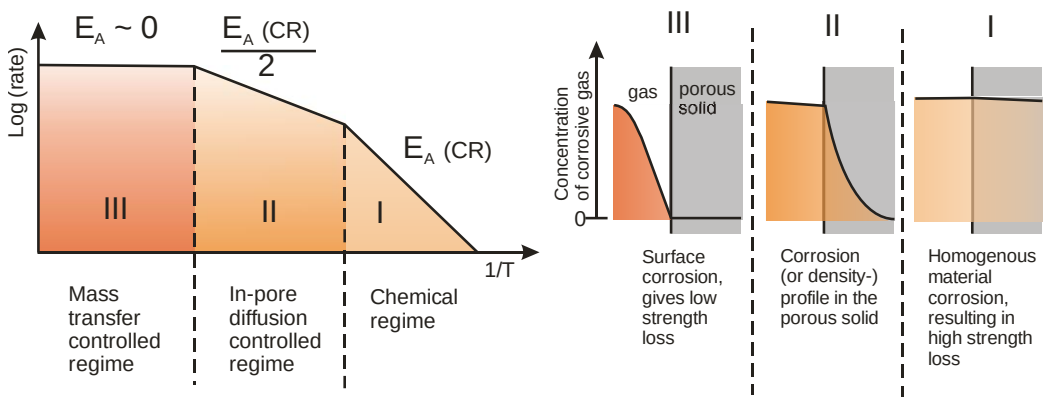

Figure 7.1.24: Schematic view of the controversial effect of temperature on reaction rates and regime in porous media.

Separation of these steps showed to be effective for what concerns radiocarbon removal, in several cases (see e.g. Fig. 7.1.16). Further tests are in progress with different graphite grades.

7.2 Release Isotherms – Merlin and Oldbury2

The release isotherms for tritium and ^{14}C from Merlin graphite (material test reactor) and Magnox Oldbury 2 graphite (nuclear power reactor) in nitrogen at 1100 °C are shown in Figures 7.2.1–4. Two observations can be done:

1. The release of ^{14}C from both Merlin and Magnox graphite is relatively low.
2. The release of tritium from Merlin graphite is significantly higher than the one from Magnox Oldbury 2 graphite.

An explanation for the different release behaviour of tritium could be the irradiation temperature of the nuclear reactor. The thermal column of the Merlin reactor was irradiated at room temperature (20…25 °C), whereas the graphite sample from the Magnox Oldbury 2 reactor was irradiated at 270 °C. These different irradiation temperatures can cause different chemical bonds of tritium on graphite.

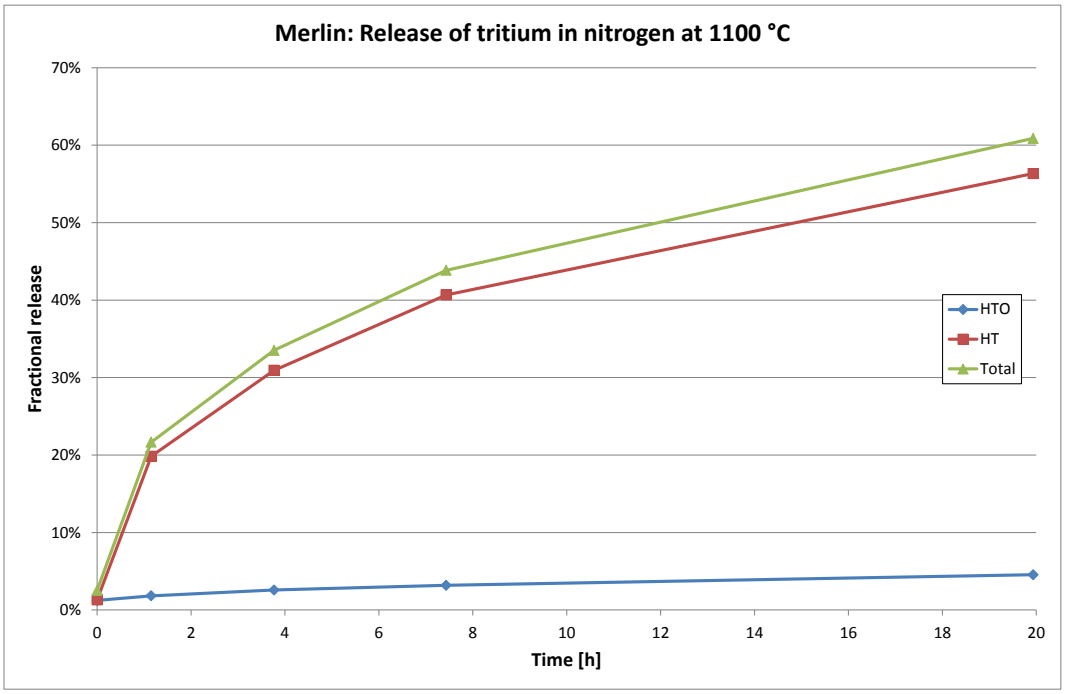

Figure 7.2.1: Release of tritium from Merlin graphite in nitrogen at 1100 °C (mass loss after 20 h: 0.20%)

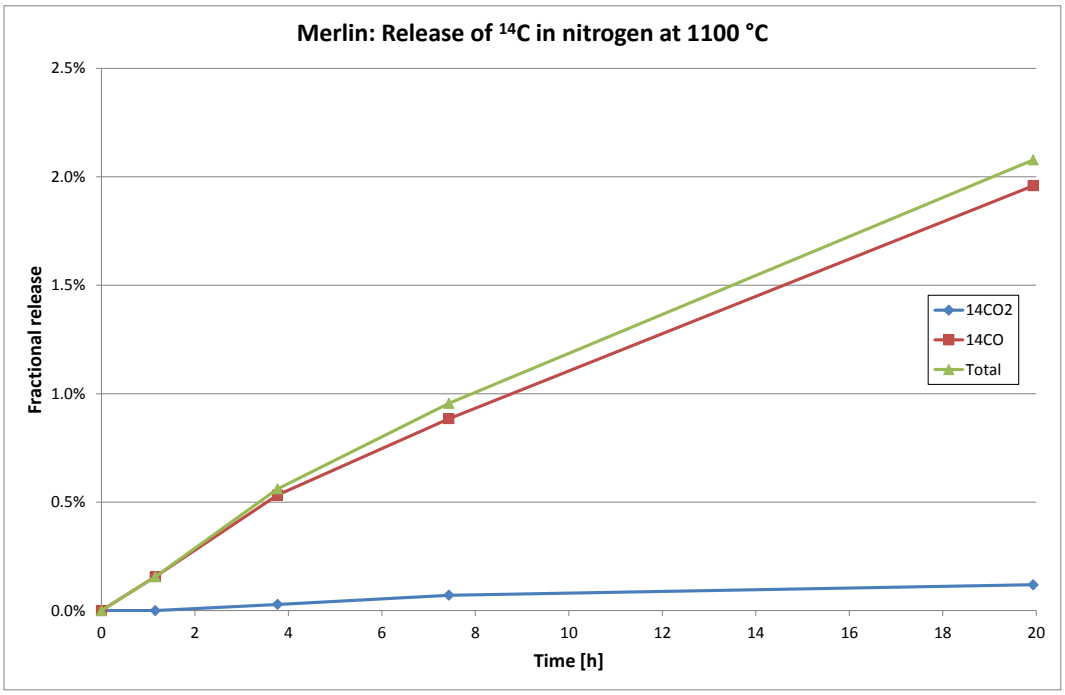

Figure 7.2.2: Release of ^{14}C from Merlin graphite in nitrogen at 1100 °C (mass loss after 20 h: 0.20%)

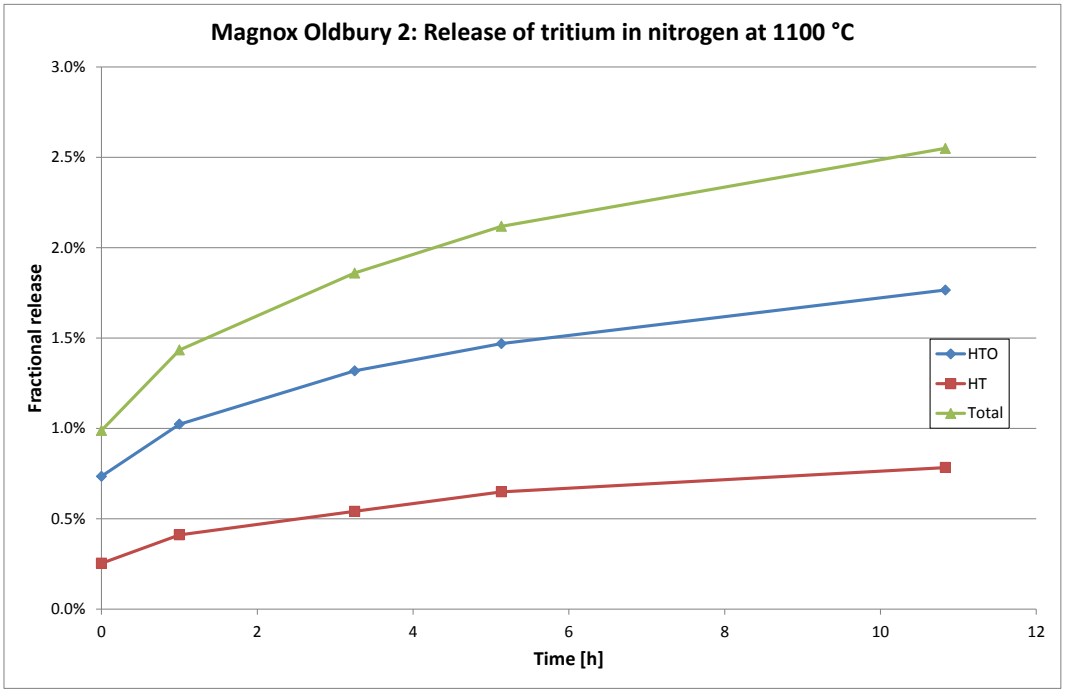

Figure 7.2.3: Release of tritium from Magnox Oldbury 2 graphite in nitrogen at 1100 °C (mass loss after 11 h: 0.14%)

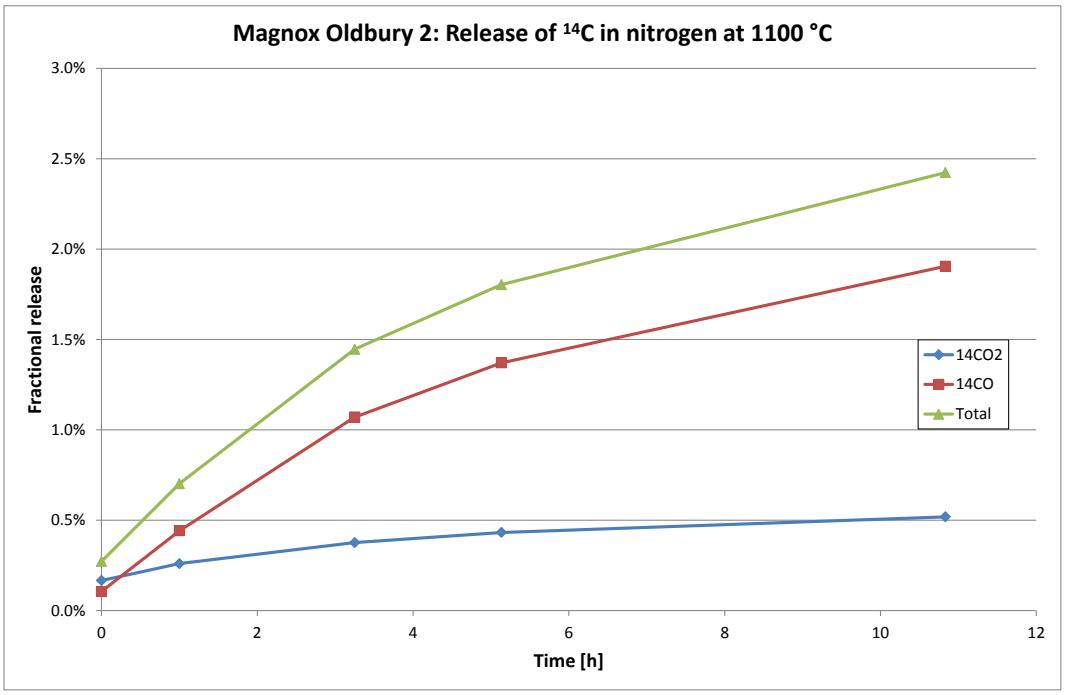

Figure 7.2.4: Release of ^{14}C from Magnox Oldbury 2 graphite in nitrogen at 1100 °C (mass loss after 11 h: 0.14%)

7.3 Special case: Detection and removal of surface contaminations

A special case is when the radionuclide contamination is on the surface of the graphite sample. In Figure 7.3.1 the release of ^{14}C from Magnox Oldbury 2 graphite in N_2 with 0.1% O_2 at 900 °C is shown. The release isotherms for ^{14}CO and $^{14}CO_2$ are quite linear (Figure 7.3.1). This means that the release process is not mainly a diffusion process but a simple oxidation of ^{14}C with the added amount of O_2 in the treatment gas. The released amount of ^{14}C compared to the mass loss of the graphite sample is also significant: 57.7% of ^{14}C could be released with a mass loss of only 0.70%. This high amount of released ^{14}C was never reached in any other experiment in FZJ. Therefore, the surface of the thermally treated graphite sample was analysed by autoradiography and significant shadows, typical for surface contaminations, were found (see Fig. 7.3.2). This is also in accordance with the information of the graphite sample´s supplier: the surface of the sample is a real surface (not artificial), which was in contact with the coolant gas of the Oldbury 2 reactor during operation. The coolant gas was CO_2; it is reasonable to expect that the coolant gas contained ^{14}C compounds or ^{14}C-containing particles and deposited them on the surfaces of the reactor internals. In this way, a thin film with a high concentration of ^{14}C was formed on the surface of the graphite sample. Such surface contamination can be easily removed by slight oxidation of the graphite sample.

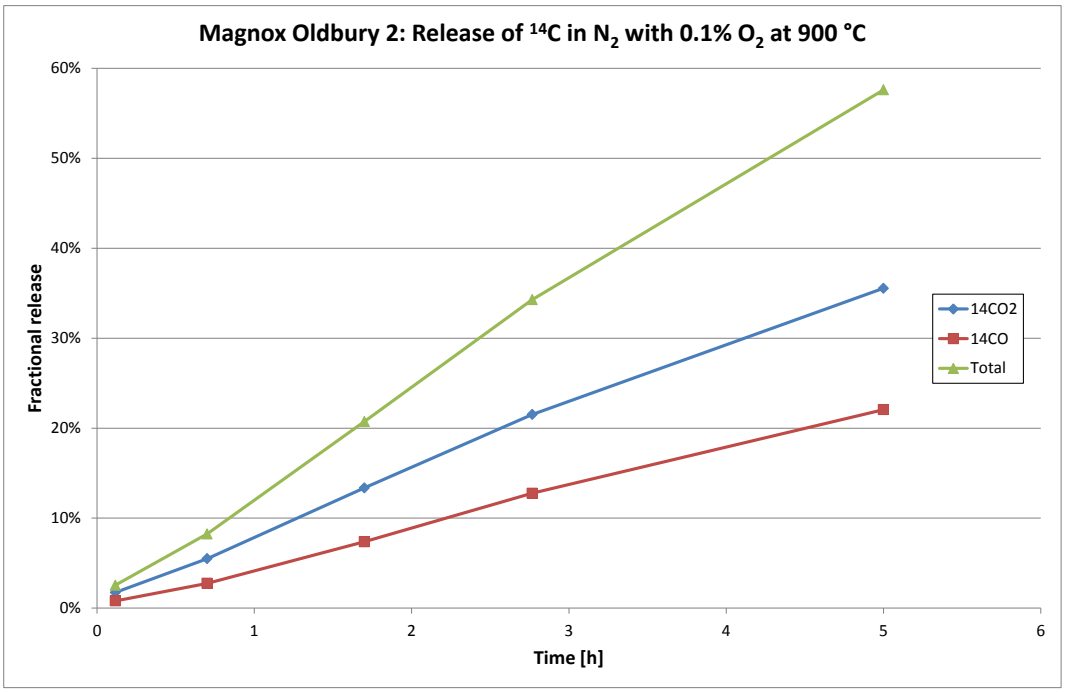

Figure 7.3.1: Release of ^{14}C from Magnox Oldbury 2 graphite in N_2 with 0.1% O_2 at 900 °C (mass loss after 5 h: 0.70%)

Figure 7.3.2: Spatial distribution of beta-emitters on the surface of the Magnox Oldbury 2 sample from Figure 7.3.1 after thermal treatment determined by digital autoradiography (specimen diameter: 15 mm, thickness: 5 mm, mass: 0.7684 g)

7.4 Waste Management Strategies

Considering neutron-irradiated nuclear graphite as waste, the specific radioactivity of graphite is important to decide what the best waste management strategy for it is. The specific radioactivity of Merlin graphite is relatively low, whereas the specific radioactivity of Magnox Oldbury 2 graphite is one to two orders of magnitude higher than of Merlin graphite (see Table 7.4.1). Therefore, a treatment process for Magnox graphite is more favourable than for Merlin graphite. On the other hand, the removability of tritium and ^{14}C from Magnox graphite is low in case of no surface contamination. This implicates that tritium and ^{14}C is strongly bound in Magnox graphite. For this reason, it can be concluded that Magnox graphite is a good "retainer" for tritium and ^{14}C. This facilitates the waste management strategy for Magnox graphite because the risk that Magnox graphite loses its tritium and ^{14}C content in an uncontrolled way is relatively low.

Nuclide	Specific Activity [Bq/g]	
	Merlin	Magnox Oldbury 2
^{3}H	1.00E+03	4.49E+04
^{14}C	3.24E+02	4.41E+04

Table 7.4.1: Isotopic inventory of Merlin and Magnox Oldbury 2 graphite (date: 15th June 2012)

Nevertheless, thermal treatment of irradiated graphite may be a good method for preparation of final disposal even if the removability of ^{14}C is only moderate or low. It is well-known from the manufacturing process of graphite that the graphite structure is formed by high-temperature treatment. It is also well-known that thermal treatment of irradiated graphite leads to an annealing process of structural defects. Therefore, it can be concluded that loosely bound ^{14}C on the surfaces of the graphite crystallites or between the graphite lattice planes will be incorporated more stably in the graphite lattice by thermal treatment. This can be imagined when considering Fig. 7.4.2: carbon atoms in different structural units form step by step the well-known C_6 rings of the graphite lattice planes which then form the stable graphite crystals. In this way the ^{14}C atoms are totally equal to the other $^{12,13}C$ atoms which normally form natural graphite. ^{14}C is thus immobilised and cannot be released without destruction of the graphite matrix.

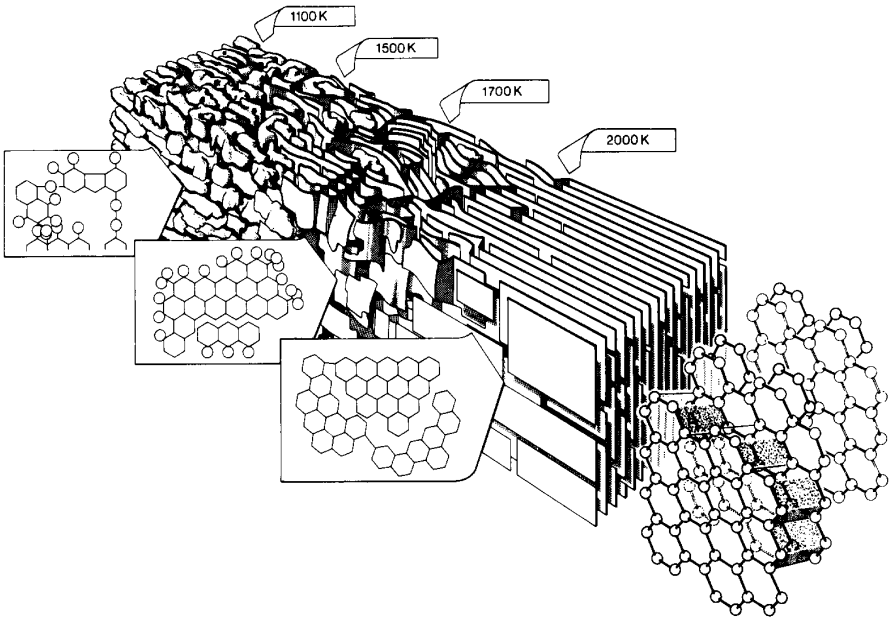

Figure 7.4.2: A model of changes from mesophase to graphite during heat treatment [19]

Conclusions

Thermal treatments have been accounted as a possible way of decontamination of i-graphite. In particular, the present deliverable dealt with thermal treatments under inert gases (Argon or Nitrogen).
Several experiments, performed on virgin graphite as on irradiated one at FZJ, underlined the presence of oxidising species in the graphite matrix, together with other impurities. Such species are e.g. adsorbed gases, adsorbed water, on the surfaces, or embedded in the graphite matrix as a result of the manufacture process and the history of the sample. The application of an inert atmosphere is favouring the desorption/pyrolysis/reaction of the above-mentioned species, resulting in a slight oxidation of the graphite, with typical mass losses lower than 0.5-1%. The intention of thermal treatments was then to operate under argon atmosphere, in order to measure the off-gases and to connect their release with the embedded species and with temperature. A general quantitative evaluation of such adsorbed/embedded species cannot be provided since the relative amounts are strongly correlated with the graphite history; in addition, the sample preparation could affect the results, especially when small samples are used; moreover, most of the times, the complete history and conditions of a graphite sample are unknown. However, what has to be underlined is the fact that an inert gas thermal treatment is involving also chemical reactions, which are leading to a partial removal of volatile radionuclides in the form of e.g. water, H_2, CO, CO_2, CH_4. Several parallelisms have been performed among the on-line gaseous emissions and the radionuclide removals, leading to a deeper understanding of the radionuclides' driving removal mechanisms.

For what concerns Tritium selective removal from i-graphite, the model which best describes the mechanism is the one developed by Atsumi (see Chapter 7.1.1.1), on which hydrogen is present in different trap-sites with different removal activation energies. The mechanism can be reproduced as a diffusion-controlled one. Experimental data from FZJ confirmed these findings on several i-graphite coming from different reactors and histories:

- Low-temperature-irradiated not-corroded graphite (as in MERLIN) showed the highest Decontamination Factors (DF), increasing with the treatment temperature, up to 30 for a treatment at 1300 °C 21 h isothermal.
- High-temperature-irradiated not-corroded graphite (as in AVR) showed lower decontamination factors due to the fact that high temperatures favoured the migration of Tritium during reactor operation; it is hypothesised that the remained Tritium is more stable (e.g. present as interstitial), fact confirmed by several experiments: higher temperatures are necessary for its removal. Moreover, it cannot be excluded that part of the Tritium diffused towards the carbon-brick insulation barrier of the reactor. Decontamination factors obtained at FZJ resulted in about 5 maximum for a treatment at 1280 °C 7h isothermal.
- Medium-temperature-irradiated and corroded graphite (as in UNGG and MAGNOX) showed very low DF (up to 1.4) due probably to the fact that the graphite experienced high radiolytic corrosion during reactor operation (up to 40%): trap 1 sites are believed to be the major fraction remained.

Diffusion coefficients for Tritium have been calculated in the order of 10^{-12} cm^2/s at 1060 °C; activation energies are in accordance with the ones reported by Atsumi and Fischer: 1.3 eV (no significant trapping), 2.6 eV (Trap 2) and 4.6 eV (Trap 1).

In general, higher temperatures provide higher decontamination factors, with different removal efficiencies depending on the graphite coming from different reactors, as described above. As a general statement, temperatures higher than 1100 °C are recommended for a tritium-removal process: treatment times are decreasing significantly by raising the temperature. These findings are in accordance to the Deuterium implantation and thermal treatment investigations performed by N. Toulhoat, N. Moncoffre and Y. Pipon (IPNL-University of Lyon), reported in D-4.2.3. It seems to be possible to remove completely the Tritium from i-graphite but further investigations, especially with massive samples, are necessary to confirm the findings here reported.
For what concerns radiocarbon, in the past no models have been established: only some experimental data was available.
Several molecular dynamics simulations performed at INBK showed that the C-14 formation process is associated with the recoil of ^{14}C atoms with a kinetic energy in the range of some keV (2.56 keV for the ^{13}C activation and 42 keV for the activation of ^{14}N) leading to its removal from the lattice site. The transfer of ^{14}C is accompanied by various interactions and ionization processes that result in a disorder of the lattice structure as well as in the formation of further displacements (interstitial atoms and vacancies). The recoiled atom showed to be displaced by a mean distance of about 50-60 nm with a starting energy of 42 keV (due to the neutron activation of N-14), with an initial smooth energy loss of about 100 eV/Å and a sudden energy drop after getting energies lower than 5 keV, probably caused by electronic interaction and ionization (Bragg-curve-like behavior). However, the result depends on the type of the potentials governing the interaction between the individual atoms in the short range and the recoil direction in relation to the orientation of the crystal lattice. Resulting from the symmetrical character of the individual atoms at the c-layers, the mean range and the transport of the primary C-14 showed not to be significantly influenced by the temperature variation. This result, however, needs to be verified by detailed modeling of the boundary conditions.
In addition, Molecular Dynamics simulations showed that a significant accumulation of C-14 in the vicinity of grain boundaries or surfaces (pores) caused only by the stopping processes (potentials) is not expected.
Assuming as the main contributor to C-14 formation the N-14 adsorbed on the surfaces, considering the MD results and in particular the recoil range of C-14, it seems to be confirmed that the removal of radiocarbon could occur because of a slight oxidation of the graphite surfaces, assuming its superficial enrichment. Experimental results showed that the removal of radiocarbon is correlated with the oxidation of graphite; FZJ and ITU experienced selective removal of C-14 during TTIA. However, the presence of e.g. small amounts of oxygen showed to increase at the same time the C-14 release and the mass loss, resulting in a less selective removal.
Following these findings the possible routes for radiocarbon removal are:

- Diffusion of C-14 atoms from interstitials or defects to the outer surface of the graphite matrix;
- Selective removal of C-14 from the enriched layers near the surfaces by slight oxidation;

Considering the possible identified removal mechanisms, the “temperature effect problem” must be considered: temperature is affecting in opposite ways the reaction rates and the established regime in the graphite sample. A separation of the steps, i.e. reactant loading and chemical reactions, could be an effective solution to remove C-14 more selectively without high corrosion of the graphite.

Concerning the C-14 DFs for graphite coming from different reactors, several experiments proven that, in general, low values can be achieved with a continuous process (up to 1.14). A special case is the graphite from UNGG and Magnox, which experienced high mass losses during operation in the reactor: the surface-enriched assumption is less reasonably applicable, since it is believed that the main contribution to the remained C-14 is C-13, supposed to be homogeneously distributed and embedded in the graphite. Considering a possible diffusion of C-14 during thermal treatment, low DFs are expected anyway in comparison with not-corroded graphite, since a "quasi in-situ treatment" already occurred.
Concerning the removable fraction of C-14, a total decontamination seems not to be achievable, unless an isotopic separation process is established. The removable fraction depends strongly on the graphite history; a particular recommendation for TTIA is the application of separate treatment steps as described above.
In order to fix some thresholds, as e.g. mass loss and C-14 removal target, a dedicated study that takes into account graphite history, together with an individual management strategy, should be established.
Concerning the creation of a dedicated model for C-14 removal in nuclear graphite, several factors have to be considered: the situation at the open surface of the crystallites is not clear, the radiation damage changes the structure and, in addition, orthogonal/parallel migration pathways have to be accounted. At the present state of the art, a model is difficult to create.

Several SIMS analyses (as reported in D-3.3.2) performed in FZJ on virgin massive samples revealed the effectiveness of a thermal treatment in inert atmosphere, with a significant removal of Cl-37 and Cl-35. The link between virgin and irradiated graphite goes through many influencing factors: final remarks cannot be done at the present state, but the above-described results give a hint about Chlorine behaviour under thermal treatment. The temperature-dependent removed fraction still needs to be deeper investigated. Other authors reported removal up to 30% for implanted Cl-37 on Saint Laurent graphite, with a peak around 350 °C followed by a shoulder at 450 °C [51]; it was reported, through XPS analyses, that the removed part was mainly the inorganic Chlorine (as HCl) [52]. It is hypothesised that, depending on the temperature, neutron flux and operational conditions, part of the most labile Cl-36 has been probably removed during reactor operation.

In the case a thermal treatment is going to be exclusively applied as the only "conditioning process" prior to final disposal, the leaching behaviour of C-14 and other residual volatile radionuclides is expected to be significantly improved. On the other hand, in the case a thermal treatment is thought to be part of a multi-step decontamination process (e.g. exfoliation, chemical separation, etc.), it is recommended to use it as the first step since it is able to remove selectively several volatile radionuclides (as H-3, C-14, Cl-36), which otherwise would be diluted in the used chemicals (e.g. acids), while metals showed to be effectively retained (except for Caesium).

In conclusion, a general recommendation is to consider any nuclear graphite with its own history as a unique case, since the effectiveness of a thermal treatment is significantly affected by several variables, as irradiation temperature, neutron flux, irradiation atmosphere, storage conditions, manufacture process and parameters, presence of impurities, etc. In addition, a systematic correlation with the above-mentioned parameters still needs to be done in order to

have a better understanding of volatile radionuclides´ removal mechanisms and to develop a variable-dependent model for every single i-graphite (UNGG, HTTR, Magnox, MTR, etc.)

In FZJ, the maximum applied temperature was 1300 °C, provided by the available equipment; higher temperatures could be achieved e.g. with an induction furnace, resulting in a more straightforward Tritium removal.

An inert gas thermal test could be a promising method to understand the key features of any i-graphite from the point of view of the release related to the mass loss: it could be a good indicator of the i-graphite treatability. Consequently, once the characterization has been performed, the relative management strategy can be assessed.

8. References

[1] J. Fachinger, W. von Lensa, T. Prodruhzina: Decontamination of nuclear graphite, Nuclear Engineering and Design 238 (2008) 3086–3091.

[2] T. Podruzhina, Graphite as radioactive waste: corrosion behaviour under final repository conditions and thermal treatment, Juel 4166, 2004.

[3] IAEA. (2011). Power Reactor Information System (PRIS). Retrieved November 23, 2011, from http://www.iaea.org/programmes/a2/.

[4] H: Nabielek, K. Verfondern, H. Werner, Selection of Benchmark Cases for Mechanical Failure Prediction, HTR-F Report, Forschungszentrum Jülich, 2005.

[5] M. A. Fütterer et al., 3rd International Topical Meeting on High Temperature Reactor Technology, Johannesburg, South Africa, 2006, p. B35.

[6] S. de Groot et al., 4th International Topical Meeting on High Temperature Reactor Technology, Washington (DC), USA, 2008, vol. 1, p. 307.

[7] P. G. Fischer, R. Hecker, H. D. Röhrig, D. Stöver, Zum Verhalten von Tritium in Reaktorgraphiten, J. Nucl. Mater. 64 (1977) 281–288.

[8] M. Florjan, Dekontamination von Nukleargraphit durch thermische Behandlung, PhD thesis, Rheinisch-Westfälische Technische Hochschule Aachen, 2009.

[9] W. Delle: Technische Notiz IRW-TN-87/83, Vergleich der bestrahlungsinduzierten Dimensionsänderungen des AVR-Reflektormaterials mit dem britischen Nukleargraphit P.G.A., Institut für Reaktorwerkstoffe, KFA Jülich, 1983.

[10] J. Fassbender, E. Münch, D. Nutbohm, Thamm, G. Die gegenwärtige und zukünftige Nutzung der Forschungsreaktoren FRJ-1 (Merlin) und FRJ-2 (DIDO) der Kernforschungsanlage Jülich. Bericht der Zentralabteilung Forschungsreaktoren, 1973.

[11] B. Bisplinghoff: AVR-Analytik, Ergebnisbericht Forschungszentrum Jülich, 2000.

[12] V. Gomez-Serrano, M.A. Acedo-Ramos, A.J. Lopez-Peinado, Thermogravimetric study of activated carbon oxidized with H2O2, Thermochimica Acta, 254, 249, 1995.

[13] J.B. Donnet, A. Schutz, Etude cinetique de l'oxydation des noirs de carbone par l'ozone Eugene Papirer, Oxidation studies of a furnace carbon black by ozone in aqueous medium, Carbon, 5 [2], 113, 1967.

[14] J.B. Donnet, P. Ehrburger, Study of the oxidation of carbons by ozone in aqueous medium, Carbon, 10 [3], 341, 1972.

[15] Gmelin Handbuch der Anorganischen Chemie, Vol. 7, Verlag Chemie, Weinheim, 1966.

[16] Chakrabartty, S.K., Kretscmer, H.O.: Studies of the structure of coals. 2. The valence state of carbon in coal, Fuel, 53, 132 (1974).

[17] Mayo, F.R., Kirshen, N.A.: Oxidation of coal by aqueous sodium hypochlorite, Fuel, 58, 698 (1979).

[18] Haag, G., Delle, W., Kirch, N., Nickel H., Reinhart, K. and Ziermann, E.: Results of the visual in-pile inspection of the inner graphite reflector of the AVR, Specialists' meeting on graphite component structural design, JAERI Tokai (Japan), Vienna, 08/09/1986, International Atomic Energy Agency, 1986.

[19] H. Marsh, A tribute to Philip L. Walker, Carbon 29 (1991) 703–704.

[20] S. de Groot et al., Nucl. Eng. Design 238 (2008) 3114.

[21] D. A. Petti et al., Nucl. Eng. Design 222 (2003) 281.

[22] J.B. Donnet, A. Schutz, Etude cinetique de l'oxydation des noirs de carbone par l'ozone Eugene Papirer, Oxidation studies of a furnace carbon black by ozone in aqueous medium, Carbon, 5 [2], 113, 1967.

[23] K. Iwamoto, The escape behaviour of non-gaseous fission products recoiled into graphite, Journal of Nuclear Materials, 29, 285, 1969.

[24] C. Marnet, M. Wimmers, Decommissioning of the AVR reactor, concept for the total dismantling, Technical committee meeting on technologies for gas cooled reactor decommissioning, fuel storage and waste disposal, Vienna (Austria), 8-9- 1997, 17, International Atomic Energy Agency, 1997.

[25] P.G. Fischer, Verhalten von Tritium in Reaktorgraphiten, Berichte der KFA Jülich, Jül-1238, 1975.

[26] V.J. Malka, R. Raitz von Frentz, Adsorption und Desorption von Tritium an Graphit, Berichte der KFA Jülich, Jül-1497, 1978.

[27] K. Ashida, K. Watanabe, Diffusion constants of tritium in graphites and compensation effect, Journal of Nuclear Materials, 183, 89, 1991.

[28] J. Wörner, W. Botzem, S.D. Preston, Heat treatment of graphite and resulting tritium emissions, IAEA Technical Committee Meeting on "Nuclear Graphite Waste Management", held from 18-20 October 1999 in Manchester, United Kingdom, 1999.

[29] McGraw-Hill: Dictionary of Scientific and Technical Terms.

[30] Hutchinson encyclopaedia.

[31] H.Atsumi, T. Tanabe, T. Shikama, "Hydrogen behaviour in carbon and graphite before and after neutron irradiation - Trapping, diffusion and the simulation of bulk retention", J. Nucl. Mat. 417, 2011.

[32] H.Atsumi, Hydrogen bulk retention in graphite and kinetics of diffusion, Journal of Nuclear Materials 307–311 (2002) 1466–1470.

[33] H. Atsumi, S. Tokura, M. Miyake, J. Nucl. Mater. 155–157 (1988) 241.

[34] E. Denisov et al., J. Nucl. Mater. 233–237 (1996) 1218.

[35] Tec.Report IT-06/4B, “Verifications under the terms of article 35 of the Euratom treaty”, May 2006

[36] C. Marnet, M. Wimmers, Decommissioning of the AVR reactor, concept for the total dismantling, Technical committee meeting on technologies for gas cooled reactor decommissioning, fuel storage and waste disposal, Vienna (Austria), 8-9-1997, 17, International Atomic Energy Agency, 1997.

[37] G. Ramos, B.M.U. Scherzer, Radiation damage, trapping and release of deuterium in diamond and HOPG-graphite, Nuclear Instruments & Methods in Physics Research Section B-Beam Interactions with Materials and Atoms, 174 [3], 329, 2001.

[38] H. Yamagishi, N. Wakayama, H. Itoh, K. Sacasai, Measurement of neutron flux in the AVR, Berichte der KFA Jülich, JUEL-2467, 1991.

[39] Gmelin Handbuch der Annorganischen Chemie, Vol. 7, Verlag Chemie GmbH, Weinheimlbergstraße, 1966.

[40] T.Fromherz, C. Mendoza, F. Ruette, "Chemisorption of atomic H,C, N and O on a cluster-model graphite surface", Mon. Not. R. Astron. Soc. 263, 851-860 (1993).

[41] K.Katayama, M. Nishikawa, "Release behaviour of tritium from graphite material", Fusion and Science Technology, vol. 41, 53-62, Jan. 2002.

[42] H.Atsumi, K. Tauchi, "Hydrogen absorption and transport in graphite materials", Journal of alloys and compounds", 356, 2003.

[43] H.Atsumi, S. Tokura, M. Miyake, J. Nucl. Mater. 155-157 (1988).

[44] H.Atsumi, J. Nucl. Mat. 313-316 (2003)

[45] R. Moormann, "A safety Re-Evaluation of the AVR", ForschungszentrumJülich, Jül-4275

[46] R. Takahashi, M. Toyahara, S. Maruki, H.Hueda, T. Yamamoto, *Investigation of morphology and impurity of nuclear grade graphite, and leaching mechanism of carbon-14*

[47] Haque, H., Feltes, W., Brinkmann, G., 2006. *Thermal response of a modular high temperature reactor during passive cooldown under pressurized and depressurized conditions*. Nucl. Eng. Des. 236, 475

[48] Schenk, W., Pitzer, D., Nabielek, H., 1988. *Fission product release profiles from spherical HTR fuel elements at accident temperatures*. Jülich Report 2234, Research Center Jülich, Germany.

[49] Kostecka, H., Ejton, J., de Weerd, W., Toscano, H., 2004. *Post-irradiation testing of HTR-fuel elements under accident conditions*. In: 2nd International Topical Meeting on High Temperature Reactor Technology , Beijing, PR China, September, p. B13.

[50] Freis, D., et al., 2010. *Post-irradiation testing of high temperature reactor spherical fuel elements under accident conditions*. J. Eng. Gas Turb. Power 132, 042901.

[51] C.E. Vaudey, N. Toulhoat, N. Moncoffre, "*Thermal Behaviour of chlorine in nuclear graphite at a microscopic scale*", J. Nucl.mat. 395 (2009)

[52] C.E. Vaudey, N. Toulhoat, N. Moncoffre, "*Chlorine speciation in nuclear graphite: consequences on temperature release and on leaching*", Radiochim. Acta 98, 2010

9. Appendix

9.1 Summary Thermal Treatment with Decontamination Factors

Revision date: 25/02/2013

Exp. No.	Sample	Irradiation conditions		Experimental conditions				Mass loss [%]	Release [%]						Decontamination factor[4)]	
		Cool. gas	T [°C]	Treat. gas	T [°C]	Treatment time [h]			HTO	HT	^{3}H total	$^{14}CO_2$	^{14}CO	^{14}C total	^{3}H	^{14}C
						Heating	Isothermal									
V4	Merlin	Air	RT	N_2 + 0.14% O_2[1)]	1300	0	10	0.89	85.9	7.7	93.6	3.4	2.5	5.9	15.4	1.05
V5	Merlin	Air	RT	N_2 + 1% O_2	900	3	2.5	6.64	10.1	0.2	10.3	8.6	3.3	11.9	1.04	1.06
V6	Merlin	Air	RT	N_2 + 1% O_2	700	2.5	7.75	7.22	26.5	0.2	26.7	14.5	7.3	21.8	1.26	1.19
V7	SLA2 9260	CO_2	258.5	N_2 + 0.14% O_2[1)]	1300	0	10.5	0.91	65.0	0.2	65.2	1.4	0.6	2.0	2.85	1.01
V8	Merlin	Air	RT	N_2 + *x*% O_2[2)]	1300	0	21	5.12	65.6	31.3	96.9	2.5	8.2	10.7	30.4	1.06
V9	Merlin	Air	RT	Pure N_2	1100	3.75	20	0.20	4.6	56.3	60.9	0.12	2.0	2.1	2.55	1.02
V10	Merlin	Air	RT	Pure N_2	1100	3.75	25.5	0.01	1.2	0.09	1.3	1.5	1.3	2.8	1.01	1.03
V11	Merlin	Air	RT	Pure N_2	1100	3.75	20.5	0.16	15.2	21.1	36.3	0.6	1.4	2.1	1.57	1.02
V12	SLA2 9260	CO_2	258.5	Pure N_2	1100	3.75	20.5	0.45	13.3	7.3	20.6	0.4	2.0	2.4	1.25	1.02
V13	Magnox	CO_2	270	Pure N_2	1100	3.75	11	0.14	1.8	0.8	2.6	0.5	1.9	2.4	1.02	1.02
V14	Merlin	Air	RT	N_2 + 0.1% O_2[3)]	750	2.5	5	0.22	1.1	0.1	1.2	0.8	0.4	1.2	1.01	1.01
V15	Magnox	CO_2	270	N_2 + 0.1% O_2[3)]	900	3	5	0.70	5.2	0.5	5.7	35.6	22.1	57.7[5)]	1.05	2.34
V16	Magnox	CO_2	270	N_2 + 0.3% O_2[3)]	900	3	5	3.90	9.0	0.1	9.1	3.8	1.3	5.1	1.06	1.01
V17	Merlin	Air	RT	N_2 + 0.3% O_2[3)]	900	3	5	1.62	30.0	0.07	30.1	9.9	4.1	14.0	1.41	1.14
V18	Merlin	Air	RT	N_2 + 0.3% O_2[3)]	900	3	5	2.72	33.0	0.4	33.4	4.7	0.9	5.6	1.46	1.03
V19	SLA2 9260	CO_2	258.5	N_2 + 0.3% O_2[3)]	900	3	5	2.43	10.3	0.06	10.4	2.8	0.6	3.4	1.09	1.01
Merlin-1	Merlin	Air	RT	Ar + steam (1.6 kPa)	1000	3.25	4	1.58	58.0	15.4	73.4	12.1	8.0	20.1	3.69	1.23
Merlin-2	Merlin	Air	RT	Ar + steam (1.6 kPa)	1000	3.25	10	3.64	74.7	18.2	92.9	16.3	12.7	29.0	13.4	1.36
FH1	SLA2 5120	CO_2	391.5	Ar	1000		40	0.70			29.4			2.4		

RT = Room temperature
Red values: Determined by assuming an averaged initial radionuclide content. Determination of the residual activity of the sample is in progress.

[1] Ceramic tube with measured ingress of O_2
[2] New ceramic tube, unknown ingress of O_2
[3] Quartz tube with defined amount of O_2 in the treatment gas
[4] The ratio of initial specific radioactivity to final specific radioactivity resulting from a separation process [McGraw-Hill: Dictionary of Scientific and Technical Terms]. 1000 and above is excellent; 10 and below is poor [Hutchinson encyclopaedia].
[5] Probably a surface contamination

9.2 Summary Thermal Treatment with Enrichment Factors

Revision date: 25/02/2013

Exp. No.	Sample	Irradiation conditions		Experimental conditions				Mass loss [%]	Release [%]						Enrichment factor[4)]	
		Cool. gas	T [°C]	Treat. gas	T [°C]	Treatment time [h]			HTO	HT	^{3}H total	$^{14}CO_2$	^{14}CO	^{14}C total	^{3}H	^{14}C
						Heating	Isothermal									
V4	Merlin	Air	RT	N_2 + 0.14% O_2[1)]	1300	0	10	0.89	85.9	7.7	93.6	3.4	2.5	5.9	105	6.7
V5	Merlin	Air	RT	N_2 + 1% O_2	900	3	2.5	6.64	10.1	0.2	10.3	8.6	3.3	11.9	1.5	1.8
V6	Merlin	Air	RT	N_2 + 1% O_2	700	2.5	7.75	7.22	26.5	0.2	26.7	14.5	7.3	21.8	3.7	3.0
V7	SLA2 9260	CO_2	258.5	N_2 + 0.14% O_2[1)]	1300	0	10.5	0.91	65.0	0.2	65.2	1.4	0.6	2.0	71.8	2.3
V8	Merlin	Air	RT	N_2 + *x*% O_2[2)]	1300	0	21	5.12	65.6	31.3	96.9	2.5	8.2	10.7	18.9	2.1
V9	Merlin	Air	RT	Pure N_2	1100	3.75	20	0.20	4.6	56.3	60.9	0.12	2.0	2.1	301	10.3
V10	Merlin	Air	RT	Pure N_2	1100	3.75	25.5	0.01	1.2	0.09	1.3	1.5	1.3	2.8	97.7	217
V11	Merlin	Air	RT	Pure N_2	1100	3.75	20.5	0.16	15.2	21.1	36.3	0.6	1.4	2.1	223	12.7
V12	SLA2 9260	CO_2	258.5	Pure N_2	1100	3.75	20.5	0.45	13.3	7.3	20.6	0.4	2.0	2.4	46.2	5.6
V13	Magnox	CO_2	270	Pure N_2	1100	3.75	11	0.14	1.8	0.8	2.6	0.5	1.9	2.4	18.4	17.5
V14	Merlin	Air	RT	N_2 + 0.1% O_2[3)]	750	2.5	5	0.22	1.1	0.1	1.2	0.8	0.4	1.2	5.3	5.3
V15	Magnox	CO_2	270	N_2 + 0.1% O_2[3)]	900	3	5	0.70	5.2	0.5	5.7	35.6	22.1	57.7[5)]	8.2	82.6
V16	Magnox	CO_2	270	N_2 + 0.3% O_2[3)]	900	3	5	3.90	9.0	0.1	9.1	3.8	1.3	5.1	2.3	1.3
V17	Merlin	Air	RT	N_2 + 0.3% O_2[3)]	900	3	5	1.62	30.0	0.07	30.1	9.9	4.1	14.0	18.5	8.7
V18	Merlin	Air	RT	N_2 + 0.3% O_2[3)]	900	3	5	2.72	33.0	0.4	33.4	4.7	0.9	5.6	12.3	2.1
V19	SLA2 9260	CO_2	258.5	N_2 + 0.3% O_2[3)]	900	3	5	2.43	10.3	0.06	10.4	2.8	0.6	3.4	4.3	1.4
Merlin-1	Merlin	Air	RT	Ar + steam (1.6 kPa)	1000	3.25	4	1.58	58.0	15.4	73.4	12.1	8.0	20.1	46.5	12.8
Merlin-2	Merlin	Air	RT	Ar + steam (1.6 kPa)	1000	3.25	10	3.64	74.7	18.2	92.9	16.3	12.7	29.0	25.5	8.0
FH1	SLA2 5120	CO_2	391.5	Ar	1000		40	0.70			29.4			2.4	42.0	3.4

RT = Room temperature
Red values: Determined by assuming an averaged initial radionuclide content. Determination of the residual activity of the sample is in progress.

[1)] Ceramic tube with measured ingress of O_2
[2)] New ceramic tube, unknown ingress of O_2
[3)] Quartz tube with defined amount of O_2 in the treatment gas
[4)] The ratio of radionuclide release to mass loss.
[5)] Probably a surface contamination

List of Figures

Figure 2.1.1: Criytalline structure of graphite.
Figure 2.1.2: Cross sections for production of C14.
Figure 2.2.1-2: Initial and Final state of single cascade in perfect lattice structure (yellow: C14).
Figure 2.2.3: Range of C-14 in dependence of recoil energy and for different potentials.
Figure 2.2.4: Displacement and energy loss of C-14 in crystalline graphite for 40 keV(right).
Figure 2.3.1-a,b: Configuration of crystaline grains for Md simulation of the boundary effect.
Figure 2.3.2-a,b: Final states of C14 near grain boundaries.
Figure 3.1.1: (a) Cross section of the reactor block (left) and (b) position of the individual graphite bricks inside the reactor block (right)
Figure 3.1.2: MERLIN Material Test Reactor (FRJ-1)
Figure 3.1.3: Graphite block from the Merlin reactor used for the high temperature treatment in Knudsen cell
Figure 3.2.1: Internal structure of AVR's core and heat exchanger chamber
Figure 3.2.2: Scheme of different histories of a nuclear-grade graphite
Figure 3.2.3: Coarse virgin material before being cut in smaller samples. Left: Unknown grade graphite, Right: AVR reflector virgin graphite
Figure 3.2.4: Massive virgin samples of AVR reflector graphite, H50Ø50 mm
Figure 3.2.5: Small sample used both in the TGA, in the small electric oven and in the Carbolite Oven, H20Ø8 mm
Figure 3.2.6: Cutaway illustration of HTR fuel element showing the outer graphite shell to be sampled.
Figure 3.2.7: Sketch of drilled fuel element with extracted carrot.
Figure 3.2.8: Cutting plan for the cylindrical carrot obtained from fuel element HFR-EU1bis/3.
Figure 3.2.9: Carrotage samples placed in the sample holders, prior to embedding in resin. The respective sample numbers are indicated in the lower right corner of each image.
Figure 3.2.10a: Photos of the surface carrotage sample "Carbowaste-1". The outer surface is shown in the large photo; the thickness of 4mm is seen in the inset photo.
Figure 3.2.10b: Photos of the surface carrotage sample "Carbowaste-2". The diameter of 1 cm is shown in the inset photo. The sample has an outer steel ring from the hollow drill bit when the sample was cut out. A pre-test Knudsen cell sample was drilled out from the centre. The left-hand photo shows some grains of the pre-test Knudsen cell sample.
Figure 3.3.1: Uses of graphite in EDF UNGG reactors; different designs were developed, in this scheme an "integrated vessel" type reactor is presented (approximate external dimensions: 50 m height / 28.5 m diameter)
Figure 3.3.2: Saint-Laurent A1 (left) and Saint-Laurent A2 (right) UNGG reactors (current state 2012)
Figure 3.3.3: Section through the graphite stack of the Saint-Laurent A2 reactor - Juelich graphite cores were sampled from the F4M10 (hexagonal cell) C19 (fuel channel).
Figure 3.3.4: Remote controlled tool used for graphite stack sampling in UNGG reactors
Figure 3.3.5: Schematic view of coring in a graphite brick
Figure 3.4.1: Saint-Laurent 2 drilled sample
Figure 3.4.2: Oldbury 2 sample
Figure 3.4.3: Oldbury 2 cut sample
Figure 3.4.4: Glove box with tools for sample preparation

Figure 3.4.5: Drilled Saint-Laurent 2 samples

Figure 4.1.1: Washing procedure of reactor tube
Figure 4.1.2: Installation for graphite thermal treatment with inert gas (T. Podruzhina, M. Florjan)
Figure 4.1.3: New installation for graphite thermal treatment with given washing solutions in each bottle (K. Baginski)
Figure 4.1.4: Photo of the new installation for graphite thermal treatment (K. Baginski)
Figure 4.1.5: Flow pattern of velocity of flow gas, vector modus (nitrogen, 1.42 L/min)
Figure 4.1.6: Flow pattern of velocity of flow gas, sample position with new sample holder (nitrogen, 1.42 L/min)
Figure 4.1.7: New sample holder with a virgin untreated graphite sample for the apparatus of graphite thermal treatment
Figure 4.1.8: Conventional sample holder for graphite thermal treatment.
Figure 4.2.1: Overview of the experimental set up with the induction oven
Figure 4.2.2: Overview of the Induction Oven Facility
Figure 4.2.3: Front view of the control and power supply unit
Figure 4.2.4: Overview of the cooling unit
Figure 4.2.5: Overview of the Induction Oven
Figure 4.2.6: Inside view of the Induction Oven during at treatment
Figure 4.2.7: Schematic representation of the pyrometer feedback action
Figure 4.2.8: Scheme of the Mass Spectrometer System (Courtesy of InProcess Instruments)
Figure 4.2.9: View of the Mass Spectrometer (left) next to the Induction Oven (right)
Figure 4.2.10-11: Upper part (left) and lower parts (right) of the original sample holder
Figure 4.2.12: Thermodynamic simulation of the original sample holder
Figure 4.2.13: Simplified thermodynamic simulation of the original sample holder, zoomed
Figure 4.2.14: Fluid dynamic simulation of the original sample holder
Figure 4.2.15: Overview of the new sample holder with thermal shield (transparent in this picture)
Figure 4.2.16: New sample holder with thermal shield, section view
Figure 4.2.17.a-b: Comparison between the old (left) and new (right) sample holder, during operation in the oven.
Figure 4.2.18: ^{14}C release vs. time during former thermal treatments [8]
Figure 4.2.19: ^{14}C release vs. ^{12}C release during former thermal treatments [2]
Figure 4.2.20: ^{14}C release vs. time during former thermal treatments under nitrogen [8]
Figure 4.2.21: ^{3}H release vs. ^{12}C release during former thermal treatments under different conditions [2]
Figure 4.2.22: ^{3}H release vs. time during former thermal treatments under nitrogen atmosphere [8]
Figure 4.3.1 Schematic overview of the Knudsen Cell for analysis of radioactive samples
Figure 4.4.1 Schematic overview of the Küfa device at JRC-ITU
Figure 4.4.2: Diagram of the Küfa device along with the cold trap for collecting & measuring the released fission gases by gamma-spectroscopy.
Figure 5.1.1: Tritium release in argon atmosphere [2]
Figure 5.1.2: Tritium release in nitrogen atmosphere [8]
Figure 5.1.3: ^{3}H release from graphite bulk samples in nitrogen, quartz tube (K. Baginski)
Figure 5.1.4: ^{3}H release from graphite bulk samples in nitrogen, ceramic tube (K. Baginski)
Figure 5.1.5: ^{14}C release from AVR and Merlin graphite in argon (T. Podruzhina)
Figure 5.1.6: ^{14}C release from AVR and Merlin graphite in nitrogen (M. Florjan)
Figure 5.1.7: ^{14}C release from graphite bulk samples in nitrogen, quartz tube (K. Baginski)

Figure 5.1.8: ^{14}C release from graphite bulk samples in nitrogen, ceramic tube (K. Baginski)
Figure 5.1.9: Incineration scheme of radioactive graphite samples
Figure 5.2.1: On-line gaseous emissions from AVR graphite, Induction Oven, sample "MAVR 2", linear plot
Figure 5.2.2: On-line gaseous emissions from AVR graphite, massive sample "AVR 2", semi-log plot
Figure 5.2.3: On-line gaseous emissions from AVR graphite, TGA, sample "CR 01", linear plot
Figure 5.2.4: On-line weight measurement of AVR graphite, TGA, sample "CR 01", Thermo Gravimetric Analyser
Figure 5.2.5: Comparison among normalized SIMS depth profiles of chlorine as Cl-, before and after thermal treatment, semilog plot
Figure 5.2.6: Comparison among normalized SIMS depth profiles of nitrogen as CN-, before and after thermal treatment, linear plot
Figure 5.2.7: Comparison among normalized SIMS depth profiles of calcium as CaO-, before and after thermal treatment, linear plot
Figure 5.2.8: Overview of AVR graphite surface, treated in experiment "AVR square 1", mag. 2400x
Figure 5.3.1: Knudsen cell results. Mass spectrometer signal as a function of time and temperature for tritium and helium. No major release was detectable.
Figure 5.3.2: Knudsen cell results. Mass spectrometer signal as a function of time and temperature for intermediate mass range. No major release traceable to ^{36}Cl was detectable.
Figure 5.3.4: Knudsen cell results. Mass spectrometer signal as a function of time and temperature for carbon & nitrogen.
Figure 5.3.3: Knudsen cell results. Mass spectrometer signal as a function of time and temperature for high mass range. No major release was detectable.
Figure 5.3.5: Gamma spectroscopy of the Carbowaste-2 sample and the 2 pre-test samples, showing the caesium-134,137 peaks and the Co-60 peaks.
Figure 6.1.1: Decontamination factors of H-3 for Merlin graphite in function of the isothermal treatment temperature
Figure 6.1.2: Decontamination factors of C-14 for Merlin graphite in function of the isothermal treatment temperature
Figure 6.2.1: Decontamination factors of H-3 for SLA2 graphite in function of the isothermal treatment temperature
Figure 6.2.2: Comparison among sample densities before and after irradiation in the reactor core at vertical position 1680 mm and 5120 mm, SLA2 sleeve graphite. Indicative values.
Figure 6.2.3: Decontamination factors of C-14 for SLA2 graphite in function of the isothermal treatment temperature
Figure 6.3.1: Decontamination factors of H-3 for Oldbury 2 graphite in function of the isothermal treatment
Figure 6.3.2: Decontamination factors of C-14 for Oldbury 2 graphite in function of the isothermal treatment temperature
Figure 6.4.1: Decontamination factors of H-3 for AVR graphite in function of the isothermal treatment temperature
Figure 6.4.2: Decontamination factors of C-14 for AVR graphite in function of the isothermal treatment temperature
Figure 6.6.1: Decontamination factors of H-3 for different graphite in function of the isothermal treatment
Figure 6.6.2-a: Decontamination factors of C-14 for different graphite in function of the isothermal treatment
Figure 6.6.2-b: Decontamination factors of C-14 for different graphite in function of the isothermal treatment temperature
Figure 7.1.1: Model of Atsumi for Hydrogen trapping sites and transport in graphite [31,42]
Figure 7.1.2: Release of tritium in inert gases at different temperatures

Figure 7.1.3: Release of HTO from Merlin graphite in nitrogen at 1100 °C plotted as diffusion reaction
Figure 7.1.4: Release of HT from Merlin graphite in nitrogen at 1100 °C plotted as diffusion reaction
Figure 7.1.5: Release of HT from Merlin graphite in nitrogen at 1100 °C plotted as first order reaction
Figure 7.1.6: Release of HT from Merlin graphite in nitrogen at 1100 °C plotted as second order reaction
Figure 7.1.7: Release of tritium in argon at 866 °C plotted as diffusion reaction.
Figure 7.1.8: Release of tritium in argon at 1063 °C plotted as diffusion reaction.
Figure 7.1.9: Release of HTO from Magnox Oldbury 2 graphite in nitrogen at 1100 °C plotted as diffusion reaction.
Figure 7.1.10: Release of HT from Magnox Oldbury 2 graphite in nitrogen at 1100 °C plotted as diffusion reaction
Figure 7.1.11: Comparison among two tritium release curves from similar experiments, with different oxygen amounts in the adduct gases
Figure 7.1.12: Release of radiocarbon in inert gas at different temperatures
Figure 7.1.13: Release of radiocarbon in inert gas at different temperatures from Fig. 7.1.8 plotted as diffusion reaction
Figure 7.1.14: Release of radiocarbon in nitrogen with 1% oxygen at different temperatures (the upper number gives the % ^{14}C released and the lower number the % carbon consumed)
Figure 7.1.15: Release of total carbon in nitrogen with 1% oxygen at different temperatures
Figure 7.1.16: Repeated thermal treatment at 900 °C under nitrogen atmosphere after intermediate exposure of the sample to air at room temperature for 20 hours (cumulated ^{14}C release: 35.5%, cumulated release of total carbon: 2.7%, ^{14}C enrichment in the gas phase: 13:1) [8]
Figure 7.1.17: Release of $^{14}CO_2$ from Magnox Oldbury 2 graphite in nitrogen at 1100 °C plotted as diffusion reaction
Figure 7.1.18: Release of ^{14}CO from Magnox Oldbury 2 graphite in nitrogen at 1100 °C plotted as diffusion
Figure 7.1.19: Model of a graphite surface with ^{3}H and ^{14}C as functional groups (surface complexes)
Figure 7.1.20: Release of $^{14}CO_2$ from SLA2 graphite in Argon at 1000 °C (mass loss after 10 h: 0.32%)
Figure 7.1.21: Release of ^{14}CO from SLA2 graphite in Argon at 1000 °C (mass loss after 10 h: 0.32%)
Figure 7.1.22: Release of $^{14}CO_2$ from SLA2 graphite in Argon at 1000 °C, isothermal section plotted as diffusion
Figure 7.1.23: Release of ^{14}CO from SLA2 graphite in Argon at 1000 °C, isothermal section plotted as diffusion reaction
Figure 7.1.24: Schematic view of the controversial effect of temperature on reaction rates and regime in porous media.
Figure 7.2.1: Release of tritium from Merlin graphite in nitrogen at 1100 °C (mass loss after 20 h: 0.20%)
Figure 7.2.2: Release of ^{14}C from Merlin graphite in nitrogen at 1100 °C (mass loss after 20 h: 0.20%)
Figure 7.2.3: Release of tritium from Magnox Oldbury 2 graphite in nitrogen at 1100 °C (mass loss after 11 h: 0.14%)
Figure 7.2.4: Release of ^{14}C from Magnox Oldbury 2 graphite in nitrogen at 1100 °C (mass loss after 11 h: 0.14%)
Figure 7.3.1: Release of ^{14}C from Magnox Oldbury 2 graphite in N_2 with 0.1% O_2 at 900 °C (mass loss after 5 h: 0.70%)
Figure 7.3.2: Spatial distribution of beta-emitters on the surface of the Magnox Oldbury 2 sample from Figure 7.3.1 after thermal treatment determined by digital autoradiography (specimen diameter: 15 mm, thickness: 5 mm, mass: 0.7684 g)
Figure 7.4.2: A model of changes from mesophase to graphite during heat treatment [19]

List of Tables

Table 3.1.1 : Content of individual radionuclides in a Merlin irradiated graphite block (320g) according to radiochemical analyses (meas. date: 25.05.2009)
Table 3.2.1: Concentrations of impurities in AVR graphite
Table 3.2.2: Activation reactions producing ^{14}C
Table 3.2.3: Total radioactivity in AVR graphite
Table 3.3.1: Some impurities and characteristic values of SLA grpahite
Table 3.3.2: Estimated radionuclide inventory of SLA2 graphite (Bq/g)
Table 3.3.3: Position, temperature and dose rate of the samples delivered to FZJ.
Table 3.4.1: Irradiation conditions of Oldbury 2 graphite provided by NNL
Table 3.5.1: Dose Rates of i-graphite samples (trepanned samples & channel bricks) selected for ITU (Mar '12). Activity & composition from ENEA (SOGIN) Italy.
Table 3.5.2: Specific activities of the main isotopes of irradiated graphite samples selected for ITU (Mar '12). Alfa emitters may be present at concentrations <0,5 Bq/g. Activity & composition from ENEA (SOGIN) Italy.
Table 4.1.1: Radioactive graphite treatment in argon atmosphere (T. Podruzhina)
Table 4.1.2: Radioactive graphite treatment in nitrogen atmosphere (M. Florjan)
Table 4.2.1: Overview of the massive samples used in the most significant experiments with the Induction Oven Facility
Table 4.4.1: General characteristics of fuel element (FE) HFR-EU1bis/3
Table 4.4.2: Parameters of the HFR-EU1bis irradiation campaign
Table 6.1.1: Overview of the performed thermal treatment experiments with Merlin graphite in “inert” atmosphere.
Table 6.2.1: Overview of the performed thermal treatment experiments with SLA2 graphite in “inert” atmosphere
Table 6.2.2: Comparison among sample densities before and after irradiation in the reactor core, indicative values.
Table 6.3.1: Overview of the performed thermal treatment experiments with Oldbury 2 graphite in “inert” atmosphere
Table 6.4.1: Overview of the performed thermal treatment experiments with AVR graphite in “inert” atmosphere. (* mass losses are only estimated due to the particular method applied, without removing the sample from the treatment chamber)
Table 7.1.1: Diffusion coefficients of H-3 at different temperatures for Merlin and AVR graphite [2]
Table 7.4.1: Isotopic inventory of Merlin and Magnox Oldbury 2 graphite (date: 15th June 2012)